

SELECTIVE CONVERSION OF CELLULOSE INTO 5-
HYDROXYMETHYLFURFURAL OVER MODIFIED
ZEOLITE CATALYSTS IN A BIPHASIC SOLVENT SYSTEM



Mr. Oluwaseyi Ojelabi

A Thesis Submitted in Partial Fulfillment of the Requirements
for the Degree of Master of Science in Petrochemistry and Polymer
Science

Field of Study of Petrochemistry and Polymer Science

FACULTY OF SCIENCE

Chulalongkorn University

Academic Year 2022

Copyright of Chulalongkorn University

การแปรรูปแบบเลือกจำเพาะของเซลล์โลสเป็น 5-
ไฮดรอกซีเมทิลเฟอร์พิวรอลบนตัวเร่งปฏิกิริยาซีโอไลต์ดัดแปรในระบบตัว
ทำละลายสองวัฏภาค



วิทยานิพนธ์นี้เป็นส่วนหนึ่งของการศึกษาตามหลักสูตรปริญญาวิทยาศา
สตรมหาบัณฑิต
สาขาวิชาปิโตรเคมีและวิทยาศาสตร์พอลิเมอร์
สาขาวิชาปิโตรเคมีและวิทยาศาสตร์พอลิเมอร์
คณะวิทยาศาสตร์ จุฬาลงกรณ์มหาวิทยาลัย
ปีการศึกษา 2565
ลิขสิทธิ์ของจุฬาลงกรณ์มหาวิทยาลัย

Thesis Title	SELECTIVE CONVERSION OF CELLULOSE INTO 5-HYDROXYMETHYLFURFURAL OVER MODIFIED ZEOLITE CATALYSTS IN A BIPHASIC SOLVENT SYSTEM
By	Mr. Oluwaseyi Ojelabi
Field of Study	Petrochemistry and Polymer Science
Thesis Advisor	Professor Chawalit Ngamcharussrivichai, Ph.D.
Thesis Co Advisor	Professor Umer Rashid, Ph.D.

Accepted by the FACULTY OF SCIENCE, Chulalongkorn University in
Partial Fulfillment of the Requirement for the Master of Science

..... Dean of the FACULTY OF
SCIENCE
(Professor POLKIT SANGVANICH, Ph.D.)

THESIS COMMITTEE

..... Chairman
(Assistant Professor DUANGAMOL TUNGASMITA,
Ph.D.)

..... Thesis Advisor
(Professor Chawalit Ngamcharussrivichai, Ph.D.)

..... Thesis Co-Advisor
(Professor Umer Rashid, Ph.D.)

..... Examiner
(Professor NAPIDA HINCHIRANAN, Ph.D.)

..... External Examiner
(Professor Attasak Jaree, Ph.D.)

จุฬาลงกรณ์มหาวิทยาลัย
CHULALONGKORN UNIVERSITY

โอลิวาเซย์ โอลิเลาปี : การแปรรูปแบบเลือกจำเพาะของเซลลูโลสเป็น 5-ไฮดรอกซีเมทิลเฟอร์ฟิวรัลบนตัวเร่งปฏิกิริยาซีโอไลต์ดัดแปรในระบบตัวทำละลายสองวัฏภาค. (SELECTIVE CONVERSION OF CELLULOSE INTO 5-HYDROXYMETHYLFURFURAL OVER MODIFIED ZEOLITE CATALYSTS IN A BIPHASIC SOLVENT SYSTEM) อ.ที่ปรึกษาหลัก : ศ.ดร.ชาลิต งามจรัสศรีวิชัย, อ.ที่ปรึกษาร่วม : Umer Rashid

ลิกโนเซลลูโลสส่วนใหญ่ประกอบด้วยเซลลูโลสซึ่งสามารถถูกเปลี่ยนให้เป็นสารเคมีมูลค่าสูงผ่านกระบวนการทางเคมีความร้อนต่าง ๆ เช่น การเร่งปฏิกิริยาดีโพลีเมโรไลเซชัน ดีไฮเดรชันที่เร่งปฏิกิริยาด้วยกรด ไพโรไลซิส แกซิฟิเคชัน ฯลฯ เพื่อการพัฒนาที่ยั่งยืนและเศรษฐกิจฐานชีวภาพ 5-ไฮดรอกซีเมทิลเฟอร์ฟิวรัล (HMF) เป็นหนึ่งในสารเคมีชีวภาพที่มีศักยภาพที่สามารถผลิตขึ้นได้โดยตรงจากลิกโนเซลลูโลสผ่านการเร่งปฏิกิริยาดีโพลีเมโรไลเซชันและ/หรือดีไฮเดรชันที่เร่งปฏิกิริยาด้วยกรดโดยใช้ตัวเร่งปฏิกิริยาแบบสองหน้าที่สำหรับการผลิตผลิตภัณฑ์หมุนเวียนต่างๆ โพรโทนิคซีโอไลต์ (protonic zeolites) เป็นตัวเร่งปฏิกิริยาชนิดกรดที่ทำงานได้สองหน้าที่ และมีสมบัติที่โดดเด่น คือ พื้นที่ผิวจำเพาะสูงทำให้โมเลกุลของสารแพร่เข้าและออกจากรูพรุนได้ง่าย และสมบัติความเป็นกรดที่สามารถควบคุมได้ง่ายด้วยกระบวนการหลังการสังเคราะห์หรือกระบวนการดัดแปร งานวิจัยนี้ใช้ซีโอไลต์เกรดการค้า 3 ชนิด ได้แก่ H-ZSM-5 (อัตราส่วนโดยโมล $\text{SiO}_2/\text{Al}_2\text{O}_3$ เท่ากับ 24), H-USY (อัตราส่วนโดยโมล $\text{SiO}_2/\text{Al}_2\text{O}_3$ เท่ากับ 6) และ H-Beta (อัตราส่วนโดยโมล $\text{SiO}_2/\text{Al}_2\text{O}_3$ เท่ากับ 28) เป็นวัสดุตั้งต้นสำหรับการเตรียมตัวเร่งปฏิกิริยาชนิดกรดแบบสองหน้าที่สำหรับปฏิกิริยาดีไฮเดรชันโดยตรงของกลูโคสและการเปลี่ยนเซลลูโลสเป็น HMF ในขั้นตอนเดียวในตัวทำละลายสองวัฏภาค (น้ำ/เตตระไฮโดรฟิวแรน) วัสดุซีโอไลต์ตั้งต้นถูกดัดแปรสภาพกรดด้วยสารละลายกรดไนตริกและถูกดัดแปรเพิ่มเติมด้วยดีบุก (tin) โดยใช้สารตั้งต้นเป็นทินคลอไรด์ ($\text{SnCl}_4 \cdot \text{H}_2\text{O}$) แม้ว่า การดัดแปรสภาพกรดจะทำให้สัดส่วนองค์ประกอบของธาตุ สมบัติทางกายภาพ และสัญญาณวิทยาของซีโอไลต์มีการเปลี่ยนแปลงเพียงเล็กน้อย แต่ปริมาณกรดรวมและการกระจายตัวของตำแหน่งกรดเปลี่ยนแปลงไปอย่างมีนัยสำคัญ การดัดแปรสภาพกรดของ H-ZSM-5 ด้วยสารละลายกรดไนตริกที่มีความเข้มข้น 0.1 โมลาร์ สกัดอะลูมิเนียมนอกโครงข่าย (non-framework) ออกจากซีโอไลต์พร้อมกันกับการเกิดไฮโดรไลซิสของโครงข่ายซีโอไลต์ ส่งผลให้สัดส่วนของโครงข่ายอะลูมิเนียมที่ไม่อิมตัวและปริมาณตำแหน่งกรดลิวอิสเพิ่มขึ้น จากการศึกษาวิเคราะห์ด้วยเทคนิค UV-vis spectroscopy พบว่าสัดส่วนโพรงอะลูมิเนียมในโครงข่ายซีโอไลต์สาขาวิชา ปิโตรเคมีและวิทยาศาสตร์พอลายมีอ็อกซิเจน

ลิเมอร์

ปีการศึกษา 2565 ลายมือชื่อ อ.ที่ปรึกษาหลัก

.....

ลายมือชื่อ อ.ที่ปรึกษาร่วม

.....

6470076323 : MAJOR PETROCHEMISTRY AND POLYMER SCIENCE

KEYWORD cellulose; glucose; 5-hydroxymethylfurfural; H-ZSM-5 H-USY H-Beta; dealumination; acid leaching; tin; impregnation; tin (IV) chloride pentahydrate

Oluwaseyi Ojelabi : SELECTIVE CONVERSION OF CELLULOSE INTO 5-HYDROXYMETHYLFURFURAL OVER MODIFIED ZEOLITE CATALYSTS IN A BIPHASIC SOLVENT SYSTEM. Advisor: Prof. Chawalit Ngamcharussrivichai, Ph.D. Co-advisor: Prof. Umer Rashid, Ph.D.

Lignocellulosic biomass mainly composed of cellulose which can be transformed through various thermochemical processes such as catalytic depolymerization, acid-catalyzed dehydration, pyrolysis, gasification, etc., into high-value chemicals for sustainable development and bio-based economy. 5-Hydroxymethylfurfural (HMF) is one of the potential platform bio-chemicals that can be obtained directly from lignocellulosic biomass via catalytic depolymerization and/or acid-catalyzed dehydration using a bifunctional catalyst for the manufacture of various renewable products. Protonic zeolites are bifunctional solid acid catalysts and are well known for their remarkable properties. Their large surface area could enable molecules to diffuse in and out of their pore systems. Moreover, their acidic properties can be easily controlled by various post-synthesis or modification procedures. In this project, three protonic commercial zeolites namely, H-ZSM-5 ($\text{SiO}_2/\text{Al}_2\text{O}_3$ ratio 24), H-USY ($\text{SiO}_2/\text{Al}_2\text{O}_3$ ratio 6), and H-Beta ($\text{SiO}_2/\text{Al}_2\text{O}_3$ ratio of 28) were used as a starting material for preparing a series of acid catalysts with bifunctionality for direct dehydration of glucose and one-pot conversion of cellulose to HMF in a biphasic water/tetrahydrofuran system. The pristine zeolites were mildly dealuminated by refluxing with dilute nitric acid solutions to adjust their acid properties and were further modified with tin metal using tin precursor, $\text{SnCl}_4 \cdot \text{H}_2\text{O}$. Although the acid treatment slightly altered the elemental composition, textural properties, and morphology of the zeolites, the total acidity and distribution of acid sites were significantly modified. Using 0.1 M acid-treated H-ZSM-5 as a reference, some non-framework aluminum (Al) oxide clusters were removed from the parent zeolite simultaneously with partial hydrolysis of the zeolitic framework. An increased fraction of coordinatively unsaturated framework Al species enhanced the number of Lewis acid sites. UV-vis spectroscopy revealed that tin was incorporated mostly at extraframework sites, thereby enhancing the weak acid sites and the overall total acidities of the zeolite catalysts. Using 0.1 M solution in the treatment process with H-ZSM-5 zeolite provided a suitable catalyst (0.1DeAl.H-ZSM-5) for glucose dehydration to HMF.

Field of Study: Petrochemistry and
Polymer Science

Student's Signature

.....

Academic Year: 2022

Advisor's Signature

.....

Year:

Co-advisor's Signature

.....

ACKNOWLEDGEMENTS

First, I acknowledge God that granted me the grace to complete my master's degree program at Chulalongkorn University successfully.

My appreciation goes to the ASEAN/NON-ASEAN Scholarship Board, the Program in Petrochemistry and Polymer Science, Chulalongkorn University, the Center of Excellence in Catalysis for Bioenergy and Renewable Chemicals (CBRC), the International Research Network: Contract No. IRN61W0003, and Thailand Science Research and Innovation (TSRI), Chulalongkorn University (CUFRB65_bcg(4)_072_23_02) for their financial support towards the success of this research program. I also acknowledge the technical support received from the Center of Excellence on Petrochemical and Materials Technology (PETROMAT), Chulalongkorn University.

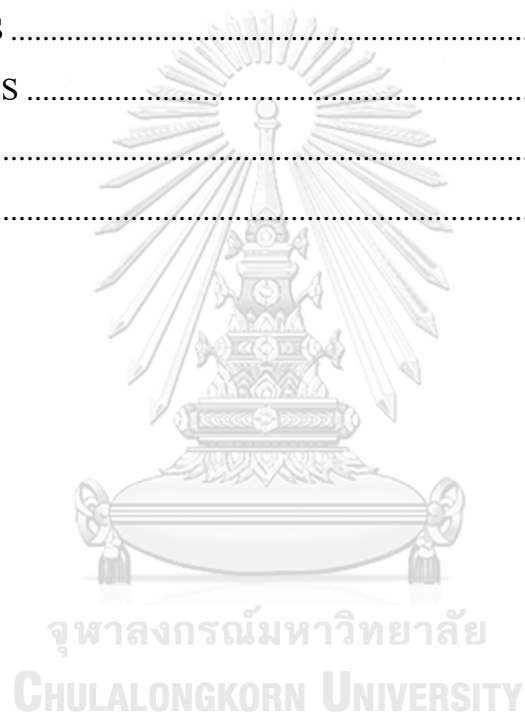
Special thanks to my thesis advisor, Professor Chawalit Ngamcharussrivichai, for his immense contributions and efforts toward the successful completion of my research work at the CBRC lab. The numerous intellectual supports and kindness I received from him during the course of my work are enormous and highly appreciated. I want to appreciate my wonderful colleagues in the CBRC lab, in the person of, Dr. Satit Yousatit, Mr. Chanasit Kaewngam, Mr. Nuttapat Thiensuwan, Mr. Atikhun Chottiratanachote, Mr. Hannarong Pitayachinchot, and Mr. Wongsakorn Khamme, for the supports they all rendered in one way or the other during the course of my research work. It was a great feeling for me to have lab colleagues that were ready to help me in the course of my research work. This would always be in my heart.

I am indeed grateful for the support I received from my family and my wife. Your continued prayers keep me going on my academic journey and success story. May God continues to be with you and bless you abundantly. I acknowledge my Nigerian Chula friends for their great contributions during my stay in Thailand.

Oluwaseyi Ojelabi

TABLE OF CONTENTS

	Page
ABSTRACT (THAI)	iii
ABSTRACT (ENGLISH)	iv
ACKNOWLEDGEMENTS	v
TABLE OF CONTENTS	vi
LIST OF TABLES	vii
LIST OF FIGURES	viii
REFERENCES	146
VITA	148



LIST OF TABLES

Page

No table of figures entries found.



LIST OF FIGURES

Page

No table of figures entries found.



CHAPTER 1

INTRODUCTION

1.1. Background

Fossil feedstock has been the primary energy source in the chemical and petrochemical industries and everyday life since the 18th century. The chemical and petrochemical industries utilize the raw materials arising from this feedstock such as crude oil, natural gas, coal, etc., and transform them into essential products for modern utilization. They originate from the anaerobic decomposition of remains of dead plants and animals which are processed to generate heat energy, electricity, transportation, jet fuels, chemicals, etc.

According to the year 2019 reports, fossil fuels account for eighty-four (84%) of the major energy consumption and sixty-four (64%) of electricity worldwide and they have also been reported to cause severe environmental consequences. Carbon dioxide, which is a major greenhouse gas is generated from their utilizations, which accounts for 80% proportion, and has been estimated around thirty-five (35) billion tons that are emitted into the atmosphere per year [1].

The major cause of global warming and climate change emanates from fossil fuel consumption, coupled with environmental and air pollution arising from their particulates and noxious gas emissions. From a global sustainability perspective, apart from their recognition of global warming and climate crisis impacts, they have been projected to go into extinction or limited supply in the future and have led to world-spread research for sustainable energy as an alternative, to put halt to their utilization.

Biomass feedstocks have drawn a lot of attention as a potential alternative for producing high-value chemicals and liquid fuels to address these concerns and lessen reliance on fossil feedstock. One of the ways to solve this challenge is the development of modern biorefineries. Interestingly, through photosynthesis, this biomass feedstock utilizes carbon dioxide that converts it to sugars and their polymers.

Biomass consists mainly of lignocellulose which can be classified into three (3) categories, and other components.

- ❖ Cellulose accounts for 40–50% and makes up the higher percentage of lignocellulosic biomass, consisting of linear chains of numerous hundreds to thousands of units of glucose monomers. They are an important structural component of the plant cell that provides rigidity and support, which are mainly connected by intra-molecular hydrogen bonds. Most of this feedstock is derived from plants such as cotton, woody trees, grasses, crops, etc., and partly from animal waste, municipal solid waste, etc. Through conventional processes such as acid or enzyme hydrolysis, fermentation, pyrolysis, gasification, etc., they can be transformed into fuels like ethanol, and biodiesel; power such as heat and electricity; chemicals products like plastics, resins, foams, solvents, adhesives, paints, chemical intermediates, etc.
- ❖ Hemicellulose makes up 16–33% of plant cells and is a branched short-chain polymer consisting of five hundred to three thousand units of diverse sugar monomers such as glucose, xylose, galactose, mannose, arabinose, etc. They

contribute to the plant cell by providing strength and serve as middle-ground support by interacting with cellulose and lignin.

- ❖ Lastly, lignin makes up 25-30% of plant dry matter and is mostly found in wood. They are majorly organic polymers cross-linked by phenolic precursors such as coniferyl alcohol, sinapyl alcohol, etc., and help in providing rigidity to plant cell walls.

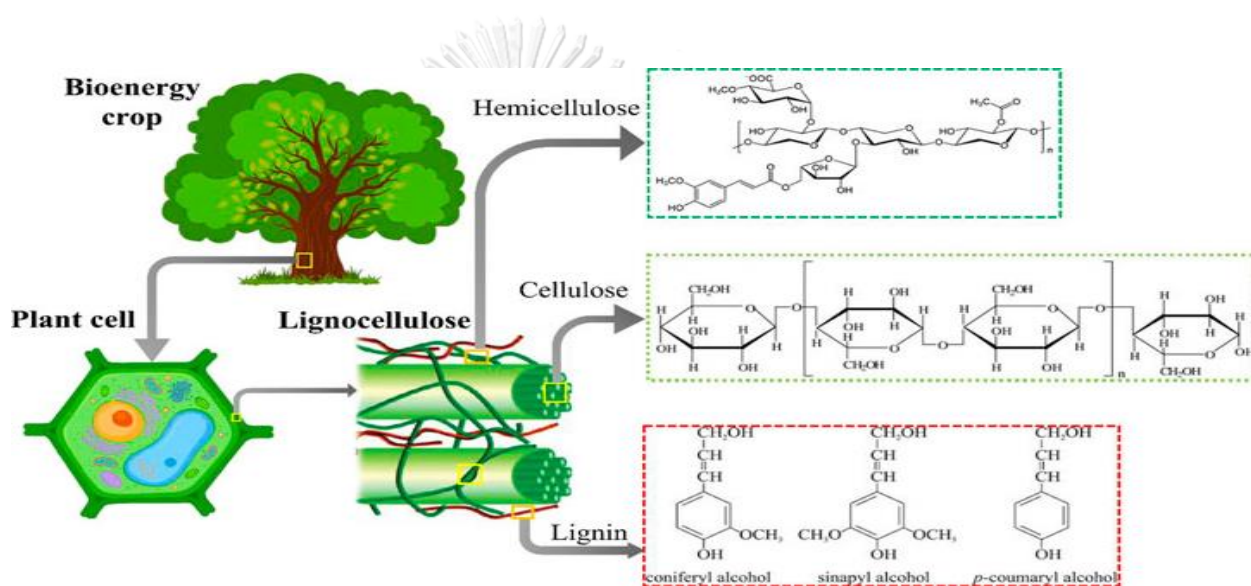


Figure 1.1. Diagrammatic representation of lignocellulosic biomass composition.

CHULALONGKORN UNIVERSITY

The minor components of biomass include oils, terpenes, and other minerals. Plants such as flax or sunflowers produce seeds where oil can be easily extracted by transforming them into biodiesel through a process known as transesterification.

An important step towards creating a potential alternative to the current fossil-based products is the development of efficient bio-refineries to produce high-value chemicals. One of these platform chemicals is 5-hydroxymethylfurfural, which has piqued the interest of many researchers.

Due to the advantageous effects of the active functional groups present, the US Department of Energy reported 5-hydroxymethylfurfural (HMF) as a major platform chemical to various high-value chemicals and biofuels derived from lignocellulosic biomass in 2004. **Figure 1.2** shows how hydrogenation and/or hydrodeoxygenation of HMF can be used to produce 2,5-dimethylfuran, a biofuel, and high-quality liquid fuel additive. Hydration of HMF can be used to produce levulinic acid, which is used in pharmaceuticals and is a precursor to ethyl levulinate, a fuel additive [2,3]. Furthermore, via aldol condensation of furfural and HMF with cyclic ketones [4,5], among other methods, bio-derived or bio-jet oil could be created directly.

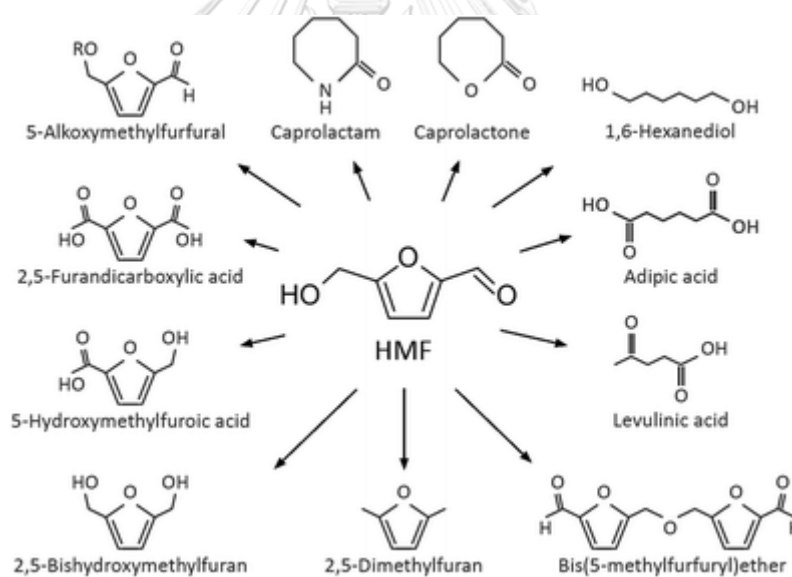


Figure 1.2. Schematic representation of high-value chemicals derived from HMF.

The synthesis of HMF involves three reaction steps from cellulose, as shown in **Figure 1.3**. The first step involves cellulose hydrolysis or depolymerization which is promoted by Brønsted acid sites and results in the production of glucose. The second step involves the isomerization of glucose to fructose, via 1,2-intramolecular hydride

shift, which Lewis acidity promotes, and the third step requires the dehydration of fructose to HMF, through the removal of three (3) molecules of water, also promoted by Brønsted acid [6,7].

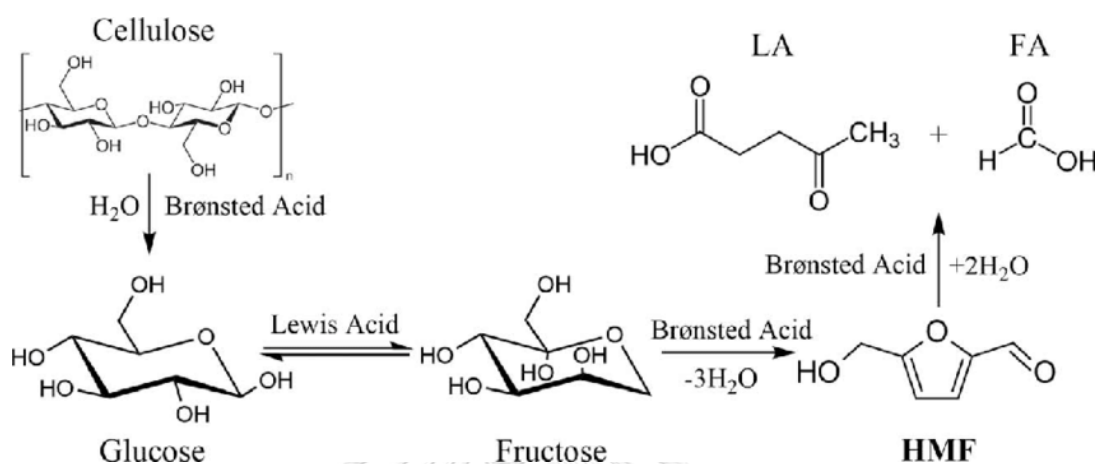


Figure 1.3. Reaction pathways to produce HMF from cellulose.

A growing interest has been shown in heterogeneous solid acid catalysts for the selective transformation of lignocellulosic biomass to high-value chemicals due to their simplicity in product separation, ease of recovery, and lack of equipment corrosion over other catalytic systems. Additionally, these catalytic systems allow for the performance of reactions in benign circumstances. Among the family of these catalysts is zeolite.

Zeolites are hydrated aluminosilicate materials that have a tetrahedral structure made of four oxygen atoms surrounding either aluminum or silicon cation. They are superior to other catalytic systems in many ways. They have the advantage of exhibiting or producing mesoporosity, which facilitates the diffusion of desired molecules inside their framework. They are known to be highly ordered microporous materials. They exhibit excellent ion-exchange capacity, which enables the use of various techniques to adjust their acid ratios, they possess good hydrothermal

stability, and the benefit of easy regeneration after thermal treatment. They also possess both Brønsted and Lewis acidity, which are necessary for lignocellulosic biomass degradation to value-added chemicals. Due to these qualities, they are highly sought-after in heterogeneous catalysis for the socio- and economically viable use of biomass for the synthesis of platform chemicals such as 5-hydroxymethylfurfural.

1.2. Research objectives and scope of work

This thesis aims to study the catalytic efficiency of zeolite catalysts namely, H-ZSM-5, H-Beta, and H-USY, for the conversion of glucose and cellulose into 5-hydroxymethylfurfural for industrial applications.

The objective is to prepare the modified forms of commercial zeolites for high-yield synthesis of HMF from glucose and cellulose. Furthermore, using the modified zeolite catalysts to investigate the effects of reaction conditions on glucose and cellulose conversion into HMF in a biphasic solvent system.

First, the post-synthesis of H-ZSM-5, H-Beta, and H-USY zeolites with different Si/Al mole ratios will be studied by acid dealumination and tin incorporation.

Second, the physicochemical properties of the catalysts will be characterized using Powder XRD, WDXRF, NH₃-TPD, Nitrogen Physisorption, Solid-state NMR, Py-FTIR, UV visible spectroscopy, and SEM.

Third, the optimum reaction conditions (catalyst loading, reaction temperature, reaction time, and substrate weight) will be investigated over the most effective catalyst(s).

Finally, the data will be analyzed, and the results will be concluded.

1.3. Thesis structure

The remaining chapters 2 to 7 discuss the development and utilization of zeolite catalysts, specifically the three selected zeolite samples (H-ZSM-5, H-Beta, and H-USY) for the catalytic conversion of glucose and cellulose into 5-hydroxymethylfurfural, detailing the new findings obtained from this work.

- ❖ Chapter 2 discusses zeolites as solid acid catalysts, their types, properties, structures, and utilization together with their synthesis and post-synthesis routes, and physiochemical characterizations. Furthermore, this chapter includes literature reviews of some of the works that have been done on glucose dehydration and cellulose hydrolysis to HMF utilizing zeolite catalysts.
- ❖ Chapter 3 contains the experimental work, materials, and chemicals used, procedures used in preparing and synthesizing the zeolite catalysts together with the techniques used for their characterizations.
- ❖ Chapters 4–6 detail the result and discussion of the new findings discovered from this study and the data obtained.
- ❖ Lastly, chapter 7 presents the conclusion drawn from this study and future recommendations on the new findings relevant to the aim of this research.

CHAPTER 2

THEORY AND LITERATURE REVIEW

2.1. Zeolites

In the year 1756, the word zeolite was first used by a Swedish researcher, Axel Fredrik Cronstedt, when a certain amount of steam was generated from a material during the process of fast rapid heating. The material was known to be stilbite. The release of the vapor was concluded to emanate from the adsorption of water that initially took place on the material. As a result of this observation, the mineralogist device the name zeolite, which originates from the Greek word “zeo” which means “to boil” and “lithos” which refers to “stone”. After the discovery by Axel, forty (40) other types of natural zeolites e.g., chabazite, clinoptilolite, natrolite, analcime, Phillipsite, etc. (**Table 2.1**). have been discovered, where most have low Si/Al mole ratios because of the absence of structure directing agents necessary for siliceous zeolites formation. More so, more than two hundred zeolites have been artificially synthesized because of these discoveries. Mordenite (MOR) and Clinoptilolite (HEU) are the two natural zeolites that have found application in industries. They find use in soil remediation, horticulture, and agronomy to ameliorate the physical and chemical properties of soil, they are used in treating effluents containing radioactive pollutants or as molecular sieves or other heavy metals. Naturally occurring zeolites can be utilized as catalysts but due to their high content of impurities and low surface areas, their catalytic activity is limited.

Table 2.1. Some natural zeolites and their properties.

Name	IZA code	Si/Al ratio	Channel size	Cations	Crystal shape
Chabazite	CHA	1.4 – 4.0	0.38	Na, K, Ca	Rhombohedral or triclinic
Clinoptilolite	HEU	4.0 – 5.7	0.31 x 0.75	Na, K, Ca	Monoclinic
Analcime	ANA	1.5 – 2.8	0.16 x 0.42	Na	Cubic
Phillipsite	PHI	1.1 – 3.3	0.38	Na, K, Ca	Monoclinic
Erionite	ERI	2.6-3.8	0.36 x 0.51	Na, K, Ca	Hexagonal
Ferrierite	FER	4.9 – 5.7	0.42 x 0.54	Ca	Orthorhombic
Laumontite	LAU	1.9 – 2.4	0.40 x 0.53	Na, K, Mg	Monoclinic
Mordenite	MOR	4.0 – 5.7	0.65 x 0.70	Na, K, Ca	Orthorhombic
Faujasite	FAU	1.0 – 2.8	0.74	Na, K, Mg	Cubic

The special nature of zeolite structures gave them unique attributes that are not commonly found in other materials. They possess excellent adsorption capacity for some target molecules, they can readily act as an ion exchanger, and due to their sizes and shapes, they can be used as molecular sieves for selective adsorption of some molecules.

Zeolite structure generally can be regarded as an inorganic polymer that originates from TO_4 tetrahedral units, where the T could be Al^{3+} or Si^{4+} and also P, Ge, Ti, B, Zn, Sn, etc. The two T atoms shared an oxygen atom that stands as a bridge between them.

2.1.1. Framework structure of zeolites

The zeolite framework's structure is mainly based on the two structural units (known as the primary building block) established by aluminum or silicon atoms and or other elements that are bonded to four O atoms. The primary building unit (PBUs) of zeolites has a tetrahedral structure while the secondary building units (SBUs) are composed of tetrahedral atoms arranged geometrically e.g., a polyhedral structure

such as hexagonal prisms, cubic or cuboctahedra structure. By repeating the secondary building blocks (SBUs), the structures can be formed and as a result, they are divided into different groups as shown below.



Figure 2.1. Zeolites' primary building unit (Left) and a typical chemical structure of zeolite (Right) [8].

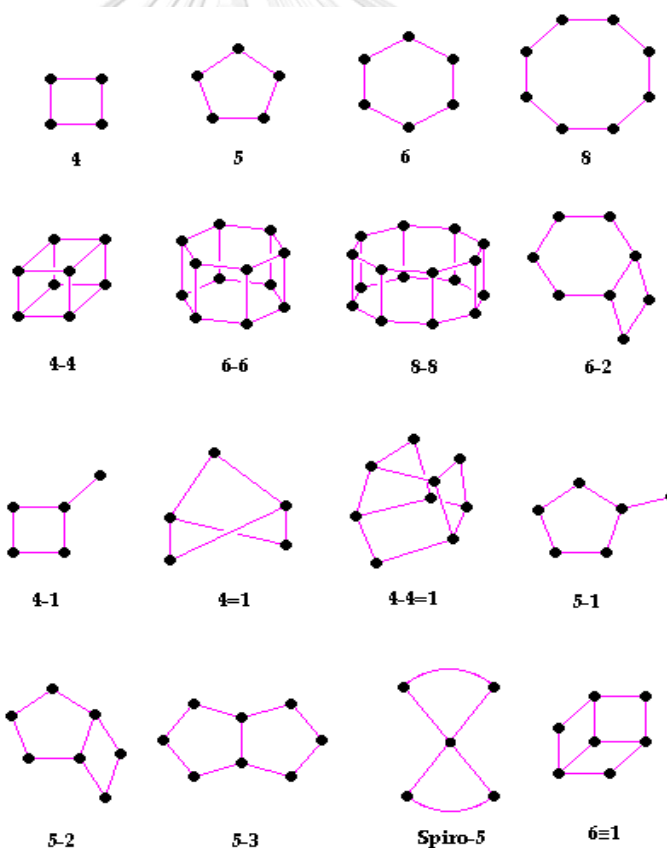


Figure 2.2. Zeolite's secondary building units. The black dots denote silicon or aluminum atoms while the colored line is the bridging oxygen atom [9].

Large numbers of secondary building units can be combined to develop the shape and structure of several different zeolites, frequently generating interconnected voids or cages. The International Zeolite Association's Structure Commission recognized 218 zeolite-type framework structures as existing as of March 2014, and they are identified by a three-capital letter code (IZA). Both the IZA website and the book by Baerlocher et al., edited by IZA and Elsevier, which is available online, provide a thorough description of the structure of each zeolite type and its code [10].

Zeolites, according to their pore system, can be roughly classified into three (3) different categories, namely.

✓ **Small pore zeolite:** Consists of channels bound by 8-member rings with a pore diameter of 4Å.

✓ **Medium pore zeolite:** Consists of channels bound by 10-member rings with a pore diameter range of 5-6Å.

✓ **Large pore zeolite:** Consists of channels bound by 12 or more member rings with a pore diameter of 7Å and or above.

The results of some common zeolite framework types and their properties according to the International Zeolite Association (IZA) are shown in **Table 2.2**.

Table 2.2. Some common zeolite types and properties

Name	IZA code	T-member Ring	Diameter of Cage (Å)	Dimension of Channels	Diameter of Channels (Å)
Clinoptilolite	HEU	8 and 10	-	2D	3.6 x 4.6, 2.8 x 4.7, 3.1 x 7.5
Erionite	ERI	8	15.1 x 6.3	1D	3.6 x 5.2
Chabazite	CHA	8	9.4	3D	3.8 x 3.8
Ferrierite	FER	8 and 10	8.3	2D	3.5 x 4.8, 0.4 x 4.2
Mordenite	MOR	12 (12 and 8)	2.6 x 5.7	1D (2D)	6.5 x 7.0 (2.6 x 5.7)
Faujasite (Linde X and Y)	FAU	12-rings	12x 12 x 12	3D	7.4 x 7.4
ZSM-5	MFI	10	8.6	3D	5.1 x 5.5, 5.3 x 5.6
ZSM-12	MTW	12	-	1D	5.6 x 6.0
ZSM-22	TON	10	-	1D	4.6 x 5.7
ZSM-23	MTT	10	-	1D	4.5 x 5.2
ZSM-48	*MRE	10	-	1D	5.6 x 5.3
MCM-22	MWW	10 + large cages	7.0 x 7.0 x 18.7	2D	4.0 x 5.5, 4.1 x 5.1
Beta	*BEA	12 and 12	13.9	3D	5.6 x 5.6, 6.6 x 6.7
Omega	MAZ	12 and 8	-	1D	3.1 x 31, 7.4 x 7.4
Linde A	LTA	8	13	3D	4.0 x 4.0
Linde L	LTL	12	-	1D	7.1 x 7.1

The ratio of silicon to aluminum atoms in the framework is frequently used to describe the elemental composition of zeolites. Due to charge limitations, AlO_4 tetrahedra PBUs naturally tend to avoid one another. As a result, the minimal Si: Al ratio that can occur in zeolites is 1: 1, which is found in structures where SiO_4 and AlO_4 are present in different ways. The behavior is referred to as Loewenstein's Rule [11]. The same criterion does not hold for silicon, hence zeolites with high Si: Al ratios are frequently seen.

The aluminum atom becomes negatively charged whereas the silicon atom remains neutral when silicon and aluminum atoms are covalently bound to four oxygen atoms. The presence of non-framework cations balances the overall negative charge that the

inclusion of aluminum in the framework causes to the zeolite crystal lattice. These cations, which are present with absorbed water molecules and are free to permeate through the pores and may be exchangeable under specific circumstances, are generally alkali metal or alkaline earth metal ions. The unit-cell formula can be used to explain the zeolite's final composition, which is represented as $M_x/n [(AlO_2)_x(SiO_2)_y] \cdot zH_2O$, where M represents an alkaline-earth or alkali cation, x and y denotes the total tetrahedral unit cell number, n is the cation's valency, and z represents the number of moles of water per unit cell and it's specifically based on their crystallographic unit cell.

As shown in **Figure 2.3**, Brønsted acid sites are created close to Si-O-Al clusters by exchanging the cations for protons (hydrogen atoms). These locations may serve as active catalytic sites with shape selectivity for a variety of acidic processes. Lewis acid sites, a different sort of acid site, can also arise because of lattice defects and the presence of extraframework aluminum. The creation or neutralization of such sites on the original catalyst might be further promoted during post-synthesis processes like steaming, which increases shape selectivity [12,13]. Zeolites are excellent candidates to take the role of traditional mineral acids in industrial applications because of the abundance of these active sites within the zeolite's pores.

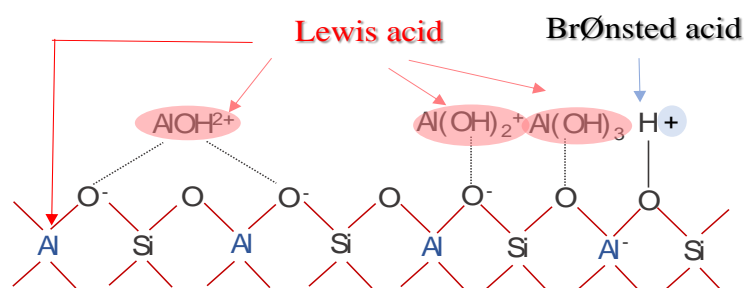


Figure 2.3. Brønsted and Lewis acid centers in protonic zeolite.

2.2. Properties of zeolites

Zeolites exhibit remarkable properties which make them unique in various chemical synthesis. Some of these properties include:

Adsorption capacity: They possess remarkable adsorption capacities as a result of their high surface area and excellent selective adsorption characteristics. Their pore structure can accommodate wide variety of molecules, including ions, liquid, and gases. Their adsorption capability can be adjusted by varying the size of the channels and cavities, allowing for specific applications in fields such as gas separation, water purification, and pollutant removal.

Porosity: They are highly porous materials with a high surface area. Their structural framework is made up of molecularly sized pores and cavities that give a large specific surface area for adsorption and catalytic processes. Because of their porosity, zeolites may selectively trap and release molecules based on their size and shape.

Molecular sieving: Zeolites' regular and well-defined pore structure allows for molecular sieving ability. They have the ability to selectively adsorb molecules based on their size and shape, allowing smaller molecules to enter while excluding bigger ones. This property is very beneficial in separation processes and catalysts because zeolites can distinguish between molecules of comparable size.

Ion exchange: Ion exchange capacity is the ability of zeolites to exchange ions inside their structure. This feature is owing to the presence of exchangeable cations inside the zeolite framework, often sodium (Na^+), potassium (K^+), or calcium (Ca^{2+}) or magnesium (Mg^{2+}). These cations can be replaced by other ions in a solution,

allowing them to be used in water softening, wastewater treatment, and selective ion removal.

Catalytic activity: Because of their unique features, zeolites are commonly utilized as catalysts. The constricted spaces within the zeolite structure, in combination with its ion-exchange and molecular sieving characteristics, provide an excellent environment for catalytic processes. The inclusion of particular cations within the framework can also improve zeolites' catalytic activity. They are used in a variety of activities, including petrochemical refining, organic synthesis, and environmental remediation.

Selectivity: In a variety of applications, zeolites demonstrate remarkable selectivity. During synthesis, their pore size and shape can be adjusted to match certain target molecules, allowing for precise separations and reactions. This selectivity is critical in industries such as gas separation, petroleum refining, and the manufacturing of specialty compounds.

Thermal stability: Zeolites have unique thermal stability, making them ideal for high-temperature applications. The zeolite framework's strong covalent connections between aluminum, silicon, and oxygen atoms contribute to its structural integrity even at high temperatures. Because of their stability, zeolites can be used as catalysts in a variety of high-temperature industrial processes.

These properties make them highly valuable materials in a variety of applications, such as adsorbents, catalysts, ion exchangers, and molecular sieves. The nature and properties of some zeolites such as the ones used in this work are discussed below.

2.2.1. Nature and properties of some specific zeolites

The protonic form of zeolites is usually generated from parent zeolites using various synthesis processes and or post-treatments, to improve their stability and catalytic activity. For instance, H-USY zeolite, commonly known as the proton form of ultra-stable Y zeolite is generated from the HY zeolite (FAU framework type) via hydrothermal treatment of H-Y zeolite, H-ZSM-5 zeolite is created from cation form-ZSM-5 zeolite with MFI framework-type by cation exchange. H-Beta zeolite is also generated by cation exchange from cation form of Beta zeolite with BEA framework type etc. The properties and nature of some zeolites such as the ones described above and used in this project are summarized in **Table 2.3**.

Table 2.3. Nature and properties of some specific zeolites

Properties	Zeolite		
	H-USY	H-ZSM-5	H-Beta
Structure	Has a 3D framework consisting of 12-membered rings with large supercages, interconnected channels, and pore size of 0.90 nm.	Has a 3D framework consisting of a 10-membered ring with one-dimensional channels with a pore size of about 0.56-0.58 nm, giving it a narrow and uniform pore structure.	Has a 3D framework consisting of a 12-membered ring with a large pore size of 0.65 nm.
SiO ₂ /Al ₂ O ₃ ratio	Silica/alumina ratio is very low. Possesses a high content of aluminum in its framework.	High silica-to-alumina (Si/Al) ratio. Moderate content of aluminum in its framework.	Typically has a high silicon-to-aluminum (Si/Al) ratio.
Acidic properties	Exhibit strongest acidity in the presence of framework and extraframework aluminum atoms. Exhibits high Lewis acidity.	Possess strong acidity. Exhibit moderate-to-high Brønsted acidity.	Possess strong acidity. Exhibit high Brønsted acidity.
Hydrothermal stability	Good hydrothermal stability.	Good hydrothermal stability.	Good hydrothermal stability.
Surface area	Possess high surface area due to extensive network of pores and channels.	High specific surface due to its intricate pore network and channels.	Possesses a high specific surface area.
Shape selectivity	High shape selective ability.	Excellent shape selectivity. Its narrowed pore structure allows the diffusion and adsorption of small to medium-sized molecules while restricting the entry of larger molecules.	Has a notable characteristic of shape selectivity.
Ion exchange capacity	Possess a high ion-exchange ability that allows cation exchange within its framework	High ion exchange capacity	High ion exchange capacity

2.3. Applications of zeolites

Zeolites find application in various fields, such as science, engineering, and environments, etc., however, their applications vary depending on the properties with which they are needed, and a clear difference must be made between synthetic zeolites which are synthesized for specific applications under well-controlled conditions and natural zeolites that are extracted in every part of the world.

Synthetic zeolites find use in industries as catalysts, desiccants, gas separation and storage, ion exchange and softeners, detergents, solar energy storage, and many more while natural zeolites due to their reduced cost are mostly used in mineral applications, building materials, in agriculture as a soil treatment, as filter additives in aquaria, and many more [9,14,15].

2.3.1. Zeolites' application in catalysis

Zeolites have proven to be an effective catalyst for so many applications due to their numerous advantages over other catalytic systems. The major advantages over other catalytic systems include.

- » They possess excellent catalytic properties e.g., high surface area and pore volumes.
- » Their acidity can be easily tuned through different processes e.g., dealumination, metal incorporation, ion exchange, etc.
- » They are thermally and hydrothermally stable under elevated conditions e.g., temperature.
- » They are favorable for reactions at lower and higher temperatures.
- » They are selective for specific products.
- » They have a unique pore structure.

- » They exhibit high ion-exchange capacity.
- » They can be easily regenerated upon thermal treatment.
- » They are highly ordered material with good shape selectivity.
- » They can act as a bifunctional catalyst depending on their synthesis mode.
- » They are easy to handle, do not oxidize, are non-toxic, and are safe to store for a long time.

Zeolites catalysis can be classified into three different categories.

- (i) Organic reactions e.g., cyclohexane (oxidation, aromatization, ring opening, isomerization), Aromatization of C₄ hydrocarbons, alkylation reaction (naphthalene, benzene, ethylbenzene, polyaromatics, biphenyl, aniline, etc.), aromatics (oxidation, hydrogenation, nitration, hydroalkylation, disproportionation, oxyhalogenation, hydroxylation, etc.
- (ii) Inorganic reaction e.g., water splitting, oxidation, and reduction of CO, NO reduction of ammonia
- (iii) Hydrocarbon conversion e.g., cracking, Friedel-craft alkylation, dehydrogenation, Fischer-Tropsch synthesis, hydrocracking, hydrogenation, alkylation, dehydration, hydrodealkylation, methanation, shape-selective reforming, isomerization, methanol to gasoline, etc.

2.3.2. Acidity of zeolites

The metal cations or hydroxyl protons on zeolites' extra-framework are what give them their acidic nature. The +4 charges on the framework silicon atoms at tetrahedral positions (T position) and the -2 charges on the coordinating oxygen atoms in aluminosilicate-type zeolites result in neutral SiO₄ tetrahedra. When silicon atoms in the framework are replaced with aluminum atoms, the matching tetrahedra's charges can be changed from neutral to 1. The extra-framework metal cations or hydroxyl protons balance these negative framework charges by generating weak Lewis acid

sites or strong Brønsted acid sites, respectively, which are responsible for the zeolite materials' catalytic activity.

The first class of hydroxyl protons is those found on oxygen bridges that connect the silicon and aluminum atoms in the framework. These hydroxyl groups, also known as Si-OH-Al, are frequently donated to structural or bridging OH groups (**Figure 2.4a**). The silanol groups Si-OH, also known as terminal OH groups, are found on the outside of crystal particles and are the second most significant form of hydroxyl groups in zeolites (**Figure 2.4a**). The main cause of the creation of these silanol groups is the dealumination of the zeolite structure through calcination, hydrothermal treatment, or treatment with strong acids. Depending on the treatment circumstances, aluminum extra-framework may experience silicon migration, silanol group formation, and hydroxyl group production (**Figure 2.4c**).

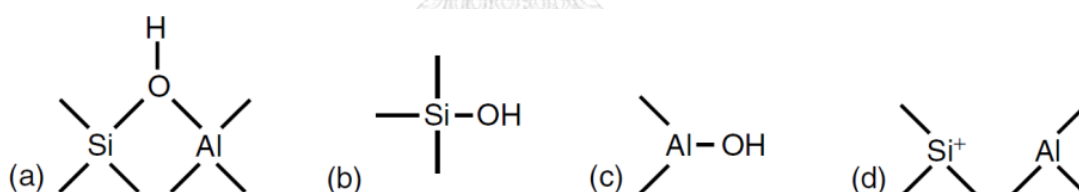


Figure 2.4. Different kinds of acid sites and hydroxyl groups in zeolites. (a) Si-OH-Al group (b) silanol group, Si-OH (c) Al-OH group, and (d) extraframework species [15]



Figure 2.5. Framework aluminum species (Left) and non-framework aluminum species (Right) in zeolite [15].

2.3.3. Zeolites synthesis

Zeolites are commonly synthesized commercially via two major methods to make them available in their pure form, be reproducible, have a uniform pore size and channels, and to be able to be post-synthesized according to their specific needs:

- ❖ The synthesis from gels
- ❖ The synthesis from silicate materials.

They utilize a wide variety of silica and aluminum sources, and the cation can be one or more alkali metal cations, an alkaline earth cation, or an organic cation in certain unique configurations. The same zeolite with various silica-alumina ratios can be synthesized by changing the concentration of specific chemicals. The chemical sources of zeolite synthesis and their functions are summarized in **Table 2.4**.

Table 2.4. Chemical sources of zeolite synthesis and their functions [24,25].

Sources	Function
AlO_2^-	Origin of the charge in the framework
SiO_2	PBU(s) of zeolite framework
OH^-	Guest molecule, mineralizer
Water	Guest molecule, solvent
Alkaline cations/template*	Guest molecule, counter-ion for AlO_2^-

*Categorized as organic or inorganic templates. Organic cations assist in the nucleation of zeolite as an additional template while the inorganic cations are mostly provided by alkali metals or alkaline earth hydroxides, and they mostly produced Al-rich zeolites.

The templates are also known as structure directing agents (SDA) and they serve as molecularly scaled scaffolds necessary for the presence of specific structures. These fall into the freshly formed pores and encourage the development of distinctive structures. A zeolite with big pores is frequently formed when a large template is used. A template-removing phase is necessary after the zeolite has been created. The x-ray diffraction patterns of some zeolite are shown in **Figure 2.6**.

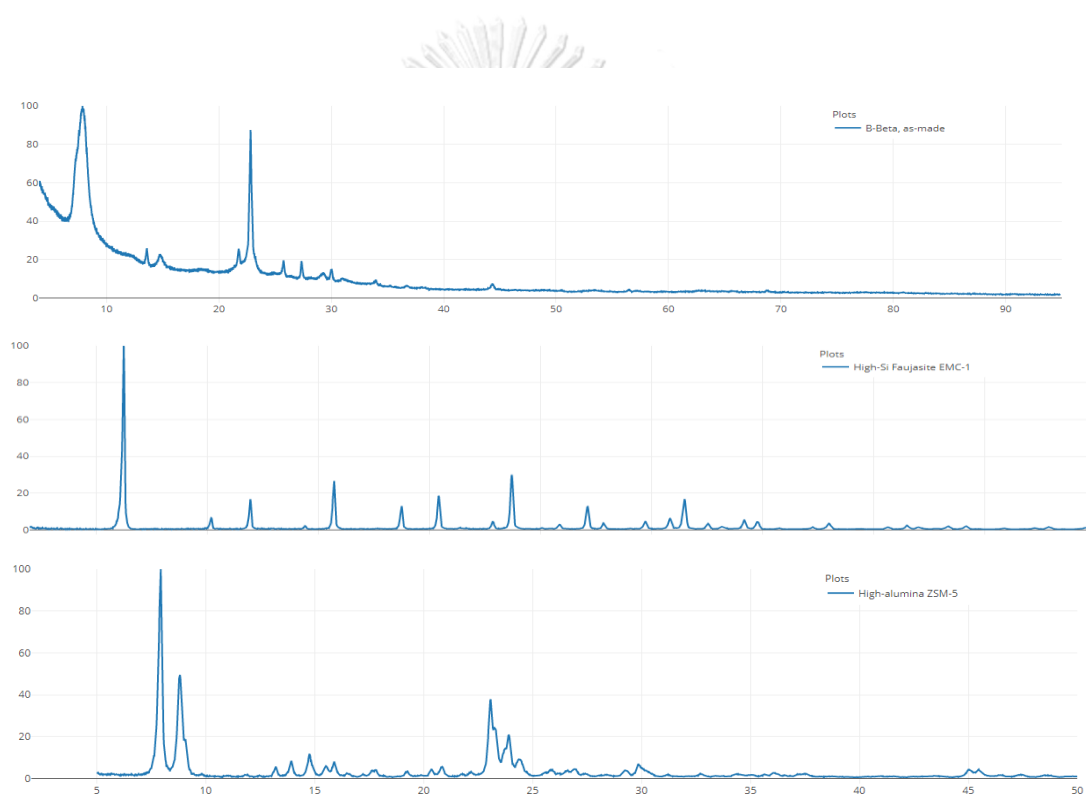


Figure 2.6. X-ray diffraction patterns of some zeolites [25].

2.3.4. Post-synthesis/modification of zeolites

Zeolite can be post-synthesized through numerous techniques to adjust its operational efficiencies and or properties. Some of these techniques include steaming or hydrothermal treatment, dealumination techniques, cation, or ion exchange processes.

2.3.4.1. Dealumination of zeolites

Dealumination is a post-synthesis technique that is used in removing some portions or parts of the framework and or extraframework aluminum atoms from the zeolite network, thus increasing the silica-alumina ratio of the zeolite. This technique, however, may not necessarily remove the aluminum atoms in the zeolite, as portions of aluminum might be present as amorphous extraframework forms in the channels, cages, pores, or aggregates on the surface of the zeolite crystals. This technique is often used for synthetic zeolites that cannot be synthesized in high silica-aluminum ratio [9,27,28].

This technique is often used to:

- ❖ Increase accessibility to Brønsted acid sites and acid strength.
- ❖ Create Lewis acid sites in the zeolite framework and or extraframework.
- ❖ Increase hydrophobicity of zeolites.
- ❖ Create secondary channel systems e.g., mesopores to enhance diffusion limitations.

The most often used dealumination techniques are:

- Steaming or hydrothermal treatment
- Acid-leaching technique

Dealumination is frequently followed by a further structural rearrangement stage in which the defect sites are filled with silica and the integrity of the structure is restored, producing a very stable and silicious framework [29]. **Figures 2.7** and **2.8** demonstrate the two steps that cause the zeolites to become more stable, with the first

demonstrating the dealumination step caused by high temperatures in the presence of steam and the latter showing the framework stabilization.

To explain the structural rearrangement that occurs, three mechanisms have been proposed.

- ❖ As postulated by Barrer [30], the elimination of the water close to the hydroxyl nests established by the loss of aluminum atoms causes a new Si-O-Si to be formed.
- ❖ According to Meher et al.'s [31], the silica that fills the defect sites comes from the crystal framework's fragments that collapsed as a result of the treatment's severity. Under steam and high temperature, the silica will migrate to the defect sites and take the place of the removed aluminum atom, rearranging the framework.
- ❖ According to Von Ballmoos [32], the created vacancies slowly migrate to the external structure and would be filled by a T-atom in the vicinity (where T is an aluminum or silicon atom). This process is referred to as T-jump. The zeolite framework is restored when this process occurs multiple times.

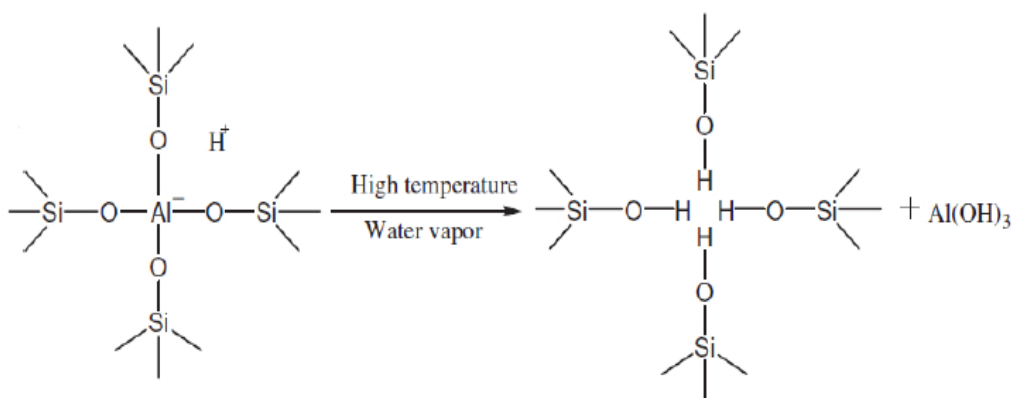


Figure 2.7. Dealumination steps caused by steam at high temperature [33].

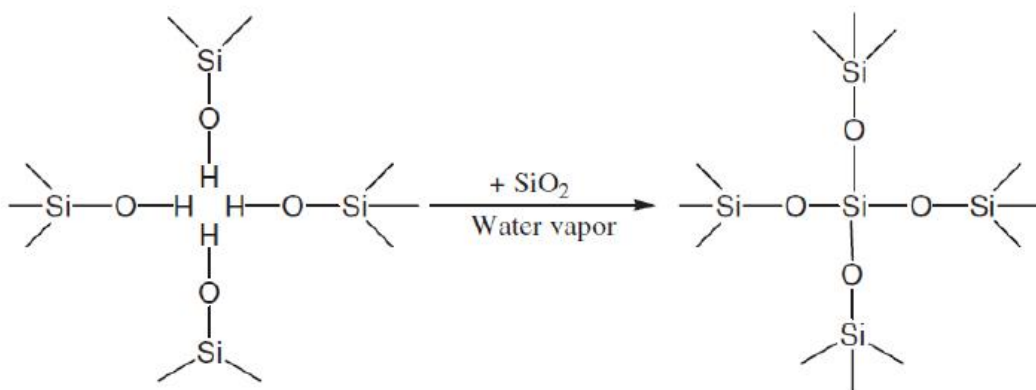


Figure 2.8. Stabilization of zeolite framework induced by silica [33].

Steaming or hydrothermal treatment: This technique involves the use of steam or water vapor at high temperatures to bring about the dealumination of zeolites. During steaming at high temperatures, the Si-O-Al bonds undergo hydrolysis and lead to the removal of aluminum in the framework or non-framework sites. The produced non-framework or extra-framework aluminum can be neutral or catalytically active in the form of Lewis acids, and it can exist within the pores or on the crystal's surface. Using hydrothermal treatment can result in up to 50% dealumination [34]. This technique shapes the cationic non-framework aluminum and produces defect sites by hydrolyzing the Al-O bonds. When silicon atoms fill the defect sites, the zeolite framework stabilizes, which leads to a higher silicon fraction being incorporated into the zeolite framework. A loss in crystallinity is typically associated with this process because silica species fill up these defect sites more slowly than the rate of aluminum species removal from the framework [35]. Because framework stabilization cannot be initiated in the beginning, a predominant collapse of the structure occurs, with the effect being much more pronounced in aluminum-rich areas [35].

Steaming or hydrothermal treatment of Y-type zeolite: Steaming or hydrothermal treatment is majorly used in transforming Y-type zeolite to its ultra-stable form (USY) in the petrochemical industry. The proton form of USY zeolite could be generated either by subjecting HY zeolite to hydrothermal treatment or directly from its ammonium form after deammoniation. The USY zeolite form has a much lower unit cell volume than the H-form due to the structure's propensity to shrink. The mechanism of steaming or hydrothermal treatment in transforming ammonium form of Y-type zeolite to H-USY zeolite is shown in **Figure 2.9**.

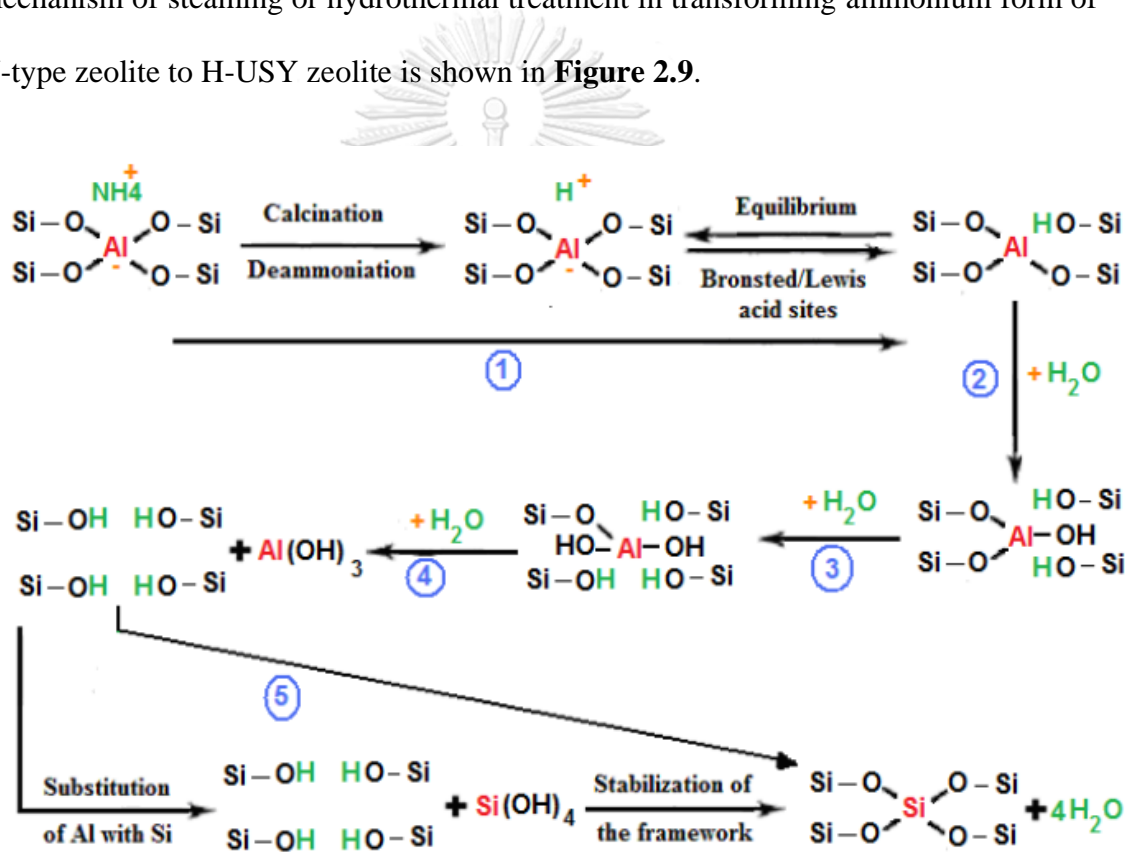


Figure 2.9. Mechanism of steam treatment of ammonium form of Y-zeolite. (1) Transformation of ammonium form to H-form (2 – 4) influence of water vapor during steaming or hydrothermal treatment (5) stabilization of the framework with silicon atoms [35]

In the steaming process, the removed aluminum atoms remain as extra-framework aluminum species inside the zeolite structure, where they may break hydroxyl bridges and lead to the creation of Lewis acid sites. While the extraframework species that form during the steaming process can block zeolite surface pore openings and potentially cause catalyst deactivation, this problem can be easily solved by additional treatment with an acid solution to remove these partially linked extraframework species from the zeolite structure.

Acid leaching technique: This technique involves the removal of aluminum atoms in the framework and or extraframework sites by using mineral acids such as nitric acid (HNO_3), hydrochloric acid (HCl), oxalic acid ($\text{H}_2\text{C}_2\text{O}_4$), tartaric acid, etc. The most used mineral acid is oxalic acid due to its ability to form stable complexes with aluminum and most metal ions. Due to its small size, it easily diffuses through and enters the zeolites' structure, where it removes aluminum from the crystal lattice effectively. A complex of aluminum ions with several water ligands and one oxalate ion is formed and can be easily removed [36]. This procedure is frequently carried out at room temperature.

Barrer and Makki proposed that the first step was the substitution of the aluminum ion with the hydronium ion, H_3O^+ , in a strong acid solution, such as HCl , followed by the removal of Al^{3+} and H_3O^+ to create the hydroxyl nest during hydrolysis, as shown in **Figure 2.10**. This process, after the extraction of aluminum from the silicate matrix, results in the generation of hydroxyl nests through the zeolite framework.

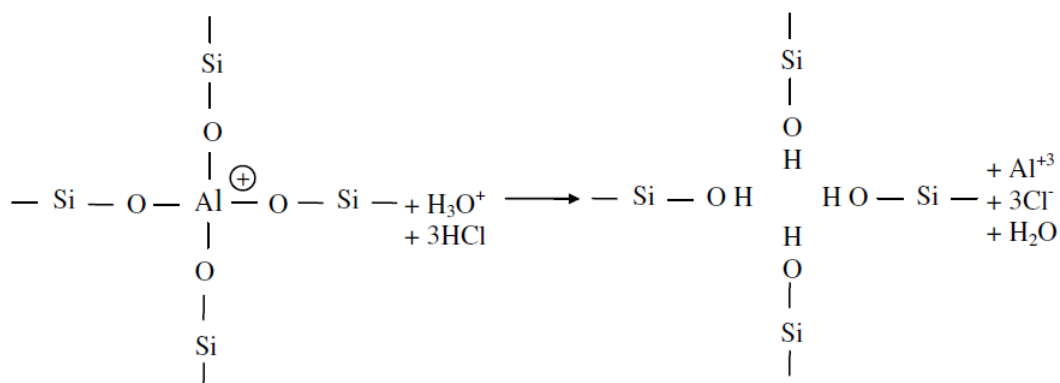


Figure 2.10. Framework's aluminum atom extraction using acid treatment [25]

The removal of neighboring aluminum ions from the zeolite's framework and replacement with silicon atoms, which introduces mesopores into the structure and enhances porosity, is the acid treatment's greatest advantage.

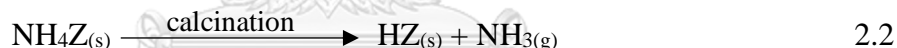
The two processes are being utilized in the chemical industry to enhance and increase the catalytic performance of zeolites for specific applications. Examples of such zeolites are mordenite for the paraffin hydroisomerization process, zeolite Y or FAU to generate ultra-stable zeolite Y (USY zeolite) [37], and MFI, which is used for octane boosting in the FCC process[38].

2.3.4.2. Ion or cation exchange process

To neutralize the overall negative charge caused by the presence of aluminum inside the framework, cations are necessary within the pores of zeolites. These cations can be incorporated into the zeolite framework during their synthesis or formation and may be positively charged organic molecules that serve as structure-directing scaffolds often known as templates, or alkali metals or alkaline earth metals [39]. The cations are free to diffuse through the structure if the size of the pores permits it and are capable of

diffusing into or out of the zeolite under specific conditions. The presence of the cations neutralizes the acid sites necessary for the zeolite's catalytic activity, hence the cations must be removed and replaced by protons in order to use the zeolite as a catalyst. The zeolite can create Brønsted or Lewis acid sites inside the structure by undergoing an ion exchange process in which the cations are exchanged for protons.

Treatments involving ion exchange often involve the use of ammonium salts with a high concentration, such as ammonium nitrate, in an aqueous solution. Ammonium nitrate can diffuse through the zeolite's structure and take the place of the existing cation. After the treatment, the protonated acid site is left behind and the ammonia is released during the calcination process. These two processes, in which sodium is exchanged for a proton [28], are shown in equations 2.1 and 2.2.



When the template is too large to easily diffuse through the pores of the zeolite during the ion exchange treatment, a Detemplation process prior to ion exchange may be necessary. Direct exchange with a mineral acid like HCl is an alternate technique. However, this procedure has the potential to cause dealumination of the framework, partial loss of its crystal structure, or possibly collapse completely.

2.3.4.3. Detemplation technique

Zeolites such as ZSM-5, USY, and Beta during their syntheses involve the use of templating agent otherwise called a structure-directing agent to coordinate and direct silica and alumina groups. These templates after their syntheses may block the pores

and accessibility to acid sites within the zeolite network or channels if present. Thus, it is imperative to remove the templates, and can be done via calcination, the Fenton process, or by using pyrolysis.

Calcination: This is the most widely used procedure for removing organic molecules or deposits within the channels of zeolite. It involves progressively heating the zeolite to a temperature until the organic template oxidizes and is transformed into CO₂ and steam. Typical heating rates between 1 and 10 °C/min and temperatures between 500 and 700 °C are commonly employed. The formation of water in the form of steam, which can cause localized dealumination of the framework and damage to the structure when combined with high temperatures, is one of the disadvantages of calcination. For instance, after the calcination step of some synthetic zeolites such as Beta zeolite, the fragile structures may partially or completely collapse [40].

According to He et al. [41], calcination successfully removes Beta zeolite's template, but at the expense of a 25–30% crystallinity loss. Furthermore, Corma et al.[42] discovered that high-temperature calcination during detemplation led to the removal of aluminum and other hetero-atoms from the structure, which had a negative impact on the surface acidity and the catalytic performance.

Fenton Process: This process involves the use of hydrogen peroxide (H₂O₂) which results in the formation of a catalytic amount of Fe or OH radicals that chemically oxidizes the templates at a lower temperature (< 80 °C). This process results in larger micropore, and mesopore volumes and a high Brønsted acid density while maintaining the structure when compared to samples detemplated by the calcination technique [9,43].

Pyrolysis: Like calcination, pyrolysis also requires high temperatures to break down the template, but it is performed in the absence of oxygen. As a result, the template is converted to coke instead of oxidizing. The coke may increase the zeolite's hydrophobicity, which will increase its affinity for organic molecules that are hydrophobic and may also cause a partial blockage of the pores and acid sites.

2.3.4.4. Desilication

This post-synthesis technique is usually done to selectively remove silicon atoms (secondary building units) from zeolite to enhance mesoporosity in a microporous zeolite system [44], with additional improvement in the diffusivity (mass transport) during the catalytic reaction process, seen as a function of pore size of catalyst [45]. This technique is seen to be particularly attractive and often applied to silicon-rich zeolites such as ZSM-5. An interconnected network of micropores and mesopores may be created by dissolving silicon atoms in an aqueous alkaline solution such as NaOH or Na₂CO₃. This technique ensures that the Si-O-Al bond hydrolysis in the presence of OH⁻ ions proceeds more slowly than the Si-O-Si bond cleavage in the absence of negatively charged AlO₄⁻ tetrahedra. As demonstrated in **Figure 2.11**, only small fractions of the surrounding Si-atoms can be dissolved because an increase in the number of neighboring aluminum ions in the framework stabilizes them.

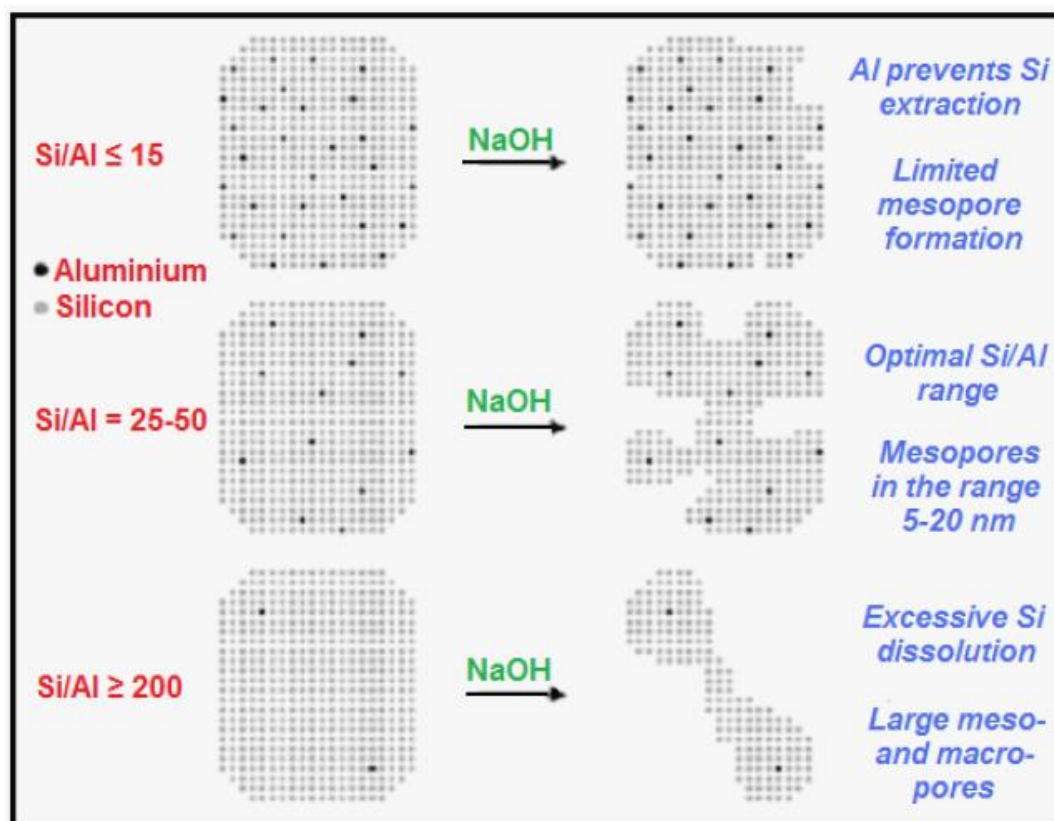


Figure 2.11. Diagrammatic illustration of the influence of desilication technique on aluminum content of MFI zeolite (ZSM-5) in NaOH solution [46].

A successive combination of treatments, such as desilication-dealumination or dealumination-desilication, is of great importance in catalyst design and optimization since they aid in the dissolution of amorphous silica from zeolites. **Figure 2.12** provides a general explanation of how dealumination and desilication approaches can be compared.

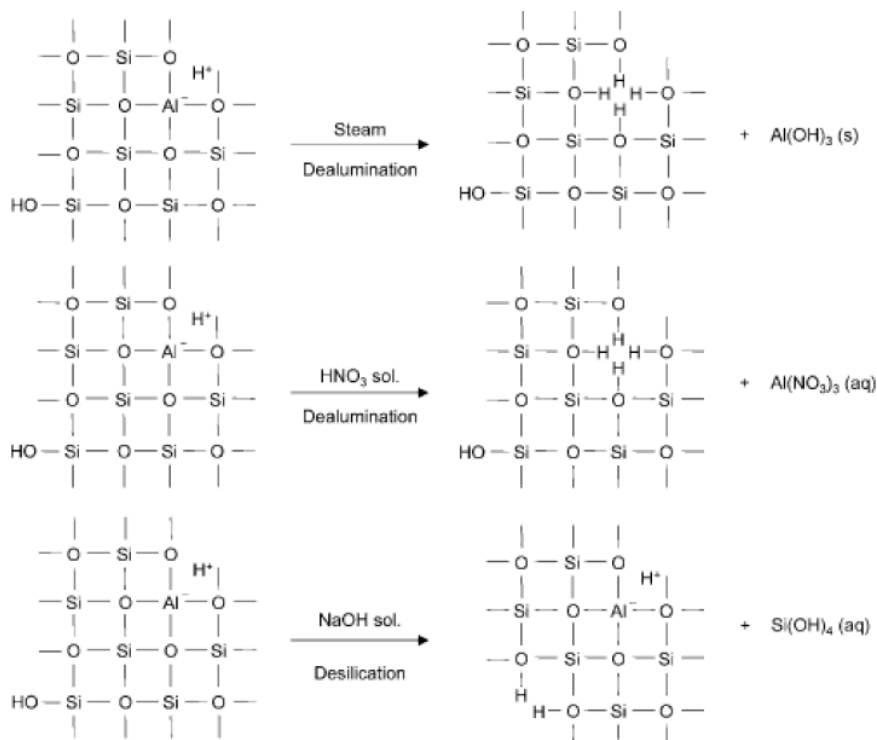


Figure 2.12. Diagrammatic illustration of post-synthesis techniques for creating mesoporosity in zeolite structure: Effect of dealumination by steaming or acid treatment and desilication by base treatment [47].

2.4. Characterization of zeolites and analytical techniques

As a result of the complex properties of various synthetic zeolites, it is imperative to characterize their properties to effectively assess the structural attributes and their interactions with other molecules. The information from these characterizations is crucial in heterogeneous catalysis to obtain the relationship between their physicochemical properties such as structure and morphology of the zeolite material, adsorption ability, chemical composition, and catalytic properties. Some of the characterization techniques used for zeolite are summarized in **Table 2.5**

Table 2.5. Some analytical techniques used for zeolite characterization.

Technique	Acronym	Functional Groups	Chemical Composition	Pore size	Structure	Coordination state
X-ray diffraction	XRD		√		√	
X-ray fluorescence	XRF		√			
Nitrogen physisorption		√		√		
Nuclear magnetic resonance (Magic angle spinning)	MAS NMR	√	√			
Electron microscopy	FE-SEM HRTEM EDX		√	√	√	
Temperature-programmed desorption	NH ₃ -TPD	√	√			
Fourier-transform infrared Spectroscopy (pyridine adsorption)	FTIR Py-FTIR	√	√			
Ultraviolet-visible spectroscopy	UV-vis				√	√
Thermogravimetry, Differential scanning calorimetry	TGA/DSC	√	√	√		
Vibrational spectroscopy		√	√	√	√	
X-ray absorption spectroscopy	XAS		√		√	
X-ray photoelectron spectroscopy	XPS	√	√			

2.5. Synthesis of 5-hydroxymethylfurfural from lignocellulosic biomass

5-Hydroxymethylfurfural (HMF) is a versatile platform chemical that is directly produced from C₆ monosaccharide fructose by acid-catalyzed dehydration. It can also be synthesized in varying yields from a variety of monomeric C₆ sugars such as glucose or by successive hydrolysis/dehydration of polysaccharides, including cellulose. Its potential lies in its ability to reduce our reliance on fossil-derived compounds, providing a green alternative to the petrochemical-based industry if available in large quantities. HMF, on the other hand, is currently unable to compete with conventional compounds due to the high costs associated with both its production and the starting materials.

HMF has the potential to be used as a general base chemical to derive several useful diverse compounds. This has the potential to transform the chemical industry by introducing new families of renewable molecules. A variety of value-added compounds derived from HMF are represented in **Figure 1.2** (in Chapter 1) amongst others may include:

- ❖ **Polymers:** 2,5-furandicarboxylic acid produced from HMF has the potential to be used as a monomer to produce a furan-based polymer. A suitable replacement for terephthalic acid in the production of polyesters, polyamides, and polyurethanes [48]. 3,5-dihydroxymethylfuran derived from HMF has found application on an industrial scale to produce polyurethane foams [49].
- ❖ **Biofuels:** 2,5-dimethylfuran produced from HMF finds application as biofuel or biofuel additive, with 40% energy density higher than that of ethanol and gasoline [50,51].

- ❖ Pharmaceuticals: Compounds derived from HMF can be modified further to produce bio-active molecules with good medicinal properties.
- ❖ Other value-added products: Levulinic acid produced from HMF serves as a potential precursor to nylon-like polymers, plastics, and synthetic rubber [52].

Due to numerous applications involved with HMF as a sustainable and renewable platform, a lot of researchers have been exploring various methods to synthesize this product in large quantities.

Following the mechanism proposed by Antal et al [53] in 1990, where HMF could be easily produced through the dehydration of D-fructose using an acid catalyst, the mechanism involving one-pot glucose conversion to HMF was proposed [54]. Zhao et al proposed that HMF can be directly produced from glucose via two reaction pathways. First, glucose under isomerization reaction to fructose, and the formed fructose is dehydrated to HMF. This opens the door to numerous research where glucose can be directly utilized for HMF synthesis using an acid catalyst. Glucose is an abundant feedstock that is less competitive in the food industry when compared to fructose as a source for HMF production.

2.5.1. Dehydration of glucose to HMF

HMF can be directly obtained from hexose sugars such as glucose and fructose, through isomerization and dehydration reactions steps. The mechanism of glucose dehydration to HMF was explained by Zhao and co-workers in an ionic liquid-catalyst system, as shown in **Figure 2.13** [54]. He proposed that the dehydration of glucose to HMF mainly occurs via isomerization and dehydration steps with the formation of some reaction intermediates. Although Zhao and coworkers'

discovery was based on an ionic liquid-catalyst system, since then a vast number of researchers have tested numerous homogeneous and heterogeneous acid catalysts with the aim of finding an efficient and effective way for HMF production. This has resulted in vast numbers of reported articles and reviews related to HMF production in the last 20 years.

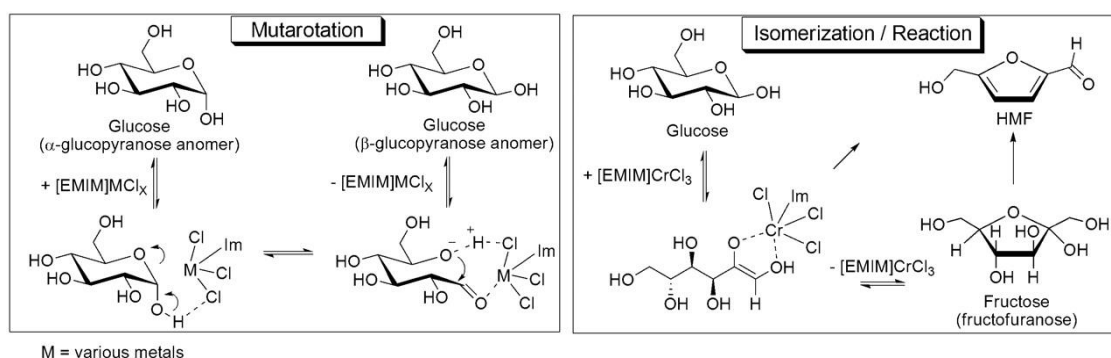


Figure 2.13. Mechanism of HMF production from glucose in ionic liquid-catalyst system [54].

The presence of an acid catalyst promotes the dehydration reaction, and various catalysts have been tested with varying degrees of success. Effective comparative studies on the kinetics of different catalysts are, however, hindered by the diverse range of reaction conditions used by the various research groups. Furthermore, in most reported studies, HMF was obtained in solution and the yield was determined using HPLC or GC, with the emphasis of the research being on optimizing the synthesis and the catalyst used. However, developing effective isolation or extraction methods is equally important.

The yield and effectiveness of the reaction of glucose to HMF are influenced by the following factors:

- ❖ **Starting material or substrate:** Various sources of biomass such as fructose, glucose, sucrose, inulin, galactose, cellobiose amongst others for HMF production have been studied with glucose and cellulose currently being sought after.
- ❖ **Catalyst:** Several catalysts have been used for HMF synthesis from the literature. Recently, bifunctional catalysts have been developed and have been on the increase to induce Lewis and Brønsted acid sites in a single catalyst for the synthesis of HMF. Various catalysts used are summarized as follows:
- Mineral acids such as HCl, H₃PO₄, H₂SO₄ [50,55-57, 59]
 - Organic acids such as levulinic and oxalic acid [56]
 - Transition metals [54,58,59,62]
 - Metal chlorides, sulfates and phosphates [54, 60,61,63]
 - Acidic resins [50,57]
 - Protonic zeolites [64-68]
 - Heteropolyacid salts [69]
- ❖ **Reaction temperature and time:** The conversion of glucose and yield of HMF is strongly correlated to the reaction temperature and time used. The reaction temperature and time control the reactivity of the starting material within the practical limit of catalyst concentration. Higher temperatures may promote higher yields and selectivity of HMF.
- ❖ **Solvent system:** The solvent system promotes the contact between the substrate and the catalyst while inducing fluidity at the same time. One of the most used solvents is water as it acts as a good solvent for reactants and

products. The dehydration reaction releases three water molecules for every HMF formed and as a result a water separation step will be required during large-scale production, regardless of whether water is used as a solvent. However, the presence of water as a solvent will shift the dehydration equilibrium and increase reaction times because water is one of the products formed. In addition, the formed HMF may react with water at high temperatures to produce levulinic acid and formic acid, which makes the conventional separation via distillation not practical. Several researchers have proposed an aqueous-organic solvent system that can retain the solvent properties of water while shifting the reaction equilibrium to the dehydration step and inhibiting further HMF hydrolysis. Most polar organic solvent have shown to be promising towards HMF synthesis, some of which include:

- Water
- Tetrahydrofuran (THF)
- Methyl tetrahydrofuran (MeTHF)
- Dioxane
- Dimethyl sulfoxide (DMSO)
- 2-butanol
- Methyl isobutyl ketone (MIBK) amongst others.

❖ **Biphasic Solvent System:** A biphasic system is a two-phase liquid system that is made up of aqueous and organic solvents, as shown in **Figure 2.14**. It is used to extract compounds such as HMF from the aqueous or organic phase using the liquid-liquid

extraction method. The system is unique by its low viscosity, ease of recovery, and short settling time. The biphasic solvent system method provides advantages over traditional extraction techniques such as environmental friendliness, low cost, simplicity of scaling-up, and efficiency for many types of experiments, particularly the concentration and purification of biochemical products.

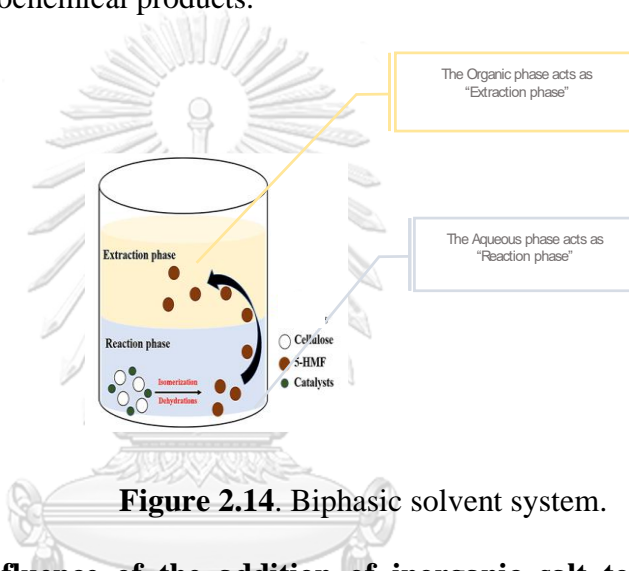


Figure 2.14. Biphasic solvent system.

- ❖ **Influence of the addition of inorganic salt to the solvent system:** Inorganic salts have been reported to have a significant influence on the HMF synthesis process. In a biphasic solvent system, the addition of inorganic salts to the aqueous phase greatly enhances HMF partitioning into the organic phase. The electrolytes alter the intermolecular bonding interactions between liquid components, increasing the immiscibility of the aqueous and organic phases. Some inorganic salts used in HMF synthesis include sodium chloride (NaCl), magnesium chloride (MgCl₂), potassium bromide (KBr), potassium chloride (KCl),

sodium ethanoate (CH_3COONa), sodium nitrate (NaNO_3), sodium sulfate (Na_2SO_4), Lithium chloride (LiCl), Lithium ethanoate (CH_3COOLi), Lithium nitrate (LiNO_3), and Lithium sulfate (Li_2SO_4) [93,94]. Among these salts, NaCl has the highest extraction coefficient, resulting in the most efficient extraction of HMF from the aqueous to the organic phase [94].

2.5.1.1. Zeolite-catalyzed dehydration of Glucose

Several zeolite catalysts have been reported to show great potential for the effective dehydration of lignocellulosic biomass to HMF. Although, with numerous advantages of zeolite as one of the promising solid acid catalysts over a homogeneous system, the yield of HMF is still lower. Some zeolite-containing catalysts used in the synthesis of HMF from glucose and cellulose as reported in the literature are summarized in **Table 2.6**.

The major aim of this work, utilizing zeolite catalysts, is to determine whether different modification procedures or post-synthesis treatments could enhance the conversion and yield of HMF.

Table 2.6. Some of the work done by other researchers with zeolite catalysts.

Entry	Catalyst	Substrate and Conditions	Conversion (%)	HMF Yield (%)	Reference
1	Bimodal-HZ-5	0.25 g Cellulose H ₂ O, 190 °C, 4 h	67	46	[70]
2	Hf/ β	100 mg Cellulose H ₂ O-NaCl/THF, 200 °C, 4 h	86.3	53.4	[71]
2	H-ZSM-5	Glucose, H ₂ O/THF/NaCl, 160 °C, 90 min	94	61	[67]
3	ZSM-5 Comm	Glucose, Water/Dioxane, 120 °C, 24 h	59.4	17	[72]
4	H-ZSM-5	Glucose, H ₂ O/MIBK, 195°C, 30min	80	42	[66]
5	Sn- β -F, HCl	Glucose, Water/THF/NaCl, 190 °C, 70 min	90	53	[73]
6	5%Hf-HZSM-5	Cellulose, H ₂ O/THF/NaCl, 190 °C, 2 h	Not reported	67.5	[68]
7	Cr-ZSM-5	Glucose, [BMIM]Cl, 130 °C, 60 min	-	54.5	[62]
8	Cu-Cr-ZSM-5	Glucose, DMSO, 140 °C, 4 h	57.5	50.4	[74]
9	Cr-USY	Cellulose, BMIMCl, 140 °C, 60min	Not reported	37	[62]
10	Cr-USY	Cellulose, BMIMCl, 160 °C, 90min	Not reported	35%	"
11	Cr-Beta	Cellulose, BMIMCl, 130 °C, 60min	Not reported	34.1	"
12	Cr-ZSM-5	Cellulose, BMIMCl, 130 °C, 60min	Not reported	4.1	"
13	H-USY	Glucose, BMIMCl, 130 °C, 60min	Not reported	21.5	"
14	H-Beta	Glucose, BMIMCl, 130 °C, 60min	Not reported	13.60	"
15	H-ZSM-5	Glucose, BMIMCl, 130 °C, 60min	Not reported	15.3	"
16	Cr-USY	Glucose, BMIMCl, 130 °C, 60min	Not reported	54.5	"
17	Cr-Beta	Glucose, BMIMCl, 130 °C, 60min	Not reported	58.5	"

2.5.2. Cellulose and its derivatives

Cellulose is the most abundant polymer on the earth's crust. It is a complex carbohydrate that forms the primary structural component of plant cell walls. It is a glucose polymer with a long chain, made up of repeating units of glucose molecules linked together by β -1,4 glycosidic bonds. Because cellulose is insoluble in water, it is

a very stable and durable material. Cellulose is formed in plants as a result of photosynthesis, and nature is estimated to be capable of producing a global annual yield of 1.3×10^9 metric tons of cellulose, with one average-sized tree capable of producing approximately 13.7 g of cellulose daily [75]. Cellulose fibers are relatively stiff, and their primary function is to provide plants with the structural rigidity they require. Cellulose fibers are held together by lignin and hemicellulose. The percentage of cellulose derived from biomass varies greatly. **Table 2.7** shows the composition of some sources of cellulose.

Table 2.7 Percentage composition of some lignocellulosic biomass [76].

Source	Cellulose	Hemicellulose	Lignin
Wheat straw	38.2	21.2	23.4
Corn fiber	14.3	16.8	8.4
Poplar	49.9	17.4	18.1
Corn stover	37.5	22.4	17.6
Pinewood	46.4	8.8	29.4
Wheat straw	38.2	21.2	23.4
Paper (pulp)	68.6	12.4	11.3

The number did not add up to 100% due to minor components that are not listed.

Wood pulp remains the most important source of cellulose for industrial applications, with the vast majority being processed for paper and cardboard production, and only about 2% of the processed cellulose being chemically modified into cellulose esters and ethers [77]. These can then be used for a variety of purposes, including coatings, laminates, optical films, and sorption media, among many others, ranging from building materials to pharmaceuticals and cosmetics.

Chemically, cellulose is made up of glucose monomers that are linked together by (1,4) glycosidic bonds. Each glucose unit is oriented in the same direction and is arranged in a linear chain. Cellobiose is the repeating unit of cellulose, and it is a dimer that is composed of two glucose molecules linked together by β -1,4 glycosidic bonds.

It is a homopolymer, which means it contains only one type of monomer, glucose. Strong hydrogen bonds between the hydroxyl (-OH) groups on adjacent glucose molecules hold the glucose molecules in cellulose together. Because of these hydrogen bonds, cellulose has a high tensile strength and is resistant to chemical and biological degradation.

The rigidity of cellulose is caused by the long linear chains on glucose units that are held together by a series of intra- and inter-molecular hydrogen bonds. Despite being significantly weaker than the covalent bonds that hold the monomer units together, the former is present in such large numbers that they allow for the formation of crystalline domains, making the material more resistant. As a result, cellulose solubility is highly dependent on the degree of polymerization. Cellulose with 1 to 6 glucose units dissolves easily in water, 7 to 13 glucose units dissolve partially in hot water, and chains larger than 30 glucose units form a dense network of intramolecular hydrogen bonds, which gives cellulose its characteristic properties such as resistance to chemical and biological degradation and insolubility in most known solvents [78].

These two factors significantly impede the process of catalytic depolymerization of cellulose to its glucose units, and the cellulose may require a pre-treatment to expose

the chemical bonds to the catalyst and increase reactivity. The chemical structure of cellulose is represented in **Figure 2.15**.

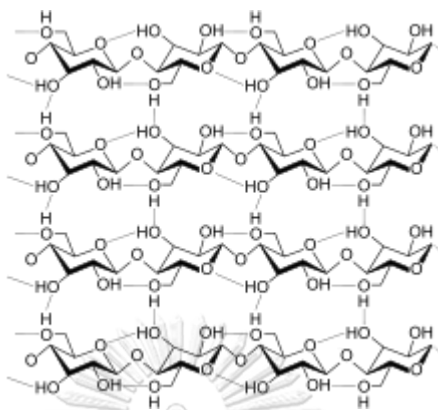


Figure 2.15 Cellulose structure [79]

2.5.2.1. Acid-catalyzed degradation of cellulose to HMF

The degradation of lignocellulosic biomass through catalysis has been the center of attraction for the past few decades, which has resulted in the development of techniques and knowledge in this aspect. Due to the emergence of these techniques, cellulose can be easily hydrolyzed by inorganic acids such as sulfuric acid (H_2SO_4), hydrochloric acid (HCl) [80-84], etc. These techniques, however, have not been applied industrially for large-scale applications due to complications accompanying the usage of these catalysts. Equipment corrosion, catalyst recovery, intensive energy demands, and decomposition of saccharides formed occur [105], with H_2SO_4 having to be neutralized with a CaO/CaSO_4 mixture, resulting in the formation of large amounts of gypsum as waste [86].

By using heterogeneous catalysts, the drawbacks of the catalysts on the process become less severe; however, using solid acid catalysts introduces a new set of challenges due to the nature of cellulose, which is not easily solubilized in the

reaction medium. The crystalline nature of cellulose greatly limits the effectiveness of heterogeneous catalysts, and this becomes a critical limitation on the effectiveness of solid catalysts. Physical barriers such as crystallinity, morphology, and surface area, among others, have a significant impact on the catalyst's effectiveness [87].

To resolve this, cellulose depolymerization can be performed in a reaction medium capable of breaking down the crystalline structure of the cellulose, or the cellulose must be subjected to a pre-treatment to disrupt the cellulosic material's supramolecular structure. Both options have the potential to increase the reactivity of cellulose to hydrolysis. These two fields have gradually evolved into their own research topics, with research groups choosing only one type of solvent or cellulose pretreatment and testing the catalytic performance of the chosen heterogeneous catalyst under the chosen conditions.

- ❖ **Reaction Media:** Since cellulose is insoluble in most solvents used in the chemical industry, research into new solvent types for this particular application is now possible. A solvent must be able to disrupt the cellulose fibers and make the hydroxyl groups and β - glycosidic linkages available for catalytic attack in order to be used with a heterogeneous catalyst. From the perspective of "Green" processes and sustainability, additional requirements are imposed, where solvent and catalyst recovery are preferred along with ease of product separation without the need for energy-intensive processes.
- ❖ **Pretreatments of cellulose:** Many studies have been conducted on various strategies to encourage the disintegration of cellulose apart from employing

solvents to disrupt the crystalline structure of cellulose. They can be divided into the following three categories:

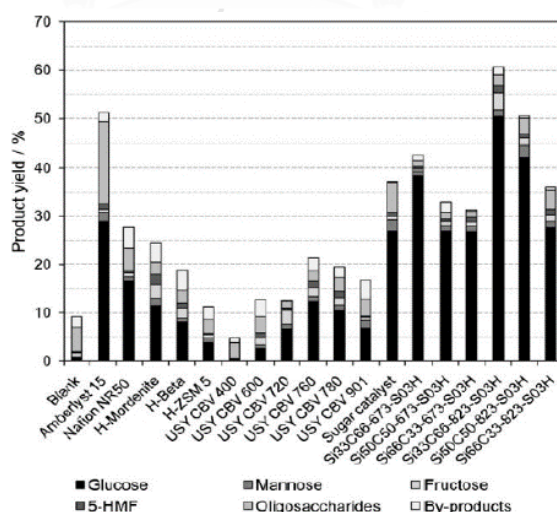
- Partial degradation with chemicals such as formic acid where cellulose is allowed to react with formic acid without the use of a heterogeneous catalyst [88].
- Swelling: By treating cellulose with salts where the hydrogen bonds in cellulose can be degraded.
- Mechanical comminution such as ball-milling: Here cellulose can be ground mechanically by ball-milling and allowing the crystalline cellulose to be converted to an amorphous form [89].

2.5.2.2. Hydrolysis of cellulose catalyzed by solid acids

Research into the use of solid acid catalysts for cellulose hydrolysis has been the main area of focus by various groups in recent years, primarily due to their numerous advantages over homogeneous catalyst systems. However, the yields obtained by utilizing these catalysts are lower when used in the same reaction condition as their homogeneous counterparts, due to diffusion limitation caused by the solid acid catalysts. The cellulose microfibrils are significantly larger than the micropores in the solid material, forcing the reaction to occur only at the solid's surface, with some authors proposing that the catalytic reaction occurs as a result of the formation of H_3O^+ species, which is released into the reaction medium [90]. **Table 2.5** shows several used zeolite catalysts for cellulose hydrolysis, their conversion, and HMF yields. References are made particularly to zeolite-containing catalysts as part of the family of solid acid catalysts for the relevance of this work.

In addition, Onda et al. [91] tested several acid catalysts under comparable reaction conditions and discovered that materials with sulfonated active groups outperformed other solid acids, even when their acid site densities were equivalent. This was explained as a result of the density of the $-SO_3H$ sites, which are assumed to be concentrated primarily on the catalyst's surface, whereas the acid-active sites of zeolites are concentrated within the pores and channels. Onda et al.'s work was followed by Sels et al. [92], who expanded the work to incorporate more catalysts such as zeolite USY, among others. **Figure 2.16** shows the results of his investigation, which shows the yield of glucose along with other components. He demonstrated that heterogeneous catalysts containing sulfonated groups were highly active and effective for this reaction in his work.

The basis of this research follows the observation from various literature reported on inducing strong acid density of zeolite-containing catalyst for the transformation of cellulose to HMF.



Reactions conditions: Ball-milled cellulose 0.05 g, catalyst 0.05 g, water 5 mL, reaction temperature 150 °C, time 24 h.

Figure 2.16. Hydrolysis of cellulose over solid acids [92]

CHAPTER 3

EXPERIMENTAL

All chemicals used in this project were of analytical grade without purification or further treatments. The zeolite materials used in this project were purchased commercially and were further post-synthesized and modified for the purpose of this research.

3.1. Post-synthesis/modification process of the commercial zeolites

3.1.1. Materials

Protonic form zeolites (H-ZSM-5, $\text{SiO}_2/\text{Al}_2\text{O}_3 = 24$, H-USY, $\text{SiO}_2/\text{Al}_2\text{O}_3 = 6$, H-Beta, $\text{SiO}_2/\text{Al}_2\text{O}_3 = 28$) were purchased from TOSOH Corporation Limited, Japan. Ammonium chloride (99.8%) and tin (IV) chloride pentahydrate (98%) were purchased from Sigma-Aldrich, USA. Nitric acid (65%) was supplied by QRëC, New Zealand.

3.1.2. Catalyst preparation

Dealumination: Acid-leaching technique was employed for the dealumination of commercial zeolites, by treating 3 g of the commercial zeolites with 120 mL of x M nitric acid solution ($x = 0.1, 0.2, 0.3$ & 0.4). The treatment was performed using a single-necked round bottom flask with a magnetic stirrer and refluxed at $80\text{ }^\circ\text{C}$ for 2 h using an oil bath connected with a proportional-integral-derivative thermocouple. After acid treatment, the samples were cooled, filtered, washed to neutral pH, and dried overnight at $80\text{ }^\circ\text{C}$.

Impregnation (ion exchange): Excess water impregnation technique was employed for the metal incorporation. 1 g of each uncalcined dealuminated zeolite sample was impregnated with a certain mass of the metal precursor in 15 mL of deionized water and stirred mechanically for 30 min. After ion exchange, the resulting mixture was dried at 80 °C overnight and denoted as $x\text{wt}\%\text{Sn-0.1DeAl.H-K}$, where x is equivalent to 1 wt%, 3.84 wt%, 5 wt%, 7 wt%, and 10 wt% of the metal (based on the relative percentage of tin in $\text{SnCl}_4 \cdot 5\text{H}_2\text{O}$) and K is the zeolite.

Calcination: Calcination was performed in a muffle furnace to remove impurities or contaminants and ensure the pure form of the catalysts. The dried solids obtained after both dealumination and impregnation procedures were calcined in a crucible at 550 °C for 6 h at a heating rate of 5 °C/min.

Hydration: This technique was employed for the solid-state NMR analysis of the dealuminated zeolites to keep the samples in their hydrated forms for analysis capture. The samples were hydrated with saturated NH_4Cl solution before analysis. In a typical hydration procedure, a saturated solution of Ammonium Chloride was prepared at room temperature and kept in a desiccator along with 1 g of the sample for 3 d. After hydration, the samples were sealed and taken for analysis.

3.1.3. Analytical techniques

XRD: Powder x-ray diffraction was employed to determine the crystallinity of the catalysts, by using Bruker Model D8 ADVANCE diffractometer, operated at 40 kV and 30 mA with $\text{Cu-K}\alpha$ radiation ($\lambda=1.541\text{\AA}$). X-ray diffractograms were recorded at a 2-theta angle from 5° to 80°.

XRF: Elemental compositions of the catalysts were recorded on Wavelength Dispersive X-ray Fluorescence, Rigaku Model ZSX Primus III+.

Nitrogen Physisorption: The textural properties of the catalysts were analyzed with Micromeritics 2020 ASAP Surface Area and Porosity Analyzer. The samples were degassed at 300 °C for 60 min before analysis. Subsequently, the nitrogen physisorption analysis was examined at -196 °C. The BET surface area was calculated in the relative pressure (P/P_0) range of 0.05 to 0.25 from the adsorption data, employing the BET equation. The adsorption branch at $P/P_0 = 0.99$ was used to obtain the total volume of the pore. The t-plot method from the adsorption data was used to quantify the surface area of the micropore.

SEM: Field emission scanning electron microscopy (FE-SEM) was employed to determine the morphology and particle sizes of the commercial and modified zeolite catalysts. The images were captured on JEOL JSM-7610F instrument, conducted at 5.0 kV, at a magnification of 30,000 - 150,000. Prior to capturing, the samples were carefully dispersed on carbon tape, and afterward, they were sputter-coated with gold to enable image capturing.

Solid-state MAS NMR: The chemical environments of aluminum (Al) and silicon (Si) in the zeolite catalysts were respectively investigated by solid-state ^{27}Al and ^{29}Si magic-angle spinning (MAS) nuclear magnetic resonance (NMR) spectroscopy. The NMR spectra were recorded on a BRUKER/AVANCE III HD/Ascend 400 WB Fourier transform NMR spectrometer at room temperature. The chemical shifts of ^{27}Al and ^{29}Si MAS NMR spectra are represented in parts per million (ppm) using aluminum chloride hexahydrate ($\text{AlCl}_3 \cdot 6\text{H}_2\text{O}$) and sodium

trimethylsilylpropanesulfonate (DSS) as reference standards, respectively. The samples were hydrated with saturated ammonium chloride (NH_4Cl) solution for 3 d before the analysis.

UV-vis spectroscopy: UV-vis near-infrared spectroscopy was performed on PERKIN ELMER LAMBDA 950 to determine the coordination states of tin species in the zeolite catalyst after successful incorporation.

Ammonia-TPD: NH_3 -TPD analysis was conducted to determine the distribution and amount of acid sites of the catalysts. The analysis was carried out by using the following procedure: the catalysts were calcined for 6 h at 550 °C before analysis. Then, ~80 mg of the catalyst sample in a quartz U-tube was pretreated at 550 °C for 30 min under helium gas flow (50 mL/min), at a ramp rate of 10 °C/min. After pretreatment was completed, the sample was allowed to cool down to 50 °C and afterward, it was equilibrated with ammonia gas (10 vol.% NH_3 in He) for 30 min. Following equilibration, the catalyst was flushed with helium for 30 min to remove the physisorbed NH_3 gas. Finally, ammonia desorption was measured with a thermal conductivity detector (TCD) at a temperature region of 50 °C to 800 °C (10 °C/min heating rate). The data were quantified by deconvoluting the temperature-programmed desorption profiles with external software (OriginPro).

FTIR spectroscopy: *In-situ* FTIR spectroscopy was used for pyridine adsorption (Py-FTIR), with the aid of Thermo-Fisher Scientific NICOLET iS10 FTIR spectrometer, to determine the Brønsted and Lewis acid contents of the catalysts, using a wavenumber range of 400 - 4000 cm^{-1} at spectra recording of 96 scans. The fresh catalyst powder was formed into a 2-cm diameter self-supported wafer and then

placed in a quartz cell. The catalyst was then pretreated at 500 °C for 1 h in a vacuum atmosphere to remove contaminants. Thereafter, the cell was cooled to 50 °C and was exposed to pyridine vapor at 500 Pa for 30 min. Finally, degassing was done from 100 °C to 500 °C at 15 min intervals.

3.2. Glucose dehydration to HMF

3.2.1. Materials

D (+) Glucose was supplied by Kemaus, Australia. D-Fructose was provided by LOBA Chemie, India. 2,5-furan dicarboxylic acid (97%), levulinic acid (98%), HMF (analytical grade), and furfural (99%) were all purchased from Sigma-Aldrich, USA. Tetrahydrofuran (99.5%) and ethyl methyl ketone (also called 2-butanone, 99.5%) were supplied by QRëC, New Zealand. Sodium chloride crystals (99%) was provided by J.T Baker, USA.

3.2.2. Apparatus and instruments used

- Autoclave reactor: Reactions were performed in stainless-steel autoclave reactors that are lined with Teflon. The autoclave, as shown in **Figure 3.1** has a capacity of 60 ml and offered the possibility of performing a reaction up to a heating temperature of 200 – 250 °C.



Figure 3.1. Stainless-steel autoclave reactor used in this research work.

- Hot-plate equipped with a mechanical stirrer and proportional-integral thermocouple – Served as a heat source for reaction, as depicted in **Figure 3.2**.



Figure 3.2. Heat source for reaction.

- Reflux condenser: As shown in **Figure 3.3**, the apparatus was used to cool the vapor that the heated mixture of the acid-treated zeolites emits over dealumination time.



Figure 3.3. Reflux condenser set-up for acid dealumination.

- Refrigerator – used as a cooling system for reflux condenser. It was also used as a storage system for reaction products for HPLC analysis.
- Glassware – Beakers, volumetric flask, round-bottom flask, analytical bottles, glass bottles, measuring cylinders.
- Centrifuge machine– used in separating catalyst from liquid products.
- Heat-box jacket – used in preventing heat dissipation during reactions.
- Screwdriver – used to seal autoclave reactors.
- Suction machine – used for mechanical filtration.
- Oven – used to dry samples or material.
- Muffle furnace – used for calcination.
- Fume hood – For keeping used and hazardous chemicals.
- Others – Silicone oil bath, micro-pipette, 0.2 μL PTFE syringe filter, 0.2 μL PTFE syringe filter, magnetic stirrer, syringe, suction, suction tubes, pH paper, nitrile gloves, weighing balance and paper, Whatman Filter paper, test tubes, ceramic crucibles.

3.2.3. Catalytic test procedure

The catalytic dehydration of glucose to HMF was conducted in water: THF system, saturated with sodium chloride, at a 1:2 volume ratio using an autoclave reactor. An aqueous solution composing 3.6 wt% anhydrous glucose and 20 wt% NaCl was made by dissolving 3.6 g of glucose and 20 g of NaCl in 100 mL deionized water. Then, 10 mL of an aqueous solution of glucose was mixed with 20 mL of THF and introduced into the autoclave, as well as 0.5 g of freshly prepared catalyst. Thereafter, it was pressurized with 10 bar nitrogen gas. The temperature of the reaction was regulated with a silicone oil bath on a hot plate equipped with a proportional-integral-derivative thermocouple and stirrer. The starting reaction time was recorded when the target temperature was attained. The reactor was quenched in a bath containing ice after reaction time, and the liquid product was recovered by centrifugation. The experiment was also performed thermally without a catalyst with the procedure described above.

3.2.4. Product analysis

The organic and aqueous products were analyzed by HPLC using an Agilent HPLC 1100 Series fitted with a Bio-Rad HPX87-H column. A Diode Array Detector (DAD) operating at a wavelength of 240 nm was used to analyze the organic phase product-containing internal standard (2,5-furan dicarboxylic acid). The analyte from the aqueous phase containing internal standard (2-butanone) was analyzed with a refractive index detector (RID), by using a column temperature of 60 °C, a mobile phase of 5 mM H₂SO₄, a flow rate of 0.5 mL/min, and an injection volume of 10 μL at an analysis (retention) time of 60 min. The experiments were run on multiple occasions and their average and standard deviation values were determined. Glucose

conversion, yields of products, and selectivity of HMF were determined based on the following equations.

Glucose conversion (%)

$$= \frac{(\text{concentration of glucose before reaction} - \text{glucose concentration left after reaction}) \times 100}{\text{concentration of glucose before reaction}}$$

$$\text{Yield (\%)} = \frac{\text{Concentration of desired product} \times 100}{\text{concentration of glucose before reaction}}$$

$$\text{Other byproducts (\%)} = \text{Conversion (\%)} - \text{Total products yield (\%)}$$

$$\text{Selectivity of HMF (\%)} = \frac{\text{Yield of HMF} \times 100}{\text{Glucose conversion}}$$

3.3. Cellulose conversion to HMF

3.3.1. Materials

Microcrystalline cellulose powder, 2,5-furan dicarboxylic acid (97%), levulinic acid (98%), HMF (analytical grade), furfural (99%), and tin (IV) chloride pentahydrate (98%) were all obtained from Sigma-Aldrich, USA. Tetrahydrofuran (99.5%) and ethyl methyl ketone (also called 2-butanone, 99.5%) were supplied by QR&C, New Zealand. Sodium chloride crystals (99%) was provided by J.T Baker, USA. D (+) Glucose was supplied by Kemaus, Australia. D-Fructose (extra pure) was purchased from LOBA Chemie, India.

3.3.2. Apparatus and instruments used

Same as above.

3.3.3. Catalytic test procedure

The degradation of cellulose to HMF was conducted in an autoclave reactor as follows: 0.18 g of microcrystalline cellulose was accurately weighed into the

autoclave. 5 mL of deionized water saturated with 1 g of sodium chloride, and 10 mL of THF, as well as 0.25 g of freshly prepared catalyst, were then introduced. Thereafter, the reactor was sealed and pressurized with 10 bar N₂ gas. The reaction temperature was controlled by a heat-box jacket on a hotplate equipped with a stirrer and proportional-integral-derivative thermocouple. Reaction time was recorded when the target temperature was reached. After the reaction time, the autoclave was quenched in an ice bath and the liquid product, unreacted cellulose, and catalyst were recovered by centrifugation technique. The experiment was performed thermally without a catalyst with the same procedure described above.

3.3.4. Product analysis

The aqueous and organic liquid products were analyzed with HPLC with the same procedure described above. The reactions were run on multiple occasions and their mean & standard deviation values were determined, owing to experimental errors. Cellulose conversion was calculated based on the weight difference of cellulose before and after the reaction, with an experimental error of $\pm 2\%$. The yield and selectivity of products were calculated based on the equations described by Nandiwale et al. [70].

$$\text{Mass of unreacted cellulose} = \text{Total mass of solid recovered} - \text{Mass of catalyst}$$

$$\% \text{ Cellulose conversion} = \frac{(\text{Mass of charged cellulose} - \text{Mass of unreacted cellulose}) \times 100}{\text{Mass of charged cellulose}}$$

$$\% \text{ Selectivity} = \frac{\text{Concentration of desired product} \times 100}{\text{Total concentration of products}}$$

$$\% \text{ Yield} = \frac{\% \text{ cellulose conversion} \times \% \text{ selectivity of desired product}}{100}$$

RESULTS AND DISCUSSION

The result and discussion section is divided into three chapters, chapters 4–6. Chapter 4 and 5 discuss the results obtained from glucose dehydration to HMF with modified zeolite catalysts while Chapter 6 details the conversion of cellulose to HMF over the modified zeolite catalysts.

CHAPTER 4

4. Glucose dehydration to HMF

This part was conducted via three steps.

- ❖ First, a preliminary study was carried out to evaluate the catalytic performance of the commercial zeolites and their similar modified forms for glucose dehydration to HMF.
- ❖ Second, the most effective acid-treated zeolite from the first category above was selected for further study by acid dealumination with higher nitric acid-concentration solutions.
- ❖ Finally, the reaction conditions over the best-modified zeolite catalyst were optimized, and optimum reaction conditions were determined.

4.1. Preliminary studies of the catalytic performance of commercial zeolites and their modified forms

Studies were conducted without catalysts and with commercial zeolites and their similar modified forms for glucose dehydration, as shown in **Table 4.1**. The result without a catalyst was poor and confirmed the significant role of bifunctional heterogeneous catalyst in glucose conversion to HMF. The yield of fructose was seen to be high without a catalyst, indicating that the rate of dehydration was slow.

Out of the three commercial zeolites and their dealuminated forms, 0.1DeAl.H-ZSM-5 exhibited the superior catalytic performance owing to its suitable acidity, as depicted in **Table 4.2**. Meanwhile, among the metal-modified dealuminated zeolite catalysts, 3.84wt%Sn-0.1DeAl.H-ZSM-5 exhibited the highest selectivity for HMF

due to improved total acid sites. H-USY and 0.1DeAl.H-USY zeolite possessed the highest acidity among the commercial and acid-treated zeolites. High acidity has been demonstrated to promote the formation of by-products by deteriorating HMF yield, and this led to the high content of other products observed with the two catalysts.

From this study, acid-treated H-ZSM-5 and tin-modified-acid-treated H-ZSM-5 zeolites were further investigated for glucose dehydration to HMF.

Table 4.1. Catalytic study^a of the three commercial zeolites and their modified forms for glucose dehydration.

Entry	Sample	Glucose conversion (%)	Yields [%]					HMF selectivity (%)
			Fructose	LA ^b	Furfural	HMF	Others ^c	
1	No catalyst	38.0	13.2	1.5	0.2	17.1	5.1	-
2	Commercial H-Beta	98.5	0.0	0.0	0.8	63.8	31.6	-
	0.1DeAl.H-Beta	77.3	2.6	0.0	0.8	65.5	6.1	-
	3.84wt%Sn-0.1DeAl.H-Beta	77.9	2.4	0.0	0.6	51.3	21.8	65.9
3	Commercial H-USY	98.6	0.0	1.2	0.0	48.8	48.7	-
	0.1DeAl.H-USY	100.0	0.0	0.0	0.6	53.1	44.5	-
	3.84wt%Sn-0.1DeAl.H-USY	100.0	0.0	0.0	1.0	14.7	81.4	14.7
4	Commercial H-ZSM-5	97.8	0.0	0.0	0.6	59.6	35.6	-
	0.1DeAl.H-ZSM-5	99.0	0.4	0.9	0.8	64.7	30.0	-
	3.84wt%Sn-0.1DeAl.H-ZSM-5	83.9	3.2	1.5	0.7	62.3	14.1	74.3

^a Reaction conditions: catalyst loading, 0.25 g; glucose concentration, 3.6 wt%; reaction temperature, 170 °C; reaction time, 60 min.

^b Levulinic acid

^c Mainly humins

Table 4.2. Comparison of the acidities of commercial zeolites and their modified forms for glucose dehydration.

S/n	Catalysts	Total acidity ^a (mmol/g)	Si/Al mole ratio ^b	Sn content ^c
1	Commercial H-Beta	1.065	26.00	n/a
	0.1DeAl.H-Beta	0.737	54.33	n/a
	3.84wt%Sn-0.1DeAl.H-Beta	0.993	51.64	3.751
2	Commercial H-USY	1.191	5.52	n/a
	0.1DeAl.H-USY	1.279	8.92	n/a
	3.84wt%Sn-0.1DeAl.H-USY	1.041	9.47	3.464
3	Commercial H-ZSM-5	1.134	21.07	n/a
	0.1DeAl.H-ZSM-5	1.189	22.09	n/a
	3.84wt%Sn-0.1DeAl.H-ZSM-5	1.336	22.11	3.666

^a obtained from ammonia-TPD analysis

^{b-c} obtained from XRF analysis

n/a means not available

4.2. Acid dealumination of commercial H-ZSM-5 zeolite

Acid dealumination was studied on commercial H-ZSM-5 zeolite to adjust its Si/Al mole ratio and to correspondingly adjust its physicochemical properties for efficient glucose dehydration to HMF. Commercial H-ZSM-5 was mildly dealuminated with a nitric acid solution (ranging from 0.1 – 0.4 M) and tested for glucose dehydration to HMF. The results of the characterization methods used for the catalysts before and after preparation are discussed below. Their catalytic performances for glucose dehydration to HMF are also discussed in detail.

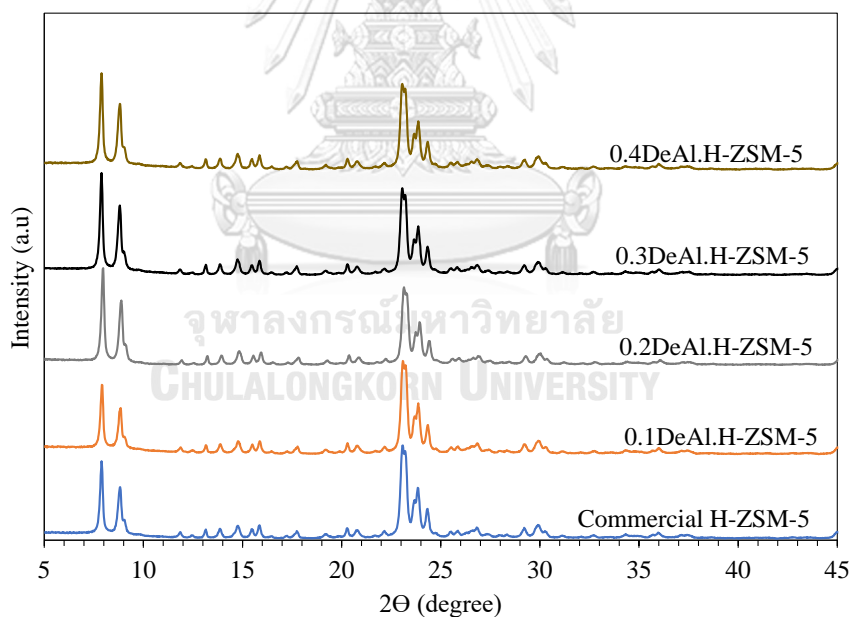
4.2.1. Physicochemical properties of dealuminated catalysts

The X-ray diffraction patterns of the commercial and acid-treated H-ZSM-5 zeolite samples are shown in **Figure 4.1**. The result confirmed that the MFI structure of commercial H-ZSM-5 was preserved after acid treatment with different concentrations. The crystallinity of the commercial H-ZSM-5 zeolite was also maintained after the dealumination processes.

The result of the XRF analysis is reported in terms of Si/Al mole ratio as shown in **Table 4.3**. The parent zeolite's silica and alumina mole ratio increased slightly after acid treatment, indicating that a certain degree of dealumination occurred. There was no notable difference in the aluminum content based on the concentration of the nitric acid solution used (0.1 – 0.4 M). This observation is attributed to the recalcitrant nature of the H-ZSM-5 zeolitic framework to low acid concentrations [95]. The result obtained follows the work reported in the literature by Triantafillidis et al. where the alumina content of commercial H-ZSM-5 zeolite (Si/Al ratio = 27) decreased by just 7 wt% following the dealumination with 1.5 M hydrochloric acid at 90 °C for 24 h [96].

Table 4.3. Textural properties and Si/Al ratio of commercial and acid-treated H-ZSM-5 zeolites.

Sample	$S_{\text{BET}}^{\text{a}}$ (m^2/g)	$S_{\text{micro}}^{\text{b}}$ (m^2/g)	$S_{\text{ext.}}^{\text{c}}$ (m^2/g)	D_{p}^{d} (nm)	$V_{\text{micro}}^{\text{e}}$ (cm^3/g)	$V_{\text{meso}}^{\text{f}}$ (cm^3/g)	$V_{\text{pore}}^{\text{g}}$ (cm^3/g)	SiO ₂ /Al ₂ O ₃ ratio ^h	Crystallinity ⁱ (%)
Comm. H-ZSM-5	343	253	90	2.76	0.133	0.105	0.238	21.07	100
0.1DeAl.H-ZSM-5	377	261	116	2.78	0.128	0.135	0.263	22.09	100
0.2DeAl.H-ZSM-5	318	218	100	2.99	0.115	0.123	0.238	22.13	100
0.3DeAl.H-ZSM-5	276	210	66	2.8	0.111	0.082	0.193	22.04	100
0.4DeAl.H-ZSM-5	362	259	103	2.89	0.137	0.125	0.262	22.16	100

^a BET surface area^b Micropore surface area^c External surface area^d Pore diameter obtained by the BJH method^e Volume of the micropore^f Volume of mesopore ($V_{\text{meso}} = V_{\text{pore}} - V_{\text{micro}}$)^g Total pore volume^h Determined by XRFⁱ Calculated from XRD patterns at 2-theta angles of 14.81°, 23.10°, 23.86°, and 24.37°**Figure 4.1.** X-ray diffraction patterns of commercial and acid-treated H-ZSM-5 zeolite.

The N₂ physisorption isotherms of the commercial and acid-treated H-ZSM-5 zeolites are shown in **Figure 4.2**. All the H-ZSM-5 zeolite catalysts display the type I isotherm of a typical microporous material. The presence of the hysteresis loop at P/P₀

> 0.4 indicates the mesoporosity of the zeolite samples [67]. The origin of mesopores is related to the interparticle voids located between the H-ZSM-5 zeolite particles and/or inside its particles agglomerate. As shown in **Table 4.3**, the commercial H-ZSM-5 zeolite exhibited the BET surface area and total pore volume of $343 \text{ m}^2/\text{g}$ and $0.238 \text{ cm}^3/\text{g}$, respectively. The acid treatment with 0.1 nitric acid solution slightly increased the textural properties of the commercial zeolite, possibly due to a decreased degree of particle agglomeration. 0.1DeAl.H-ZSM-5 possessed the highest surface area and porosity. By increasing the acid concentration further, up to 0.3 M, the surface area and total pore volume of the catalysts decreased whereas the surface area and total pore volume slightly increased at a higher concentration (0.4 M).

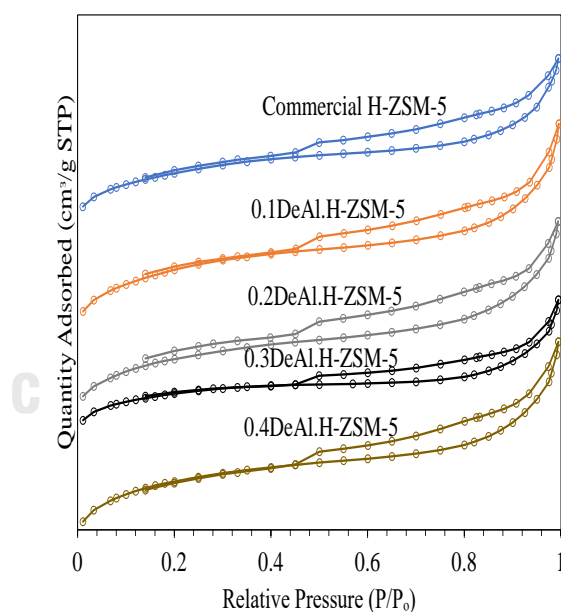


Figure 4.2. N_2 adsorption-desorption isotherms of commercial and acid-treated H-ZSM-5 catalysts.

The FE-SEM image of the commercial and acid-treated (0.1 – 0.3 M) H-ZSM-5 zeolites are shown in **Figure 4.3**. The commercial H-ZSM-5 zeolite has a rectangular-

shaped nanoparticle agglomerate, similar to the observation of Hoff et al. [97]. The shape and size of the primary H-ZSM-5 zeolite particles were maintained after the acid treatment, but the degree of agglomeration changed, particularly at a high concentration of the acid solution. A decrease in the agglomeration nature was observed after the dealumination process, which explained the changes in the textural properties of the H-ZSM-5 catalysts.

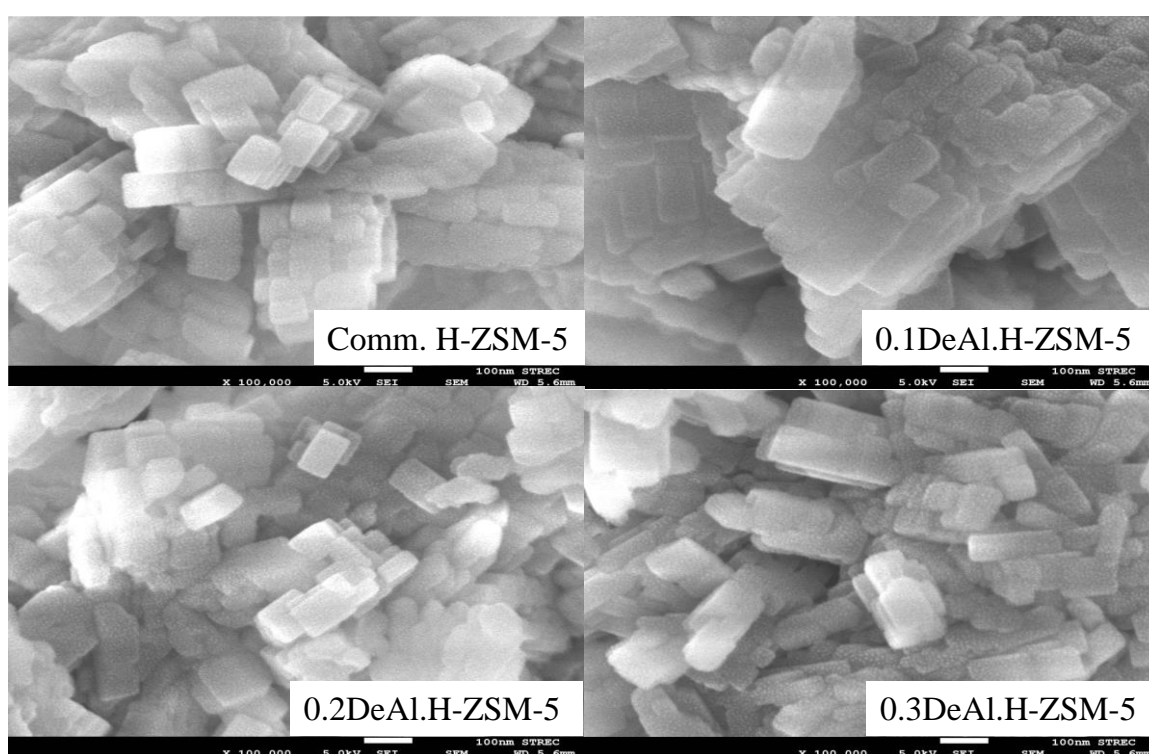


Figure 4.3. FE-SEM images of the commercial and acid-treated H-ZSM-5 catalysts at 100,000X magnification.

The solid-state ^{27}Al NMR was conducted to investigate the chemical shift that occurred in the aluminum environment of the commercial H-ZSM-5 after acid treatment. The ^{27}Al MAS NMR spectra of the commercial and 0.1 M acid-treated H-ZSM-5 zeolites are shown in **Figure 4.4A**. Three chemical shifts were observed at 54 ppm, 37 ppm, and 0 ppm. They are ascribed to the aluminum species in the tetrahedral

(Al^{IV}), pentahedral (Al^V), and octahedral (Al^{VI}) coordinations in the H-ZSM-5 zeolite network, respectively [98,99]. The pentahedral and octahedral species can be present in the commercial H-ZSM-5 zeolite as coordinatively unsaturated aluminum atoms attached in its framework and/or extraframework aluminum (EFAL) species [98]. The broad signal at -30 ppm is assigned to non-framework aluminum species in the form of a three-coordinated cationic Al³⁺ in the distorted environment and or charged neutral alumina (Al₂O₃) clusters [96,98]. The distributions (area%) of the aluminum species determined for the commercial and acid-treated zeolites are summarized in **Table 4.4**. The acid treatment removed some tetrahedral aluminum species, while the relative fraction of the pentahedral aluminum atoms notably increased. This outcome is in agreement with the work of You et al. [98]. As earlier discussed, the framework of the commercial H-ZSM-5 zeolite was not significantly perturbed with 0.1 M nitric acid solution. The change in the aluminum environment on the mild dealumination should be mostly attributed to the partial removal of extraframework aluminum species via hydrolysis and ion-exchange processes [100]. The work of Kooyman et al. demonstrated that the dealumination process was a facile method to control the types of aluminum species, and thus the acid properties of H-ZSM-5 catalysts [95].

Table 4.4. Distribution of aluminum species in the commercial and acid-treated H-ZSM-5 catalysts.

Catalyst	Al ^{IV} ^a		Al ^V ^b		Al ^{VI} ^c		Distorted EFAL ^d		Total peak area
	Peak area	Fraction (%)	Peak area	Fraction (%)	Peak area	Fraction (%)	Peak area	Fraction (%)	
Comm. H-ZSM-5	2823580	62.96	539993	12.04	750786	16.74	370188	8.25	4484547
0.1DeAl.H-ZSM-5	3512800	63.11	793055	14.25	793055	14.25	467586	8.40	5566497

^a Tetrahedral aluminum species at 54 ppm

^b Pentahedral aluminum species at 37 ppm

^c Octahedral aluminum species at 0 ppm

^d Distorted extraframework aluminum (EFAL) at -30 ppm

The solid-state ²⁹Si MAS NMR spectra of the commercial and acid-treated H-ZSM-5 zeolite are shown in **Figure 4.4B**. The spectra were deconvoluted into four (4) components, resonating at -85 ppm, -95 ppm, -105 ppm, and -111 ppm, corresponding to the silicon (Si) atoms in different coordinations with aluminum atoms; Si(3Al), Si(2Al), Si(1Al), and Si(0Al) species, respectively [98,100-101]. In addition, these chemical shifts can be assigned to Si(OSi)_{4-n}(OR)_n, where n is equivalent to 0,1,2, or 3, and R is a proton [98,101]. The relative distributions of different silicon species are summarized in **Table 4.5**. The treatment with 0.1 M acid solution predominantly increased the fraction of the band at -85 ppm, while other silicon coordinations were not significantly altered.

The result is ascribed to the increase in the number of silanol groups ($\equiv\text{Si-OH}$) due to the partial hydrolysis of the H-ZSM-5 aluminosilicate framework during the acid treatment [93]. This was evident by the FTIR spectra of these samples thermally treated at 500 °C, **Figure 4.5**. The absorption bands at ca. 3740 cm⁻¹ correspond to the silanol groups [104], while the absorption band at ca. 3680 cm⁻¹ is assigned to the hydroxyl groups attached to aluminum debris and/or partially hydrolyzed framework aluminum (FAL) [105]. It was obvious that the content of silanol groups increased by the mild acid treatment, and the absorption band of the bridging hydroxyl groups became sharp. The overall results obtained from the solid-state NMR and FTIR analysis indicated that low concentration of acid solution removed some extraframework aluminum (EFAL) species from the commercial H-ZSM-5 zeolite and slightly hydrolyzed its zeolitic framework.

Table 4.5. Fractions of silicon species in the commercial and acid-treated H-ZSM-5.

Catalyst	Si(0Al) ^a		Si(1Al) ^b		Si(2Al) ^c		Si(3Al) ^d		Total peak area
	Peak Area	Fraction (%)	Peak Area	Fraction (%)	Peak Area	Fraction (%)	Peak Area	Fraction (%)	
Comm. H-ZSM-5	229551	37.79	250494	41.24	101948	16.79	25380	4.18	607372
0.1DeAl.H-ZSM-5	236797	36.76	256296	39.79	104601	16.24	46446	7.21	644140

^a Silicon bonded with no aluminum atom or Si(OSi)₄ species at -111 ppm.

^b Silicon bonded to one aluminum atom or Si(OSi)₃(OH) in the range of -104 to -105 ppm.

^c Silicon bonded to two aluminum atoms or Si(OSi)₂(OH)₂ in the range of -92 to -95 ppm.

^d Silicon bonded to three aluminum atoms or Si(OSi)(OH)₃ in the range of -84 to -85 ppm.

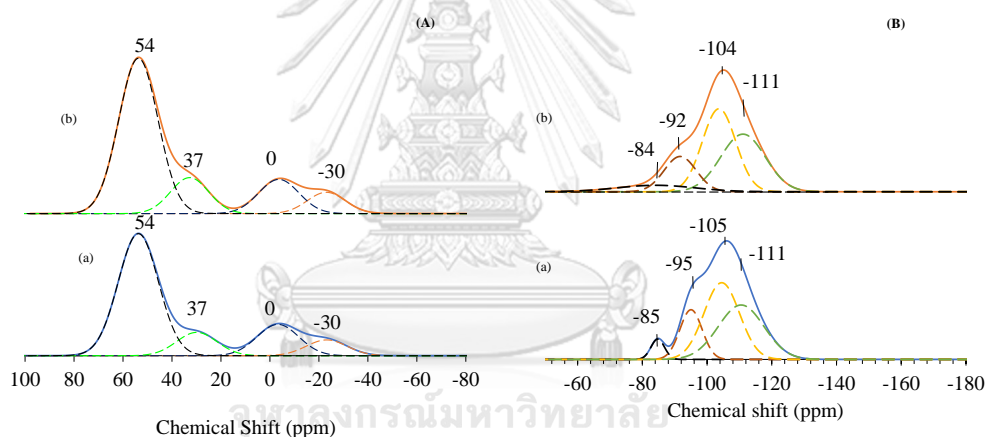


Figure 4.4. Solid-state (A) ²⁷Al and (B) ²⁹Si MAS NMR spectra of (a) commercial H-ZSM-5 and (b) 0.1DeAl.H-ZSM-5.

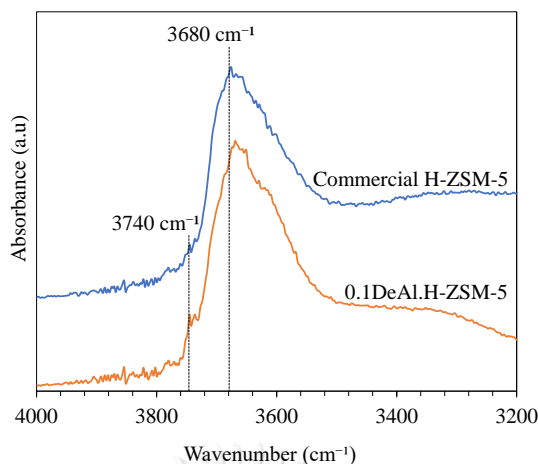


Figure 4.5. FTIR spectra of the commercial H-ZSM-5 and 0.1DeAl.H-ZSM-5 in the O–H stretching region.

The distribution of the total acidity and acid sites of the commercial and acid-treated H-ZSM-5 zeolites were characterized by the NH_3 -TPD analysis. The weak, moderate, and strong acidity corresponded to the ammonia desorption that occurred in the temperature region of 50–200 °C, 200–350 °C, and 350–500 °C, respectively, as depicted in **Figure 4.6A**. By treating the commercial H-ZSM-5 with various nitric acid solutions, the area under the TPD profiles, relative to the total acidity, was increased. The acid site distribution with different strengths is shown in **Table 4.6**. The acid treatment with 0.1 M acid solution particularly enhanced the strong acidity. Since the temperature-programmed desorption technique cannot differentiate the type of acid sites, the FTIR for pyridine adsorption was carried out to determine and quantify the Brønsted and Lewis acidity (**Figure 4.6B**). The absorption bands at 1545 cm^{-1} and 1455 cm^{-1} are attributed to the pyridine molecules adsorbed onto the Brønsted and Lewis acid sites of the catalysts, respectively, meanwhile the superimposition obtained from the vibration of the pyridine molecules that interacted

with both acid types was located at 1490 cm^{-1} [104]. Following acid treatment, the amount of Brønsted and Lewis acidity was 1.5-fold and 5.5-fold increase, respectively. As suggested by the solid-state MAS NMR analysis, this outcome was explained by partial hydrolysis of non-framework alumina (Al_2O_3) clusters as well as zeolitic framework, resulting in a diverse coordination of aluminum atoms. The extraction of some cationic extraframework aluminum (EFAL) species through ion-exchange process rendered the Brønsted acidity increased [104].

By increasing the nitric acid concentration further, the amount of weak and moderate acid sites increased, while the strong acidity was slightly changed. The content of the Lewis acid sites increased by only 2.6-fold and 3.5-fold at higher concentrations of the acid solution (0.2–0.3 M). The decreased Lewis acidity observed after further acid treatment at higher concentration of nitric acid (0.4 M) implies that both framework and extraframework aluminum were extracted by the acid solution. Yang and co-workers [137] demonstrated that the Lewis acid content of a commercial H-USY zeolite decreased significantly after the acid treatment of the zeolite with 0.5–8 M nitric acid solutions. Meanwhile, the Brønsted acid content was maintained around 1.5-fold increase after treatment with 0.2 M acid solution, whereas with 0.3 – 0.4 M acid solution, the content of Brønsted acid increased concomitantly, **Table 4.6**. As evidenced by the X-ray diffraction and X-ray fluorescence analysis, the crystallinity and elemental composition of the acid-treated zeolites were not significantly altered at high concentrations of the acid solution. However, the degree of particle agglomeration and the interparticle void volume of the modified catalysts changed significantly. Losch et al. [106] from their work demonstrated that the H-ZSM-5 zeolite with highly dispersed crystallites had superior acid properties to the

agglomerate ones. The total acidity of the acid-treated zeolite remained high even at 0.4 M acid solution.

Table 4.6. Distribution and type of acid sites of commercial and acid-treated H-ZSM-5 catalysts

Catalysts	Acid sites distribution (mmol/g) ^a				Type of acid sites (mmol/g) ^b		
	Weak	Moderate	Strong	Total	L	B	B/L ratio
Comm. H-ZSM-5	0.735	0.233	0.166	1.134	0.020	0.176	7.35
0.1DeAl.HZSM-5	0.711	0.255	0.224	1.189	0.109	0.261	2.39
0.2DeAl.HZSM-5	1.008	0.291	0.210	1.509	0.051	0.264	5.20
0.3DeAl.HZSM-5	0.976	0.257	0.199	1.432	0.069	0.374	5.39
0.4DeAl.H-ZSM-5	1.019	0.307	0.152	1.477	0.018	0.289	15.90

^a Determined by Ammonia-TPD analysis (Weak: 50–200 °C, Moderate: 200–350 °C, Strong: 350–500°C)

^b Determined by Py-FTIR analysis (L – Lewis acidity, B – Brønsted acidity)

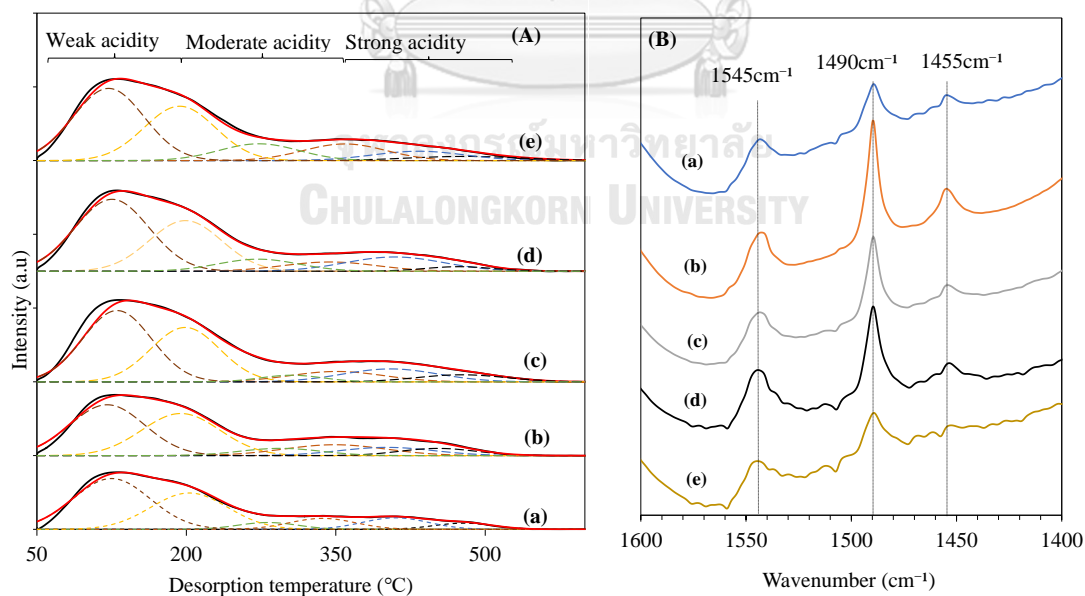


Figure 4.6. (A) NH₃-TPD profiles and (B) Py-FTIR spectra of (a) commercial H-ZSM-5, (b) 0.1DeAl.H-ZSM-5, (c) 0.2DeAl.H-ZSM-5, (d) 0.3DeAl.H-ZSM-5, and (e) 0.4DeAl.H-ZSM-5.

4.2.2. Glucose dehydration to HMF over commercial and dealuminated H-ZSM-5 zeolite

Reaction pathways for glucose dehydration to HMF: The plausible reaction pathways for the conversion of glucose to HMF and other by-products are illustrated in **Figure 4.7**. Glucose isomerization to fructose is facilitated by Lewis acid sites through 1,2-intramolecular hydride shift [107]. The fructose formed is then dehydrated at the Brønsted acid centers, removing three molecules of water to form HMF. It has been demonstrated that a high Brønsted acidity could deteriorate the yield of HMF formed by promoting its rehydration to levulinic acid (LA) and formic acid (FA) [66]. In this study, furfural was also observed as a by-product. It is a xylose dehydration product from the retro-aldol condensation of fructose intermediates, which is catalyzed by Brønsted acid sites [68]. Soluble or insoluble (polymeric) humins are inevitably formed via condensation among glucose, fructose, furans, as well as other reactive intermediates, such as 2,5-dioxo-6-hexanal (DHH) [108]. Previous works have shown that the formation of humins can be retarded, and could increase the selectivity of HMF, by optimizing not only the total number of acid sites but also a molar ratio of Brønsted/Lewis (B/L) acidity [108,109].

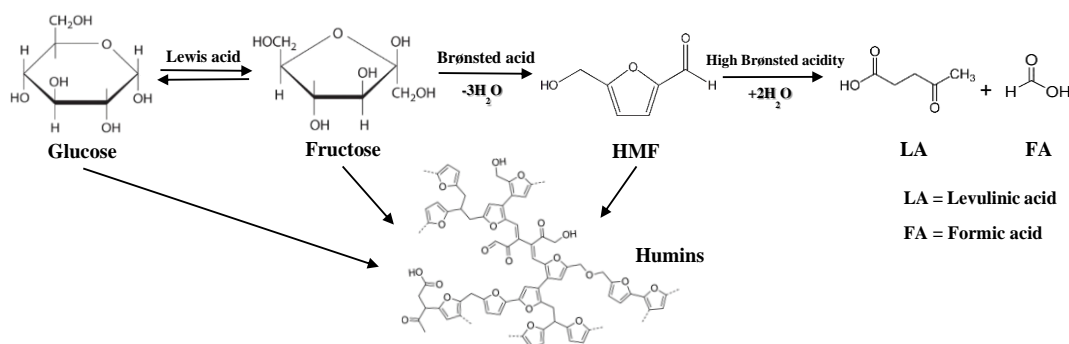


Figure 4.7. Reaction pathways for glucose dehydration to HMF

Effect of mild acid dealumination of H-ZSM-5 zeolite: As earlier stated, the dehydration of glucose without any catalyst was examined to understand the influence of bifunctional heterogeneous catalysts on HMF synthesis. As shown in **Table 4.7**, the yield of HMF was not encouraging (17.1%), while fructose yield remained high (13.2%) at 38.0% glucose conversion. The introduction of commercial H-ZSM-5 into the reaction increased glucose conversion and HMF yield significantly to 97.8% and 59.6%, respectively. The combined Lewis and Brønsted acid centers of the commercial zeolite actively promoted the isomerization and dehydration steps, respectively. Moreover, the bifunctional nature of the catalyst suppressed pentose intermediate formation as deduced from a low furfural yield (less than 1%). No trace of fructose and levulinic acid was detected. Meanwhile, a high amount of humins and other by-products (soluble oligomers) was observed, as deduced from the dark brown color of the spent catalyst and the reaction mixture. A high amount of polymeric products in the reaction suggests that the acid properties of the commercial H-ZSM-5 needed optimization for more efficient synthesis of HMF.

Table 4.7. Glucose dehydration^a over commercial and dealuminated H-ZSM-5 catalysts.

Catalyst	Glucose conversion (%)	Yield (%)				
		Fructose	LA	HMF	Furfural	Others ^b
No catalyst	38.0	13.2	1.5	17.1	0.2	5.1
Comm. H-ZSM-5	97.8	0.0	0.0	59.6	0.6	35.6
0.1DeAl.HZSM-5	99.0±1.3	0.4±0.0	0.9±1.1	64.7±0.1	0.8±0.3	30.0±3.5
0.2DeAl.HZSM-5	96.4±2.6	1.2±0.6	6.5±5.6	60.4±0.6	0.8±0.1	25.1±1.4
0.3DeAl.HZSM-5	95.6±2.0	1.5±0.6	2.2±0.1	61.7±0.6	0.8±0.1	27.1±3.3
0.4DeAl.H-ZSM-5	97.3±1.0	1.0±0.1	3.9±2.0	63.1±2.1	0.9±0.0	25.8±5.0

^a Reaction conditions: catalyst loading, 500 mg; glucose concentration, 3.6 wt%; reaction temperature, 170 °C; reaction time, 60 min.

^b Mainly humins

When 0.1DeAl.H-ZSM-5 was used as a catalyst, HMF yield notably increased to 64.7% at a near complete conversion of glucose. As depicted in **Table 4.7**, this result was attributed to an increased content of total acid sites, especially in the strong acidity, from 0.166 mmol/g to 0.224 mmol/g for the commercial and 0.1 M acid-treated zeolite catalysts, respectively. Khumho et al. [110] in their work investigated the catalytic conversion of glucose into HMF with niobium oxides supported on carbon/silica nanocomposite. They found out that the catalyst with the highest amount of strong acid sites gave the highest yield of HMF. Besides, the mild dealumination process reduced the yield of humins by 5.6%. This result should be related to a decreased B/L molar ratio of the commercial zeolite from 7.35 to 2.39 after the dealumination (**Table 4.7**). Yousatit et al. [111] from their work demonstrated that the catalyst with a higher proportion of isomerization active sites was more suitable than that of Brønsted acid sites in the selective synthesis of HMF. This is related to the fact that glucose isomerization to fructose is the rate-determining step [112], and Brønsted acid sites are responsible for the aldol addition and condensation of HMF to humins [113]. It is worth noting that the suitable B/L ratio of the bifunctional catalysts used in the direct conversion of glucose was significantly different from the ones reported in the literature [113–115]. It should be attributed to the difference in other physicochemical properties of the catalysts, such as specific surface area, pore size, and hydrophobicity, as well as the difference in the reaction conditions studied.

The glucose conversion dropped slightly to 96.4%, 95.6% and 97.3% in the presence of 0.2DeAl.H-ZSM-5, 0.3DeAl.H-ZSM-5 and 0.4DeAl.H-ZSM-5 catalysts, respectively. Although the yield of HMF was still maintained at higher than 60%, there was a significant change in the distribution of other products. The outcome of

this result was attributed to the acid properties of the dealuminated catalysts. 0.2DeAl.H-ZSM-5, 0.3DeAl.H-ZSM-5, and 0.4DeAl.H-ZSM-5 exhibited an increased content of weak-to-moderate acidity, while the strong acid sites were reduced (**Table 4.7**). This should lower their catalytic activity in glucose isomerization and fructose dehydration. Obviously, the high B/L ratio observed with the three catalysts was not suitable for higher HMF formation, and in turn, promoted hydrolysis of HMF to levulinic acid. This result is explained by an increased content of weak-acidic silanol groups ($\equiv\text{Si-OH}$) in the zeolites treated with high concentrations, which increased the catalyst hydrophilicity and affinity for water required for the rehydration of HMF to obtain levulinic acid. Due to the high catalytic performance of dealuminated catalysts, reaction conditions were optimized over 0.1DeAl.H-ZSM-5 zeolite to obtain the highest yield of HMF.

4.2.3. Effect of reaction conditions on HMF synthesis over 0.1DeAl.H-ZSM-5 catalyst

Effect of reaction temperature: The acid-catalyzed dehydration of glucose was optimized over 0.1DeAl.H-ZSM-5 from a temperature of 150 – 180 °C to obtain the highest yield of HMF, owing to its superior catalytic performance over the commercial H-ZSM-5 and other acid-treated zeolite catalysts. As shown in **Figure 4.7A**, the glucose conversion and yield of HMF were low, 62.5% and 31.2%, respectively, when the reaction was conducted at 150 °C. The yield of fructose remaining in the solution at this temperature was 15%. It indicates that the energy available in the system was not sufficient for glucose dehydration to HMF. An increase in the reaction temperature to 170 °C drove the glucose conversion to near

completion (>99%) at which the yield of HMF reached 64.7% since the isomerization and dehydration steps are endothermic processes [116,117]. Meanwhile, other by-products formed at low temperatures were reduced above 160 °C, except for humins. It was demonstrated that the formation of humins through the condensation of glucose and/or fructose has comparable activation energy (114–127 kJ/mol) to the fructose dehydration to HMF [119]. Therefore, both catalytic routes are accelerated proportionally at elevated temperatures. Further increasing the temperature above 170 °C enhanced the formation of polymeric products by consuming HMF since there was no glucose and fructose available in the reaction system. Hence, the reaction temperature of 170 °C was selected as the optimum one for screening other reaction parameters.

Effect of reaction time: Since the direct conversion of glucose to HMF is a consecutive reaction process accompanied by various side reactions, the reaction time is an important parameter to control the products' selectivity and enhance the yield of HMF. The effect of reaction time was studied in the range of 40–80 min (**Figure 4.7B**). At 40 min, the HMF yield of 56.1% was obtained at 88.0% glucose conversion, along with the fructose and LA yield of 3.8% and 2.0%, respectively. As the reaction time was prolonged to 60 min, the conversion of glucose jumped to >99% and the yield of HMF was achieved at 64.7%. There was no significant change in the glucose conversion and HMF yield at 80 min, but the distribution of by-products was altered. Atanda et al. [63] reported that the transformation of HMF to humins at a certain temperature was a function of time. Recently, the acid concentration-dependent kinetic study demonstrated that the condensation and polymerization of HMF proceeded at different reaction rates to the rehydration of HMF to levulinic acid [109].

In a strong acid-catalyzed system without any glucose and fructose, the rate of HMF conversion into levulinic acid was larger than that of HMF-derived humins formation. Considering the HMF yield and ease of product separation, the reaction time of 60 min was a suitable period for the HMF synthesis in this study.

Effect of substrate concentration: Primarily, the concentration of substrate not only controls the yield of formed products but also determines the desired product throughput and economic feasibility of the process. In this study, the glucose concentration in the aqueous phase was varied from 3.6–10 wt% (**Figure 4.7C**). It was found that 3.6 wt% of glucose was the suitable substrate concentration by which both the glucose conversion and the HMF yield became the highest values, >99% and 64.7%, respectively. Around 6–9 % of glucose remained in the reaction system once the weight of the substrate was increased above the suitable concentration. The HMF yield dropped, while the humins formation was enhanced, proportionally to the glucose concentration. An increased availability of HMF and other reactive intermediates formed at a high concentration of substrate induced the polycondensation routes to the unwanted oligomers. This result also implied the cause of catalyst deactivation due to various organic compounds depositing on the surface of the zeolite catalyst. Hence, the glucose concentration of 3.6 wt% was suitable for the HMF synthesis in this study.

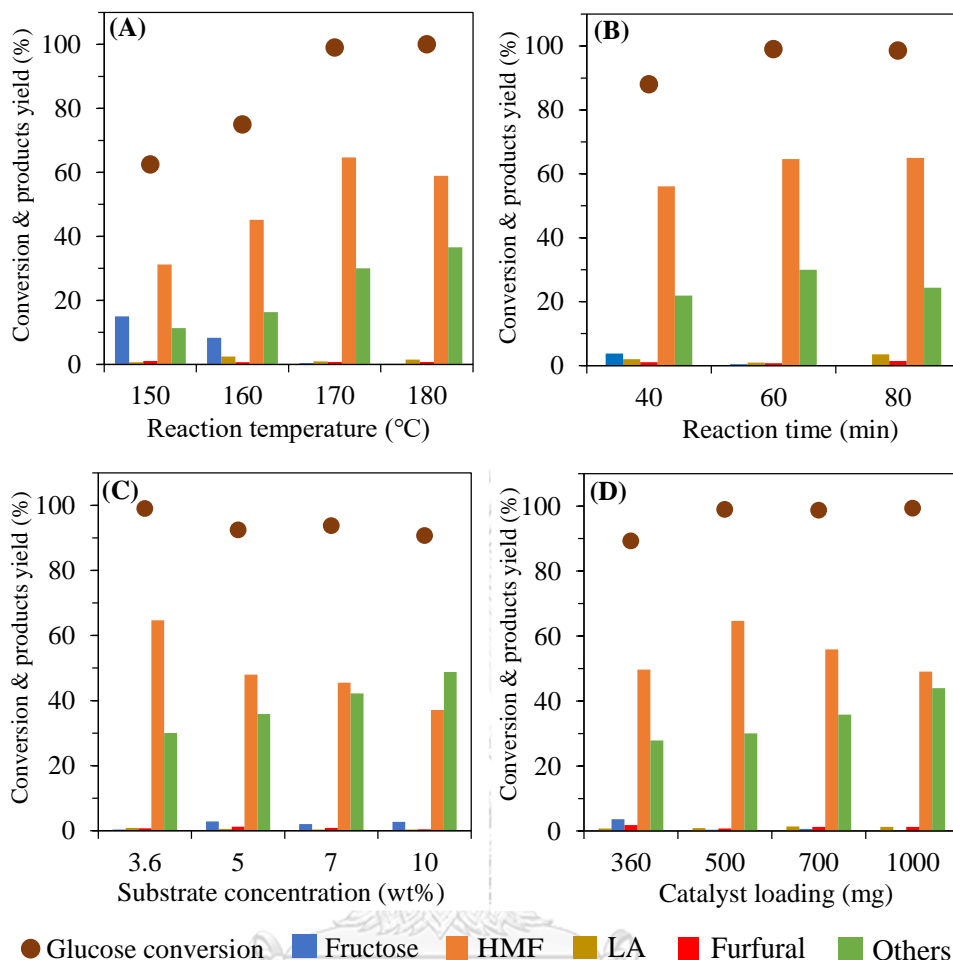


Figure 4.8. Effects of (a) reaction temperature (b) reaction time (c) substrate concentration (d) catalyst loading in the conversion of glucose to HMF over 0.1DeAl.H-ZSM-5 (Central reaction conditions: catalyst loading, 500 mg; glucose concentration, 3.6 wt%; reaction temperature, 170 °C; reaction time, 60 min.

Effect of catalyst loading: Optimizing the catalyst loading level is a facile approach to increase the amount of acid sites responsible for the glucose dehydration, and thus selectively control the HMF formation. When the amount of 0.1DeAl.H-ZSM-5 catalyst in the reaction was extended from 360 mg to 500 mg, the glucose conversion and HMF yield were increased from 89.3% and 49.7% to >99% and 64.7%, respectively. However, using higher levels of catalyst loading deteriorated the HMF

yield concomitantly with an enhanced humins yield. The observed trend was similar to the recent study by Ramesh and co-workers [119]. Zhang et al. [120] found out that the surplus catalyst provided an excess amount of active sites responsible for the HMF hydrolysis and polycondensation to form humins. Based on the result obtained, the loading level of 500 mg was suitable for the direct conversion of glucose into HMF over 0.1DeAl.H-ZSM-5.

4.2.4. Reusability study of 0.1DeAl.H-ZSM-5 catalyst

The reusability of heterogeneous catalysts generally reflects their catalytic stability and potential application for industrial chemical processes. In the direct conversion of glucose to HMF, the acidic catalysts developed so far have suffered from serious deactivation due to the presence of various reactive intermediates and oligomers that competitively adsorbed on the catalyst surface. To verify the reusability of 0.1DeAl.H-ZSM-5 as the suitable catalyst, the spent catalyst recovered from the reaction mixture was thoroughly washed with hot water (~80 °C), and then toluene (twice each). Subsequently, the washed sample was dried at 80 °C overnight, followed by calcination at 500 °C for 4 h to ensure the removal of all organic deposits. Once the regenerated catalyst was reused in the reaction under the optimized conditions, the glucose conversion and HMF yield dropped remarkably from >99% to 60.4% and from 64.7% to 32.0% respectively (**Figure 4.9**). On one hand, this result might be associated with the existence of humins that remained adsorbed on the strong acid sites of the catalyst. On the other hand, some strong acid sites in the form of extraframework aluminum species were removed from the fresh catalyst during the first run. Other organic solvents with different polarities (THF, ethanol, and

isopropanol) were tried in the washing step based on the hypothesis that an increased polarity of solvent could facilitate the removal of oxygenated organic deposits. However, using toluene with the least polarity index gave better results. It is worth noting that the performance of catalysts reused in the second and third cycles was not significantly different from the first reuse. It implied that the change in the characteristics of 0.1DeAl.H-ZSM-5 catalyst occurred just in the first contact with the reaction mixture, and then this catalyst could be reused in the HMF synthesis without noticeable loss of activity. It should be also addressed that the yield of HMF obtained over the reused catalyst was 2-fold higher than the reaction without any catalyst.

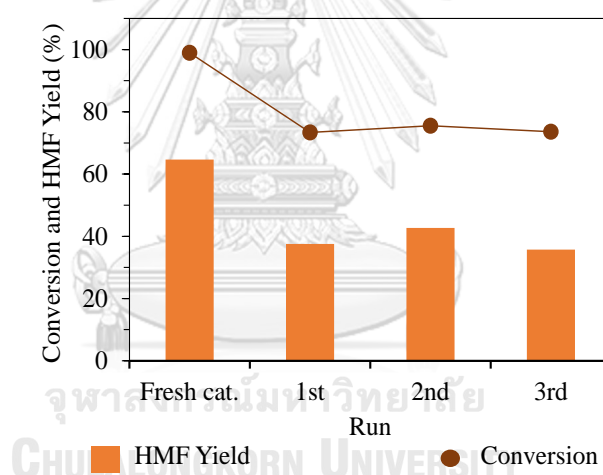


Figure 4.9. Reusability study of 0.1DeAl.H-ZSM-5 in the glucose dehydration to HMF. Reaction conditions: catalyst loading, 5 wt%; glucose concentration, 3.6 wt%; reaction temperature, 170 °C; reaction time, 60 min (except for the 1st–3rd reuse, reaction time was 90 min).

4.2.5. Comparison of the performance of 0.1DeAl.H-ZSM-5 catalyst to other zeolite-based catalysts

The catalytic performance of 0.1DeAl.H-ZSM-5 catalyst was compared to other zeolite-based catalysts in the direct dehydration of glucose into HMF as shown in **Table 4.8**. Based on the results obtained with this catalyst and the literature reported so far, 0.1DeAl.H-ZSM-5 is a good zeolitic catalyst for the synthesis of HMF from glucose, especially in a biphasic solvent system. Compared to large pore zeolites, the MFI zeolite is of great benefit for glucose dehydration to HMF due to its smaller microporous channels that limited the condensation degree of reactive intermediates to oligomers. Several attempts have been made to adjust the total acidity and the B/L ratio of zeolite catalysts through different techniques, such as modified synthesis procedures [73], metal doping [62,74], high-temperature calcination [114]. However, there have been some difficulties to control the distribution, type, and strength of newly generated acid sites. The reaction ended up with an HMF yield of <60 % in most cases. Furthermore, some of these approaches are associated with dangerous chemicals or excessive energy use. The proposed dealumination procedure herein is a simple and effective method for modifying the acid characteristics of commercial H-ZSM-5. Using mild HNO_3 acid solution in the dealumination process increased the content of Lewis acid sites in the resulting acid-treated H-ZSM-5 with the preserved microporous MFI framework and consequently promoted glucose–fructose isomerization.

Table 4.8. Comparison of 0.1DeAl.H-ZSM-5 with other zeolite-based acid catalysts.

Entry	Catalyst	Solvent	Temp. (°C)	Time (h)	Glucose conversion (%)	HMF yield (%)	Ref.
1	H-ZSM-5	NaCl-H ₂ O/THF	160	1.5	94.0	61.0	[67]
2	H-ZSM-5	H ₂ O/Dioxane	120	24	59.4	17.0	[72]
3	H-ZSM-5	H ₂ O/MIBK	195	0.5	80.0	42.0	[66]
4	H-ZSM-5	[BMIM]Cl	130	1	n.d. ^a	15.3	[62]
5	Cr-ZSM-5	[BMIM]Cl	130	1	n.d.	11.2	[62]
6	Cu-Cr-ZSM-5	DMSO	140	4	57.5	50.4	[74]
7	H-Beta-Cal750	H ₂ O-DMSO/THF	180	3	78.0	43.0	[114]
8	Sn-β-F, HCl	NaCl-H ₂ O/THF	190	1.1	90.0	53.0	[73]
9	H-USY	[BMIM]Cl	130	1	n.d.	21.5	[62]
10	0.1DeAl.H-USY	NaCl-H ₂ O/THF	170	1	100	53.1	This work
11	0.1DeAl.H-ZSM-5	NaCl-H ₂ O/THF	170	1	99.0	64.7	This work

^a n.d. means no data.



CHAPTER 5

Glucose dehydration to HMF - Acid dealumination of commercial H-ZSM-5 zeolite and metal incorporation

The acid property of the commercial H-ZSM-5 zeolite was further studied by using both acid treatment and metal incorporation processes to find a suitable acidity (Brønsted & Lewis acidity) needed to selectively synthesize a high yield of HMF from glucose. The commercial zeolite was treated with 0.1 M nitric acid solution, followed by tin impregnation at different weights. The catalysts were appropriately characterized and tested for glucose dehydration to HMF. The results obtained from their characterizations and catalytic tests are discussed below.

5.1. Physicochemical properties of catalysts

After catalysts preparation, the x Sn-modified-acid-treated H-ZSM-5 samples were analyzed with an X-ray diffractometer. Their profiles are presented in **Figure 5.1A**. All the modified samples have a similar diffraction pattern as the commercial H-ZSM-5. With a low and high content of tin, loaded on the surface of dealuminated H-ZSM-5 zeolite, no bulk phase of tin oxide was observed, indicating that the metal was fully dispersed without any structural damage of H-ZSM-5. From the peak enlargement at 2θ angle from 6° to 10° shown in **Figure 5.1B**, the parent peak position was maintained after acid treatment. Following modification with the metal, the peak position shifted moderately to a higher angle at 1 – 3.84 wt% loading, whereas at higher loading, the peak position was maintained. The unit cell values of the acid-treated and tin-modified-acid treated H-ZSM-5 showed that the cell contracted moderately at low loading of the metal, **Table 5.1**. The shift in the diffraction peak is a result of the expansion or contraction of the zeolite framework

that emanated from the diameter difference of the framework T atoms after metal insertion [121]. The relative crystallinity of the commercial and modified samples was determined by their peak intensities at two-theta angles of 7.8° , 8.8° , 22.9° , 23.8° & 24.3° respectively. As summarized in **Table 5.1**, the result showed that the crystal structure of the commercial H-ZSM-5 zeolite was maintained after acid treatment, however, the intensity of the peaks increased at different weights of the metal. This is attributed to the ion-exchange of some extraframework species in the H-ZSM-5 by the acidic metal precursor [122]. Huang et al. demonstrated that the dimension of the metal incorporated could also contribute to the crystallinity effect of the zeolite [123].

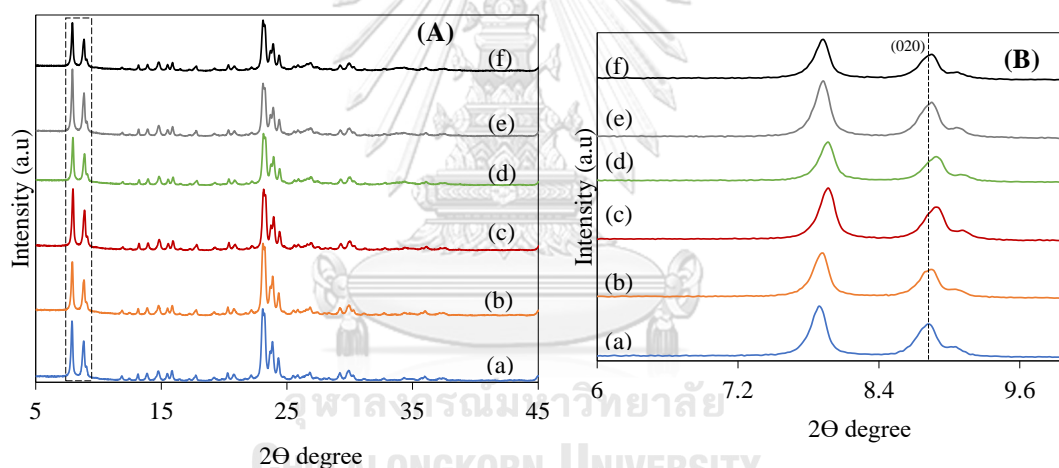


Figure 5.1. (A) Diffraction patterns and (B) peak enlargement of (a) commercial H-ZSM-5 (b) acid-treated H-ZSM-5 (c) 1wt%Sn-0.1DeAl.H-ZSM-5 (d) 3.84wt%Sn-0.1DeAl.H-ZSM-5 (e) 5wt%Sn-0.1DeAl.H-ZSM-5 (f) 7wt%Sn-0.1DeAl.H-ZSM-5

The Si/Al mole ratio of the commercial and modified H-ZSM-5 catalysts was determined by X-ray fluorescence spectroscopy and is presented in **Table 5.1**. As previously explained in Section 1A, the result of the commercial and dealuminated H-ZSM-5 showed that the degree of dealumination occurred slightly after acid

treatment. Meanwhile, the Sn-modified catalysts showed a similar silica-alumina ratio as the acid-treated H-ZSM-5 zeolite, indicating that no notable degree of dealumination occurred after impregnation with the metal precursor solution.

Table 5.1. Textural properties of the commercial and modified catalysts.

Samples	$S_{\text{BET}}^{\text{a}}$ (m^2/g)	$S_{\text{micro}}^{\text{b}}$ (m^2/g)	D_{p}^{c} (nm)	$V_{\text{micro}}^{\text{d}}$ (cm^3/g)	$V_{\text{meso}}^{\text{e}}$ (cm^3/g)	$V_{\text{pore}}^{\text{f}}$ (cm^3/g)	Unit cell $^{\text{g}}$ (\AA)			Si/Al ratio $^{\text{h}}$	Sn $^{\text{i}}$ (wt%)	Rel. Cry. $^{\text{j}}$ [%]
							a	b	c			
Comm. HZ	343	253	2.76	0.133	0.105	0.238	20	20.02	13.46	21.07	-	-
DHZ	377	261	2.78	0.128	0.135	0.263	19.95	19.98	13.46	22.09	-	100
1wt%SDHZ	311	214	3.11	0.113	0.128	0.241	19.91	19.90	13.40	22.4	1.04	179
3.84wt%SDHZ	331	221	2.88	0.117	0.121	0.238	19.89	19.90	13.38	22.11	3.67	207
5wt%SDHZ	307	204	3.12	0.108	0.131	0.239	19.93	19.98	13.42	21.9	4.83	270
7wt%SDHZ	315	210	2.88	0.112	0.115	0.227	19.95	19.98	13.42	22.14	7.09	299

^a surface area obtained by BET method.

^b Surface area of micropore

^c Average pore diameter

^d Micropore volume

^e Mesopore volume ($V_{\text{meso}} = V_{\text{pore}} - V_{\text{micro}}$)

^f Total pore volume

^g Calculated from XRD at lattice plane 040, 200 and 002

^{h-i} Determined by XRF.

^j Relative crystallinity obtained from XRD at 2θ degree (7.8° , 8.8° , 22.9° , 23.8° & 24.3°)

HZ means H-ZSM-5; DHZ means Dealuminated H-ZSM-5; SDHZ mean Sn-0.1DeAl.H-ZSM-5

The result obtained from the nitrogen physisorption analysis is shown in **Table 5.1**.

The textural properties of the commercial zeolite moderately increased after acid treatment. The BET surface area of the commercial zeolite increased by $34 \text{ m}^2/\text{g}$ while its pore volume increased by $0.025 \text{ cm}^3/\text{g}$ and more mesopores were created. The zeolite's textural properties subsequently decreased after metal incorporation, possibly due to the accumulation of the metal on the zeolite's surface. This

observation is consistent with the work of Oozeerally et al. [124] and Gautham et al. [125]. The nitrogen physisorption isotherms of the commercial and modified H-ZSM-5 catalysts are shown in **Figure 5.2**. The adsorption-desorption isotherms of all the catalysts follow a type I isotherm, attributed to a microporous material exhibiting mesopore. The mesopore observed with the commercial H-ZSM-5 at $P/P_0 > 0.45$ is related to the interparticle space (or void) located in the zeolite particle and or particle agglomerates. The mesopore however decreased after tin incorporation indicating that some secondary pore systems were blocked by tin species after impregnation.

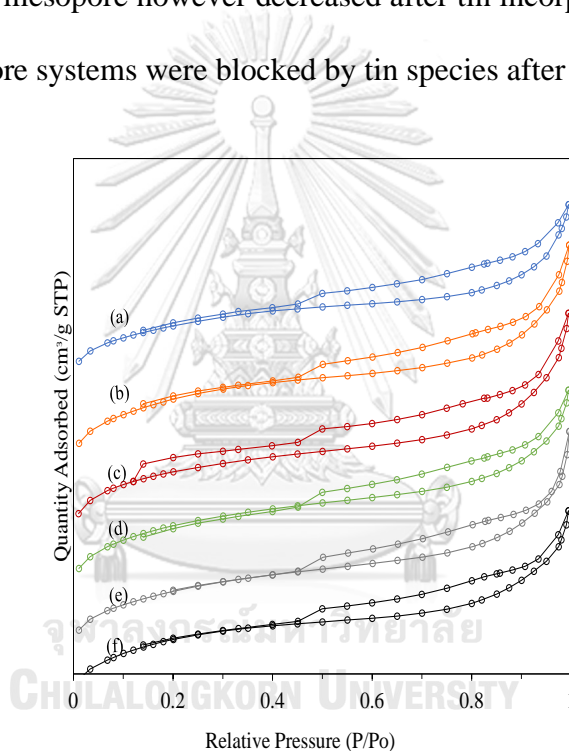


Figure 5.2. N_2 physisorption isotherms of (a) commercial H-ZSM-5 (b) acid-treated H-ZSM-5 (c) 1wt%Sn-0.1DeAl.H-ZSM-5 (d) 3.84wt%Sn-0.1DeAl.H-ZSM-5 (e) 5wt%Sn-0.1DeAl.H-ZSM-5 (f) 7wt%Sn-0.1DeAl.H-ZSM-5

The results of the FE-SEM image of the commercial and modified catalysts are shown in **Figure 5.3**. The commercial H-ZSM-5 and the acid-treated H-ZSM-5 exhibit a typical nanoparticle agglomerate with a rectangular-shaped morphology. The surface

of the zeolite became rougher after the metal was incorporated and the degree of agglomeration of primary particles increased at higher loading of the metal. The change noted in the textural properties of the x wt%Sn-0.1DeAl.H-ZSM-5 catalysts could be due to this observation.

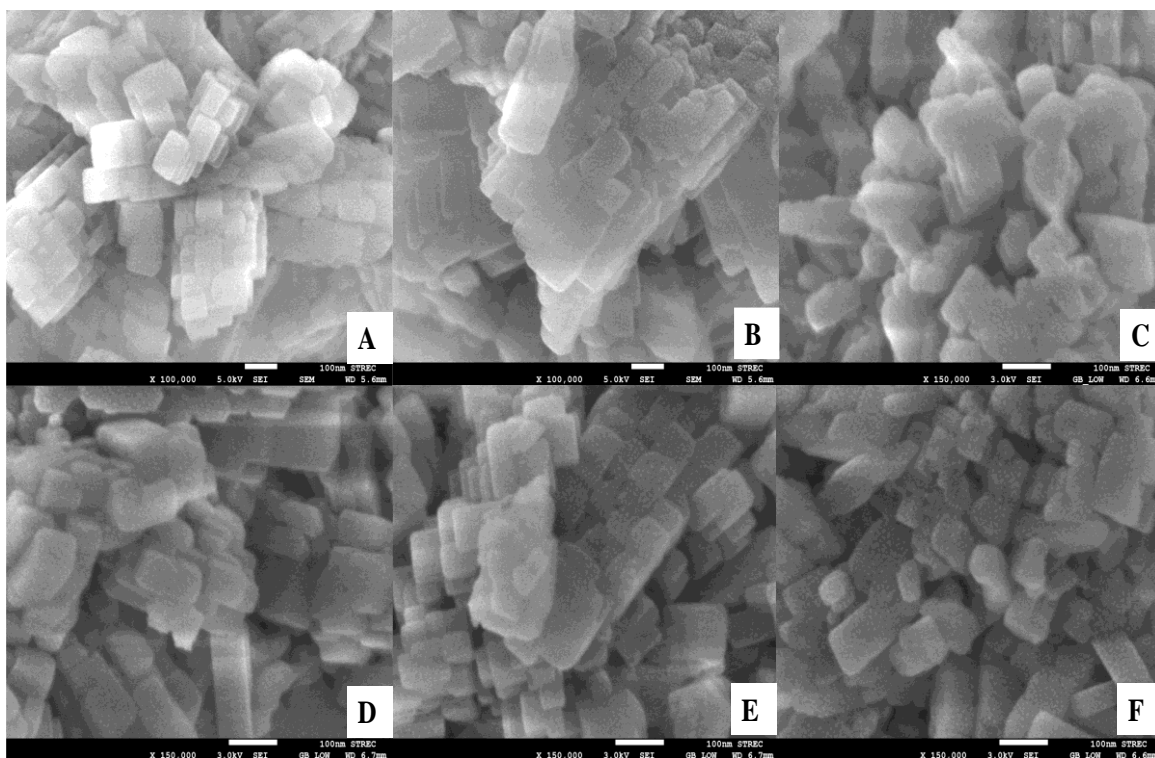


Figure 5.3. SEM images of (A) commercial H-ZSM-5 (B) acid-treated H-ZSM-5 (C) 1wt%Sn-0.1DeAl.H-ZSM-5 (D) 3.84wt%Sn-0.1DeAl.H-ZSM-5 (E) 5wt%Sn-0.1DeAl.H-ZSM-5 (F) 7wt%Sn-0.1DeAl.H-ZSM-5.

The coordination of tin species in the H-ZSM-5 frameworks, analyzed by UV-vis near-infrared spectroscopy, is shown in **Figure 5.4**. Absorption bands were observed at a wavelength of 231 nm, and 271 nm with a shoulder at 201 nm, and are characteristic frameworks of zeolite [124,130,131]. The absorption bands at a shoulder of ca. 201 nm and 231 nm are characteristic of catalytic active species in the

tetrahedral environment, while the band at ca. 271 nm is attributed to extraframework coordinated species [132]. From **Figure 5.4**, after acid treatment, the intensity of the commercial H-ZSM-5 spectrum at the tetrahedral position (ca. 231 nm) slightly increased due to the hydrolysis/ion exchange process in the zeolite framework. From the acid-treated H-ZSM-5 spectrum, the peaks at bands 231 nm and 271 nm are all sharp, with a shoulder at ca. 201 nm. After metal incorporation, the peak intensity of the band at 201 nm slightly extended in the shoulder, while the peak intensity of the bands at 231 and 271 nm was well broadened. This implies that some isolated Sn^{4+} atoms were successfully incorporated as framework coordination and also at the extraframework sites [125]. The extraframework tin species could also occur as Sn-O-Sn coordination group in the zeolite [94,124]. No peak was observed at 340 nm, which is a characteristic absorption band for SnO_2 species [125,133].

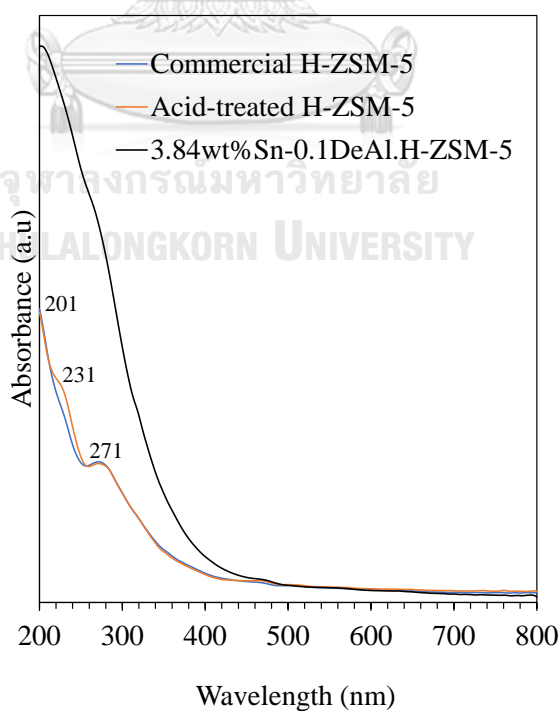


Figure 5.4. UV-visible spectra of commercial and modified catalysts.

The result obtained from ammonia temperature-programmed desorption analysis for all the catalysts is shown in **Table 5.2** and **Figure 5.5A**. The commercial zeolite possessed a weak, moderate, and strong acidity of 0.735 mmol/g, 0.233 mmol/g, and 166 mmol/g respectively, with an overall acidity of 1.134 mmol/g. After acid treatment, the weak acidity of the commercial zeolite slightly decreased from 0.735 mmol/g to 0.711 mmol/g, whereas its moderate, and strong acidity moderately increased, having an overall acidity of 1.189 mmol/g. The partial hydrolysis of alumina clusters as well as the zeolitic framework in H-ZSM-5 after acid treatment resulted in an increased silanol group which contributed to the increased acidity. From the NH₃-TPD profiles shown in **Figure 5.5A**, after tin incorporation, the acid strength of the dealuminated zeolite shifted to a lower desorption temperature, up to 5 wt% of the metal loading, implying that the strong acid sites were suppressed, and the tin atoms were mostly incorporated as weak acid sites (WAS). As computed in **Table 5.2**, at 1 wt% of the metal loading, the weak acidity of the dealuminated H-ZSM-5 zeolite notably increased from 0.711 mmol/g to 0.743 mmol/g, whereas the moderate and the strong acidity decreased with a decreased total acidity. Saenluang et al. [72] synthesized Sn- β zeolite and reported a decrease of 12.1% in the overall acidity of β -zeolite at a low weight of tin incorporation. The weak acidity significantly increased to 0.962 mmol/g when 3.84 wt% of the metal was loaded, with increased total acidity. Meanwhile, the moderate acidity slightly decreased while the strong acid sites (SAS) were significantly suppressed, implying that most of the tin atoms loaded at 3.84 wt% were also incorporated as weakly acidic sites. Strong acid site emanates from the interaction of aluminum atoms with the framework -OH group of zeolites [96]. Most of the tin species were incorporated as extraframework species, as evident from the

UV-vis spectroscopy in **Figure 5.4**. Subsequent loading of the metal at 5 wt% caused the weak, moderate, and strong acidity to decrease. Further loading at a higher weight (7 wt%) increased the weak acidity slightly by 0.006 mmol/g, but not the moderate and strong acidity. The total acidity at higher weights of the metal was obviously lowered. Song et al.[126] reported that the strength of zeolite acid site could be weakened at increasing concentrations of the tin precursor solution. At higher concentrations of the metal loading, increased accumulation of the tin species might have blocked some acid sites of the catalyst resulting in lowered acidity. This feature can however be controlled at a suitable proportion of metal loading.

The acid density in **Table 5.2** measures the acidity of the tin-modified catalysts per unit surface area. The acid density of the commercial H-ZSM-5 was lowered after acid treatment, due to hydrolysis/ion exchange process. Meanwhile, the acid density of acid-treated zeolite moderately increased after tin incorporation. 3.84wt%Sn-0.1DeAl.H-ZSM-5 possessed the highest acid density.

Table 5.2. Distribution of acid sites for commercial and modified catalysts from NH₃-TPD analysis.

Catalysts	Acid site distribution (mmol/g) ^a				Nature of acid site (mmol/g) ^b			Acid density ^c (mmol/m ²)
	Weak	Moderate	Strong	Total	L	B	B/L ratio	
Comm. HZ	0.735	0.233	0.166	1.134	0.020	0.176	7.35	3.31
DHZ	0.711	0.255	0.224	1.189	0.109	0.261	2.39	3.15
1wt%SDHZ	0.743	0.191	0.121	1.055	n.d	n.d	n.d	3.40
3.84wt%SDHZ	0.962	0.186	0.189	1.336	0.045	0.106	2.37	4.04
5wt%SDHZ	0.705	0.196	0.148	1.049	n.d	n.d	n.d	3.42
7wt%SDHZ	0.717	0.207	0.149	1.073	n.d	n.d	n.d	3.40
Regen. catalyst ^d	0.993	0.387	0	1.380	n.d	n.d	n.d	n.d

^a Determined by NH₃-TPD (Weak: 50 – 200 °C, Moderate: 200 – 350 °C, Strong: 350 – 500 °C)

^b Determined by Py-FTIR (L – Lewis acid, B – Brønsted acid)

^c Acid density = Total acidity / S_{BET}

^d regenerated 3.84wt%Sn-0.1DeAl.H-ZSM-5 catalyst after 4th reaction run

n.d – not determined

HZ means H-ZSM-5; DHZ means dealuminated H-ZSM-5; SDHZ means Sn-0.1DeAl.H-ZSM-5; Regen. means regenerated

The results obtained from the *in-situ* FTIR study and *in-situ* FTIR of pyridine adsorption are shown in **Figures 5.5B & C**. The Brønsted and Lewis acid content of the commercial H-ZSM-5, acid-treated H-ZSM-5, and 3.84wt%Sn-0.1DeAl.H-ZSM-5 zeolite were determined and quantified, **Table 5.2**. The bands at 1455 cm⁻¹, 1545 cm⁻¹, and 1490 cm⁻¹ correspond to the adsorption of pyridine that took place at the Lewis acid center, Brønsted acid center, and both Lewis and Brønsted acid center of the catalysts, respectively, at a degas temperature of 150 °C. The commercial H-ZSM-5 exhibits a Lewis acidity of 0.020 mmol/g, Brønsted acidity of 0.176 mmol/g, and a

B/L acid ratio of 7.35. After acid treatment with the commercial zeolite, the Lewis and Brønsted acid content increased by 5.45-fold and 1.5-fold and gave a significant adjustment to the B/L acid ratio, **Table 5.2**. The result of the *in-situ* FTIR studies shows that all three (3) samples have a distinct absorption band at 3680 cm^{-1} , and 3740 cm^{-1} . These bands are attributed to the extraframework hydroxyl group and silanol group ($\equiv\text{Si-OH}$) in the zeolite frameworks [104, 127]. The silanol group of the commercial zeolite increased after acid treatment as a result of the partial hydrolysis of alumina clusters in the zeolitic framework. This feature gave rise to the increased Brønsted and Lewis acidity respectively.

Following metal insertion on the acid-treated zeolite (at 3.84 wt%), the content of Lewis and Brønsted acid decreased significantly (by 2.4-fold for the former, and 2.5-fold for the latter). The decrease observed proportionally contributed to a lower B/L acid ratio. Tin interaction with framework T atoms is known to induce strong Lewis acidity. Meanwhile, tin inserted at the extraframework sites coupled with the terminal Sn-OH is known to induce Brønsted acidity in zeolite [128,129]. However, the intrinsic properties of the medium pore MFI zeolite could, however, counter this effect [125]. From **Figure 5.5C**, it is clearly seen that the bands for the silanol and the extraframework hydroxyl group of this catalyst were all weakened after metal insertion, implying that Sn condensed with Si-OH groups to form Si-O-Sn linkages which resulted in the decreased content of the Lewis and Brønsted acidity observed (**Table 5.2**).

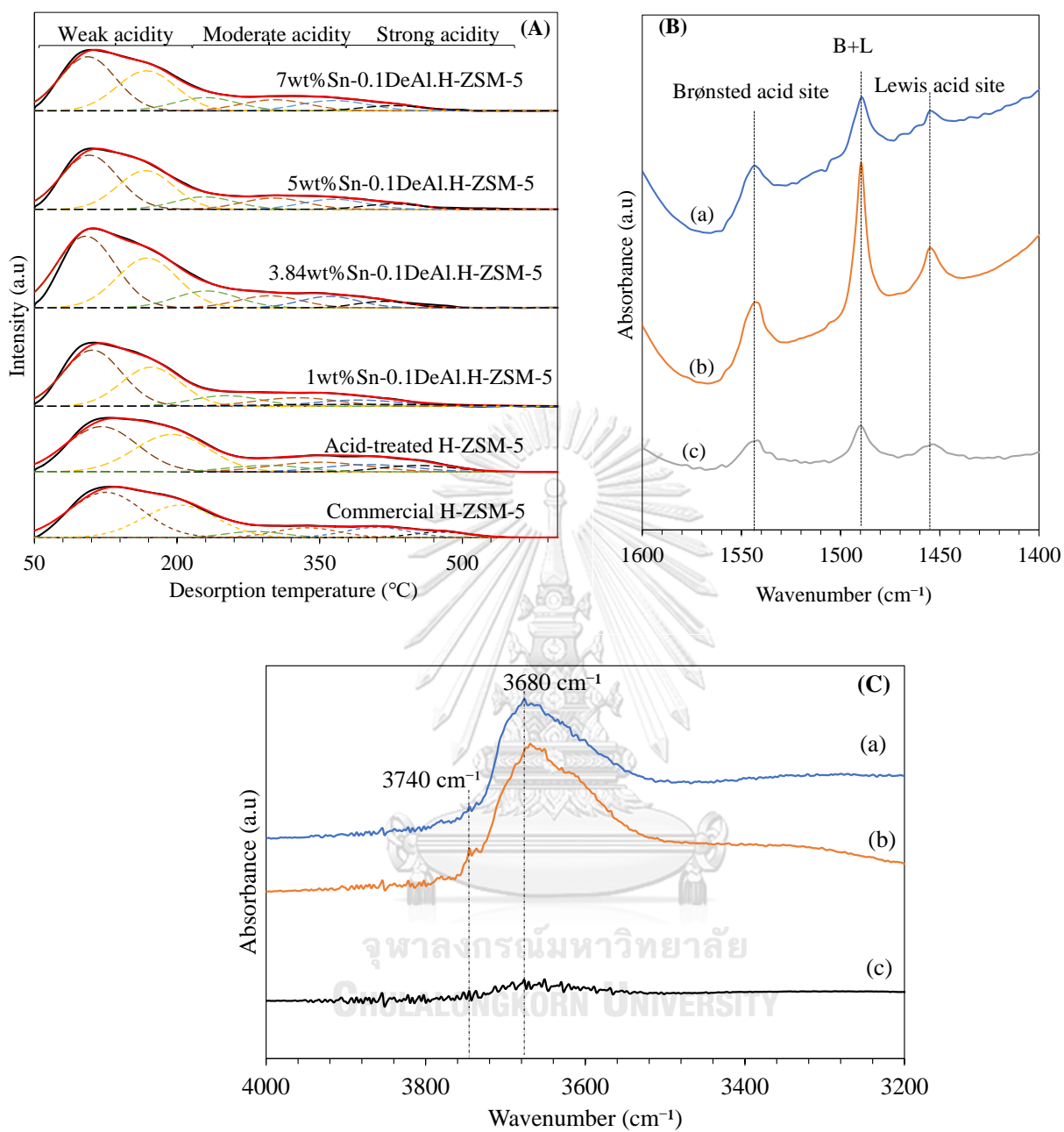


Figure 5.5. (A) deconvoluted TPD Profile of all catalysts (B) Py-FTIR spectra and (C) FTIR study of (a) commercial H-ZSM-5 (b) acid-treated H-ZSM-5 (c) 3.84wt% Sn-0.1DeAl.H-ZSM-5 catalysts.

5.2. Effect of tin incorporation with acid-treated H-ZSM-5 zeolite on glucose dehydration to HMF

The results obtained with different weights of tin on the acid-treated H-ZSM-5 zeolite for glucose dehydration to HMF are shown in **Table 5.3**. Glucose conversion decreased progressively with all weights of the metal used (1 – 7 wt%). At 1 wt% metal loading, the yield of HMF was similar to that of the commercial zeolite but the selectivity of HMF slightly increased, and humins/other byproducts reduced.

When the metal was loaded at 3.84 wt%, the yield and selectivity of HMF increased, with a lower formation of other byproducts. The improved HMF selectivity is attributed to the high acid density possessed by this catalyst. At higher weights of the metal insertion, the yield and selectivity of HMF dropped progressively. The decreased conversion observed with all metal weights used is associated with the agglomeration that occurred on the zeolite covering the active sites [126] while the trend in the decreased HMF yield (at 5 – 7 wt%) and the increased fructose trend (1 – 7 wt%) is a result of limited accessibilities to Brønsted active sites of the catalysts. Levulinic acid yield, a product from HMF's rehydration, varies from 1 - 1.6% while furfural yield was observed from 0 – 1% for all weights. The formation of other byproducts decreased with all metal weights. Song et al. [126] and Ordonsky et al. [134] demonstrated that a strong correlation exists between zeolite's ability to catalyze glucose dehydration to HMF and the nature of their acidities. Therefore, 3.84wt%Sn-0.1DeAl.H-ZSM-5 exhibited a suitable acidity and showed a good catalytic performance towards HMF synthesis.

Table 5.3. Glucose dehydration^a to HMF over commercial and Sn-modified acid-treated H-ZSM-5 catalysts

s/n	Sample	Conversion [%]	Fructose Yield [%]	LA Yield [%]	HMF [%]		Others ^b [%]
					Yield	Selectivity	
1	Comm. HZ	97.8	0.0	0.0	59.6	61.0	35.6
2	1wt%SDHZ	93.7±3.3	1.9±0.8	1.2±1.0	58.8±1.0	62.5±0.7	28.2±3.2
3	3.84wt%SDHZ	83.9±0.1	3.2±0.6	1.5±0.2	62.3±1.9	74.3±2.1	14.1±3.0
4	5wt%SDHZ	81.7±4.3	3.5±0.8	1.6±0.6	53.6±5.7	68±0.00	18.7±0.1
5	7wt%SDHZ	79.2.09±8.2	4.1±1.8	1.0±0.0	49.26±6.8	62.5±2.1	21.6±3.2

^a Reaction conditions: catalyst loading, 250 mg; glucose concentration, 3.6 wt%; reaction temperature, 170 °C; reaction time, 60 min; Pressure, 10 bar N₂ gas.

^b Mainly humins

HZ means H-ZSM-5; DHZ means dealuminated H-ZSM-5; SDHZ means Sn-0.1DeAl.H-ZSM-5

5.3. Effect of reaction conditions on HMF synthesis over 3.84wt%Sn-0.1DeAl.H-ZSM-5 catalyst

Effect of reaction temperature and time: The effects of reaction temperature and time were systematically studied for efficient dehydration of glucose to HMF with the modified catalyst. It has been widely demonstrated that energy consumption and length of reaction are crucial for the conversion of hexose sugars to HMF [135]. The reaction was carried out from a range of temperature of 160 – 180 °C at a fixed reaction time. Subsequently, the reaction was conducted from 40 – 80 min after a suitable temperature was obtained.

As depicted in **Figure 5.6A**, the conversion of glucose significantly increased from 68.7% to 99% as the reaction temperature was increased from 160 – 170 °C, which was favorable for more HMF formation, obtaining an increased yield of 62.3% from 52%. Fructose dehydration notably accelerated as the temperature was increased from 160 – 180 °C.

By extending the temperature further (at 180 °C), the yield and selectivity of HMF dropped to 56% and 55% respectively. Other by-products (mainly humins) were notably high in this medium. It was also clearly observed in the organic phase of the reaction mixture and in the color of the spent catalyst. It implies that high temperature accelerated unwanted product formation through polymerization and or condensation routes by consuming HMF to form humins or soluble oligomers. This outcome is consistent with the work of Song et al. [126] who demonstrated that higher temperatures deteriorate the yield of HMF to humins formation. The yield of levulinic acid was found between 1.4% to 1.7% as the reaction temperature increased from 160 – 180 °C while furfural was seen in traces (<0.7%).

Figure 5.6B shows the results obtained when the reaction time was optimized. The conversion of glucose increased from 80% to 88% as the reaction time was increased from 40 to 80 min. HMF yield and its selectivity increased from 57% and 71% to 62.3% and 74.3% for the first 20 min interval from 40 min. Meanwhile, no notable change in the yield and selectivity of HMF when the time was increased further, whereas byproducts distribution changed. Levulinic acid yield was found between 1.5 – 3% as the reaction time progressed. Furfural as a byproduct was seen in traces

(<1%). By considering HMF yield and selectivity, 60 min reaction time was chosen as the suitable period for the synthesis of HMF in this study.

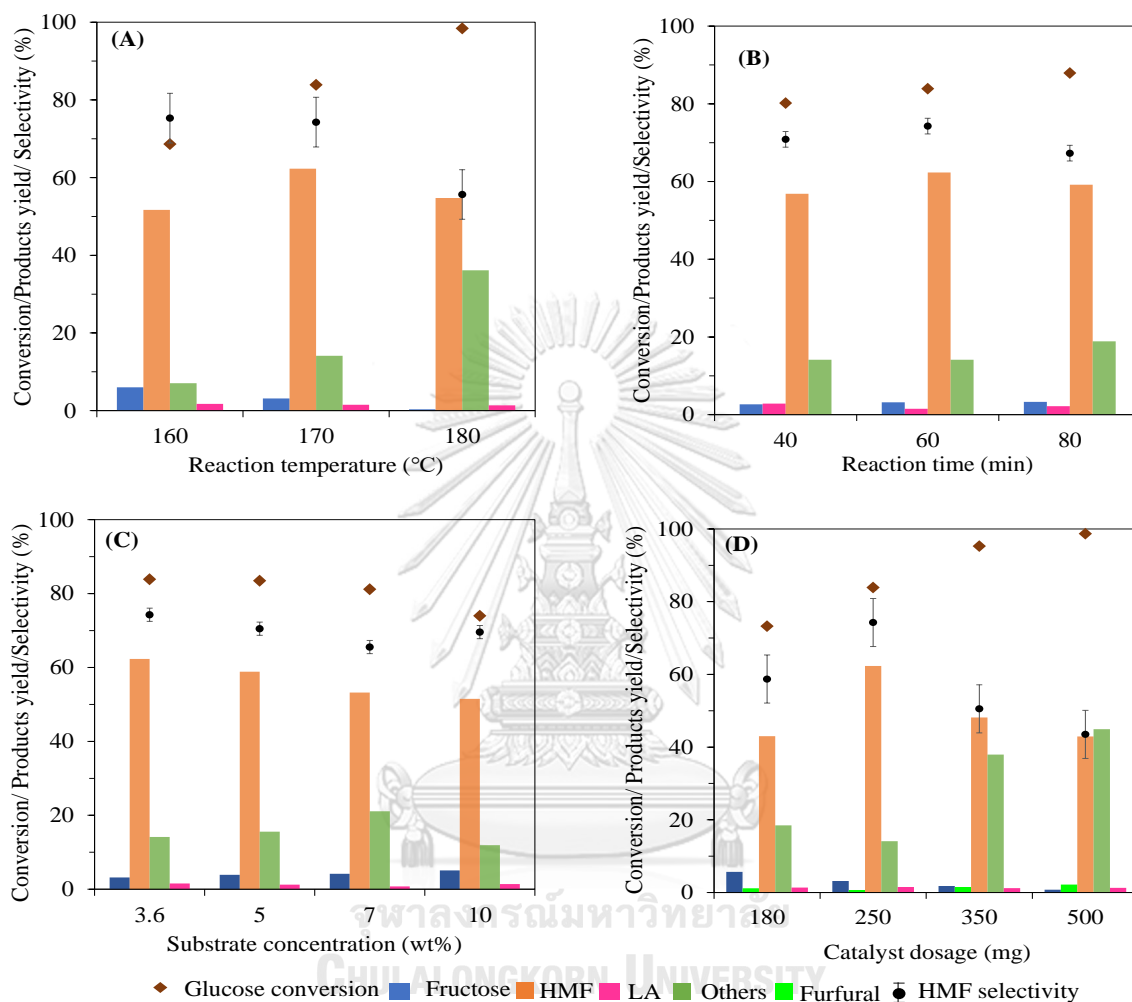


Figure 5.6. Effects of (a) reaction temperature (b) reaction time (c) substrate concentration (d) catalyst dosage in glucose dehydration to 5-hydroxymethylfurfural over 3.84wt%Sn-0.1DeAl.H-ZSM-5 (Central reaction conditions: catalyst loading, 250 mg; glucose concentration, 3.6 wt%; reaction temperature, 170 °C; reaction time, 60 min).

Effect of substrate concentration: Studies were carried out by using 3.6 – 10 wt% of the substrate concentration. As shown in **Figure 5.6C**, 3.6 wt% substrate concentration gave the highest conversion, HMF yield, and selectivity (84%, 62.3%,

and 74.3%). Subsequent studies with higher concentrations caused a decline in the conversion, yield & selectivity of HMF. A high amount of the substrate concentration in the reaction system was more than what the catalyst required, and the limited amount of the active sites (Brønsted and Lewis acid sites) slowed down the isomerization and dehydration rate. Hence, the trend of the decrease observed with glucose conversion and the increase observed with fructose yield. Side reactions were also accelerated at higher concentrations, giving rise to a darker polymeric product known as humins or soluble oligomers. The yield of levulinic acid and furfural varies from 0.8 – 1.4% as the substrate concentration was increased from 3.6 – 10 wt%. From this study, 3.6 wt% of substrate concentration was selected as optimum for further study.

Effect of catalyst dosage: Glucose conversion and HMF yield were studied with different catalyst dosages, ranging from 180 – 500 mg, as shown in **Figure 5.6D**. The conversion of glucose increased from 73% to 99% as the catalyst weight was increased from 180 – 500 mg, implying that the Lewis acid amount increased as the catalyst dosage increased. Fructose dehydration was simultaneously accelerated as the dosage increased. HMF yield and selectivity increased from 43% and 59% to 62.3% and 74.3% as the catalyst weight was increased from 180 – 250 mg. Subsequent loading at a higher dosage (350 – 500 mg) caused HMF yield and selectivity to drop. Higher catalyst dosage in the system deteriorated the yield of HMF simultaneously and enhanced humins generation. Levulinic acid and furfural yield varies from 0.7 – 2% as catalyst dosage increased. Based on these outcomes, 250 mg of catalyst dosage was suitable for HMF synthesis for glucose conversion.

5.4. Reusability study of 3.84wt%Sn-0.1DeAl.H-ZSM-5 catalyst

The reusability of the catalyst was done following the procedure reported in **Chapter 4**. However, the catalytic result of the regenerated catalyst under optimized reaction conditions was not encouraging, achieving a glucose conversion and HMF yield of 46% and 26.68% respectively. The reduced catalytic performance may be associated with polymeric humins that remain adsorbed on the strong acid sites of the catalyst or as a result of metal leaching [126].

To achieve high catalytic performance as the freshly prepared catalyst, the reaction temperature was raised to 190 °C for the regenerated catalyst, keeping all other reaction parameters constant. From **Figure 5.7**, the conversion of glucose was greatly enhanced (~99%) with the regenerated catalyst at a slight increase in HMF yield (~33%). Meanwhile, the selectivity was very low (at 33.5%) with a high content of humins/other by-products. Glucose conversion was maintained around ~98% while the yield and selectivity of HMF increased progressively after the 4th run, reaching an HMF yield of 62.34% at a selectivity of ~64%. Other byproducts notably decreased following each run. It implies that the catalyst characteristics changed during contact with the reaction mixture at each run. The total acid content of the regenerated catalyst after the 4th reaction run notably increased, as summarized in **Table 5.2**.

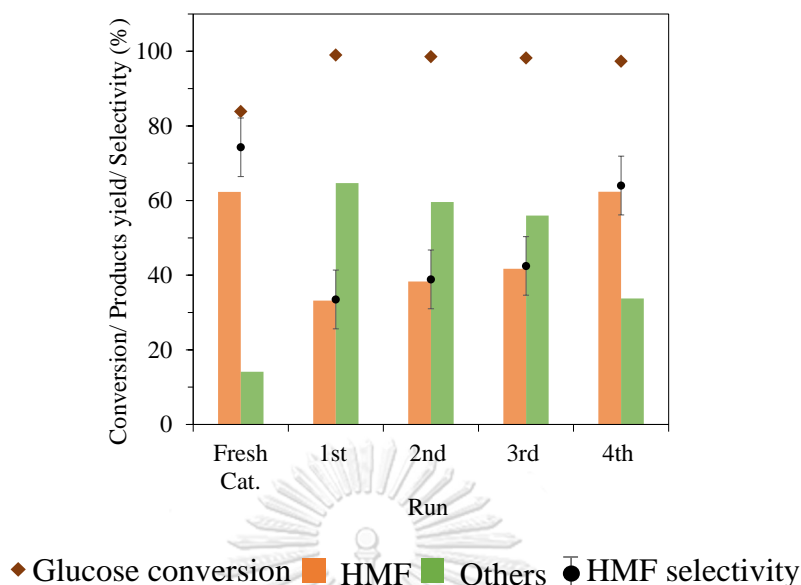


Figure 5.7. Reusability study of 3.84wt%Sn-0.1DeAl.H-ZSM-5 catalyst for glucose conversion to HMF. Reaction conditions: catalyst loading, 5 wt%; glucose concentration, 3.6 wt%; reaction temperature, 170 °C (excluding 1st – 4th reuse, reaction temperature was 190 °C); reaction time, 60 min.

5.5. Catalyst stability and deactivation study

The x-ray diffraction patterns of the fresh and the regenerated 3.8wt%Sn-0.1DeAl.H-ZSM-5 catalyst are shown in **Figure 5.8**. The crystal structure of the catalyst was preserved after the fourth reaction run at 190 °C, which implies that the stability of the catalyst was maintained.

NH₃-TPD analysis of the regenerated catalyst after the 4th reaction cycle (**Table 5.2**) revealed that the strong acid sites of the catalyst disappeared. This implies that metal leaching occurred in the reaction mixture. The weak and moderate acid sites increased from 0.962 and 0.186 mmol/g to 0.993 and 0.387 mmol/g with a total acidity of 1.380 mmol/g. Some catalytic active species might have been superficially hydrolyzed

during the course of the reaction, which increased the acid content [147]. In addition, the ion exchange of protons present in the catalyst with sodium ions from the salt solution could also have shifted the catalyst's acidity. The formation of other byproducts (humins) decreased progressively, **Figure 5.8**. This indicates that the degree of catalyst deactivation was suppressed.

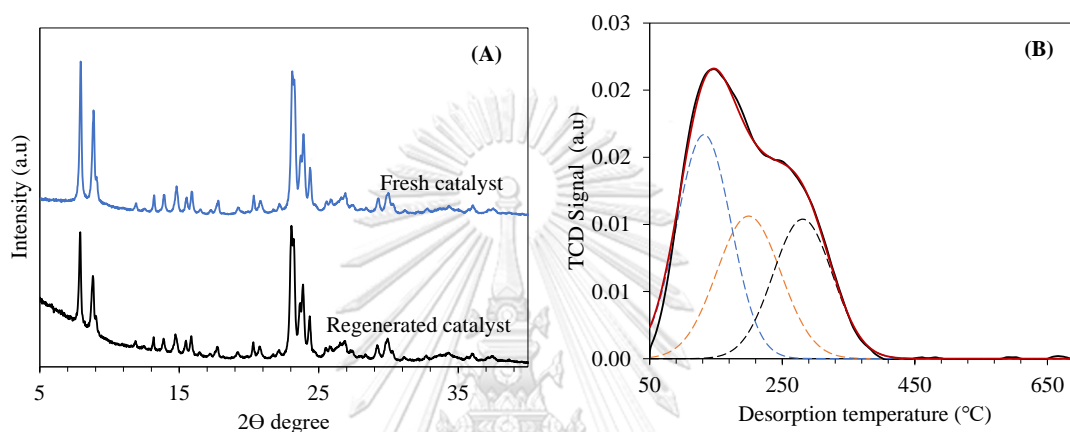


Figure 5.8. (A) XRD patterns of fresh and regenerated catalysts (B) NH_3 -TPD profile of regenerated catalyst.

5.6. Comparison of the performance of the 3.84wt%Sn-0.1DeAl.H-ZSM-5 catalyst to other zeolite-based catalysts

The catalytic activity of 3.84wt%Sn-0.1DeAl.H-ZSM-5 was compared to other metal-containing zeolite catalysts, as shown in **Table 5.4**. Based on the literature reported so far and our results, 3.84wt%Sn-0.1DeAl.H-ZSM-5 exhibited superior catalytic performance for selective synthesis of HMF from glucose under a biphasic solvent system. Several procedures were utilized by other researchers to introduce the metal into the frameworks of zeolites with the aim of adjusting the distribution of the acid sites and B/L acidities. Some of the methods used include the incipient wetness technique [124], solid-state ion exchange method [92,94], solid-gas reaction [143] wet

impregnation technique [7,126], *in-situ* hydrothermal procedures [72]. However, most of these procedures come along with some demerits such as high degree of agglomeration after metal insertion, limiting diffusion rates and acid distributions. Meanwhile, in most of the cases, HMF selectivity was achieved at <72%. Our study pointed out that, mild dealumination of zeolite and tin insertion via excess water impregnation could lower the degree of metal agglomeration. Using excess water impregnation with the tin precursor resulted in a decreased content of Lewis and Brønsted acid sites of the catalyst which aided the suitable B/L acidity needed for glucose dehydration to HMF significantly.

Table 5.4. Comparison of 3.84wt%Sn-0.1DeAl.H-ZSM-5 with other zeolite-based acid catalysts.

Entry	Catalyst	Solvent	Temp. (°C)	Time (h)	Glucose conversion (%)	HMF Yield (%)	HMF Selectivity (%)	Ref.
1	Sn-deAl-HY	DMSO	140	3	70	22.0	n.d	[124]
2	Sn-Beta-HCl	Water-THF/NaCl	180	1.1	79	56.9	72.0	[94]
3	Sn-Beta	Water-Dioxane	120	24	98.4	42.0	42.7	[72]
4	Hier-Sn-0.06-Beta	DMSO/THF	160	2.5	99	41.6	42.0	[143]
5	Sn-SAPO-34	NaCl-H ₂ O/THF	150	1.3	98.5	64.4	n.d	[126]
6	Sn-Mon	THF/DMSO	160	3	98.4	53.5	n.d	[7]
7	Sn-Al-Beta-4-8	[C4MIM]Cl	120	2	81	54.0	n.d	[102]
8	Cr-ZSM-5	[BMIM]Cl	130	1	n.d.	11.2	n.d	[62]
9	Cu-Cr-ZSM-5	DMSO	140	4	57.5	50.4	n.d	[74]
10	3.84wt%SDHB	H ₂ O-NaCl/THF	170	1	77.9	51.3	65.9	This work
11	3.84wt%SDHZ	H ₂ O-NaCl/THF	170	1	84	62.3	74.3	This work

^a n.d. means no data.

SDHB means Sn-0.1DeAl.H-Beta; SDHZ means Sn-0.1DeAl.H-ZSM-5

CHAPTER 6

Cellulose conversion to HMF

The part was carried out in four distinct steps.

- ❖ First, a preliminary study was conducted to determine the catalytic performances of the commercial zeolites under a reaction temperature of 170 °C.
- ❖ Second, further investigation was conducted to determine the catalytic efficiency of the commercial zeolites and their similar modified forms at a higher temperature.
- ❖ Third, the best zeolite from the second step was then selected for further study through metal modification procedure and tested for cellulose conversion to HMF.
- ❖ Finally, the reaction conditions over the best-modified zeolite catalyst were optimized, and optimum reaction conditions were determined.

6.1. Preliminary study of the catalytic performance of commercial zeolites under a reaction temperature of 170 °C.

Studies were conducted without a catalyst and with the three commercial zeolites for cellulose conversion to HMF under a reaction temperature of 170 °C, as shown in **Table 6.1**. The results obtained with cellulose conversion and HMF yield using the three commercial zeolite catalysts were very low. The parent H-USY gave the lowest catalytic performance in this medium. This could be attributed to the lowest acid strength of H-USY compared to the other zeolites. Moreover, it could also be related to

the energy supplied that was not capable of breaking down cellulose units even with the presence of the catalytic acid sites. Based on these results, the reaction was further conducted at 190 °C to further evaluate their performances.

Table 6.1. Preliminary study^a of commercial zeolites for cellulose conversion to HMF at 170 °C.

Entry	Sample	Cellulose conversion (%)	Products Yield [%]					HMF selectivity (%)
			Glucose	Fructose	LA ^b	FF ^c	5-HMF	
1	Thermal	24.2±2%	12.0	0.0	0.0	3.5	8.7	36.1
2	Parent H-Beta	44.5±2%	7.9	2.0	5.1	5.1	24.5	55.1
3	Parent H-USY	36.0±2%	9.9	2.3	10.2	2.9	10.7	29.7
4	Parent H-ZSM-5	38.7±2%	4.8	0.0	0.0	5.1	28.8	74.3

^a Reaction conditions: catalyst loading, 0.25 g; microcrystalline cellulose, 0.36 g; NaCl, 2 g; Water, 5 ml; THF, 10 ml; reaction time, 60 min.

^b Levulinic acid

^c Furfural

The results obtained at 190 °C for the commercial zeolites and their modified forms are shown in **Table 6.2**. The conversion of cellulose increased from 44.5%, 36%, and 38.7% to 87.9%, 64.1%, and 74.8% while HMF yield increased from 24.5%, 10.7%, and 28.8% to 54.3%, 46.3%, and 52.9% with commercial H-Beta, H-USY, and H-ZSM-5, respectively. At 190 °C, the degradation of cellulose was significantly enhanced in the presence of catalytic acid sites (**Table 6.2**). Cellulose, due to its strong intermolecular hydrogen bonding, has a rigid structure. Although a strong correlation exists between zeolites' acidity and the conversion of cellulose to HMF, the availability of suitable energy in the systems is also crucial. Using a temperature of 190 °C caused responsive hydrolysis of cellulose to glucose and subsequent

dehydration of glucose formed to HMF at the Brønsted acid sites of the zeolite catalysts.

The conversion of cellulose and HMF yield increased further after the zeolites were dealuminated, excluding H-Beta. The removal of aluminum atoms rendered their Brønsted acidity increased and in turn promoted the rate-limiting step (hydrolysis) and dehydration step. The conversion of cellulose and HMF yield were further ameliorated as their dealuminated forms were modified with tin, with H-USY zeolite achieving the highest. Tin is an acidic metal, and its insertion further enhanced their acidities and improved their catalytic performances. Meanwhile, the HMF yield obtained with acid-treated and tin-modified-acid-treated H-Beta might be a result of limited Lewis and Brønsted acid contents after dealumination and metal incorporation. Beta zeolite has been mostly investigated in the catalytic conversion of carbohydrates into HMF due to its large micropore size, 3-dimensional porous channel connectivity, and high Brønsted acidity. However, the low content of Lewis acid sites limits its activity in the glucose isomerization step [145], and consequently, cellulose conversion to HMF. Based on this outcome, acid-treated H-USY was selected and was further studied with different weights of the metal for cellulose conversion to HMF.

Table 6.2. Catalytic study of the commercial zeolites and their similar modified forms for cellulose conversion to HMF.

Sample	Cellulose conversion (%)	Products Yield [%]					HMF selectivity (%)
		Glucose	Fructose	LA ^b	FF ^c	HMF	
Comm. H-Beta	87.9±2%	18.8	4.8	9.9	0.0	54.3	61.8
0.1DeAl.H-beta	75.1±2%	23.8	2.1	3.4	4.8	41.1	54.7
3.84wt%SDHB	84.2±2%	35.5	3.0	4.1	4.0	37.6	44.7
Comm. H-USY	64.1±2%	9.8	1.2	6.8	0.0	46.3	72.3
0.1DeAl.H-USY	88.7±2%	11.4	0.0	7.4	5.3	64.6	72.9
3.84wt%SDHU	>99%	7.1	1.7	17.1	5.9	68.2	68.2
Comm. H-ZSM-5	74.8±2%	11.1	1.3	5.7	3.8	52.9	70.7
0.1DeAl.H-ZSM-5	81.7±2%	7.5	1.7	7.6	6.0	58.9	72.2
3.84wt%SDHZ	83.1±2%	12.8	1.4	4.7	4.1	60.2	72.4

^a Reaction conditions: catalyst loading, 0.25 g; microcrystalline cellulose, 0.18 g; NaCl, 1 g; Water, 5 ml; THF, 10 ml; reaction temperature, 190 °C; reaction time, 60 min; Pressure, 10 bar N₂ gas.

^b Levulinic acid

^c Furfural

SDHB means Sn-0.1DeAl.H-Beta; SDHU means Sn-0.1DeAl.H-USY; SDHZ means Sn-0.1DeAl.H-ZSM-5

6.2. Modification of acid-treated H-USY with different weights of tin for cellulose conversion to HMF

The dealuminated H-USY obtained from the acid treatment of commercial H-USY with 0.1 M nitric acid solution was modified with the tin precursor at different weights, ranging from 1 – 10 wt% of the relative metal content in the metal precursor.

The commercial zeolite was treated with the acid solution to remove some aluminum in the T atoms and or extraframework of commercial H-USY, where the metal can then be inserted. The resulting catalysts were appropriately characterized and elucidated for cellulose conversion to HMF. The physicochemical properties and catalytic performances of the catalysts are discussed below in detail.

6.2.1. Physicochemical properties

The x-ray diffractograms of the commercial, acid-treated, and x Sn-modified-acid-treated H-USY obtained from XRD analysis are shown in **Figure 6.1A**. The acid-treated sample follows a similar diffraction pattern as the commercial H-USY, indicating no occurrence of structural damage after acid treatment. Meanwhile, the crystallinity of the commercial zeolite slightly decreased by 9%. Heda and co-workers [136] reported a similar observation with H-USY zeolite (Si/Al ratio of 15) with the same acid concentration. The Sn-modified samples have the same diffraction pattern as the acid-treated zeolite, which means that tin metal was highly dispersed and no appearance of SnO₂ peak. By taking the crystallinity index of the dealuminated zeolite as 100% (**Table 6.3**), the crystallinity of the zeolite was maintained at a low weight of the metal insertion (1 wt%), however, the crystallinity correspondingly decreased at higher weights, as shown in **Table 6.3**. Huang et al. [143] and Yang et al. [137] demonstrated that the dimension of the metal inserted into the framework and the degree of dispersion could alter the crystallinity of zeolite. This observation is consistent with the work of Wang et al. [138]. From the peak enlargement at 2θ angle from 22.4° to 24.8° shown in **Figure 6.1B**, the diffraction peak of commercial H-USY slightly shifted to a higher angle after acid treatment due to hydrolysis/ion-exchange

processes. Meanwhile, the peak position of the acid-treated zeolite shifted slightly to a higher angle at 1 wt% and moderately at 7–10 wt% of the metal loading whereas at 3.84 – 5 wt%, the peak shifted to a lower angle. This result can be explained by the contraction and expansion of the unit cell in the H-USY crystal lattice, as shown in **Table 6.3**, consistent with the work of Tang et al. [139]. Luo and co-workers [121] reported that the expansion or contraction of the zeolitic framework occurs during metal incorporation which causes a shift in the diffraction peaks. They explained that the phenomenon emanated from the diameter difference of the framework T atoms.

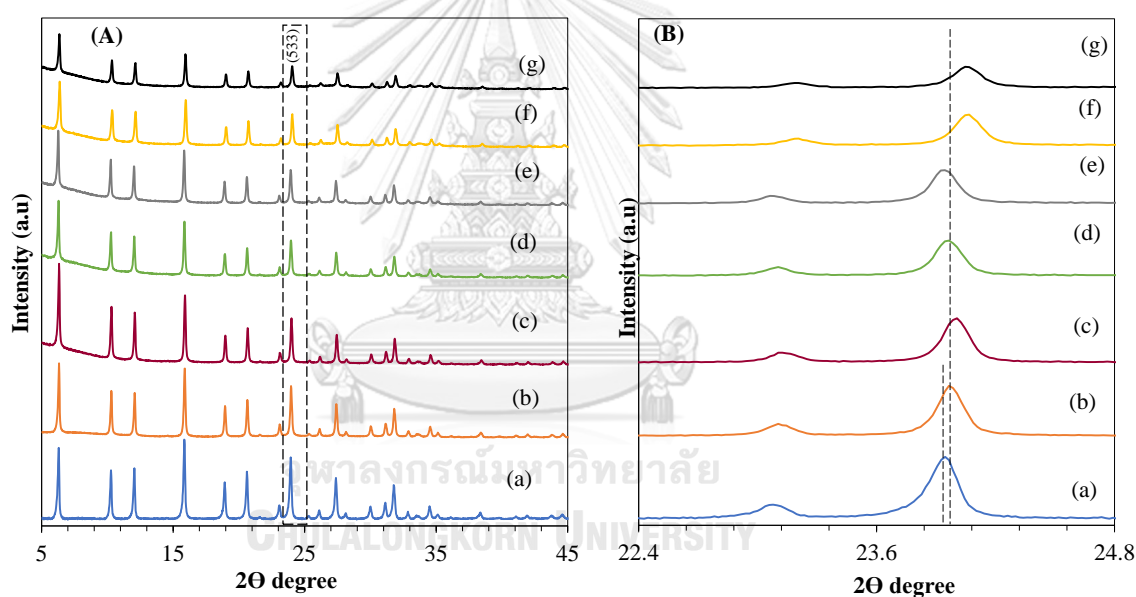


Figure 6.1. XRD pattern of (a) commercial H-USY (b) dealuminated H-USY (c) 1wt%Sn-0.1DeAl.H-USY (d) 3.84wt%Sn-0.1DeAl.H-USY (e) 5wt%Sn-0.1DeAl.H-USY (f) 7wt%Sn-0.1DeAl.H-USY (g) 10wt%Sn-0.1DeAl.H-USY.

The result obtained from XRF analysis showed that the Si/Al mole ratio of the commercial zeolite increased by 3.4 (from 5.52 to 8.92) after acid treatment, indicating that some framework and or extraframework aluminum atoms were

removed. The increased Si/Al mole ratio of the x Sn-modified-dealuminated samples confirmed that dealumination also occurred with the metal precursor solution, although at a low degree. The metal precursor solution exhibited a pH value of 1, implying that the metal precursor solution itself is acidic.

Table 6.3. Textural properties of commercial and modified H-USY zeolites.

Sample	$S_{\text{BET}}^{\text{a}}$ (m^2/g)	$S_{\text{micro}}^{\text{b}}$ (m^2/g)	D_{p}^{c} (nm)	$V_{\text{micro}}^{\text{d}}$ (cm^3/g)	$V_{\text{meso}}^{\text{e}}$ (cm^3/g)	$V_{\text{pore}}^{\text{f}}$ (cm^3/g)	Unit cell ^g (Å)	Si/Al ratio ^h	Sn ⁱ (wt%)	Rel. Crystallinity ^j (%)
Comm. H-USY	514	419	2.86	0.220	0.147	0.367	24.42	5.52	-	-
DHU	689	573	2.89	0.302	0.197	0.499	24.35	8.92	-	100
1wt%SDHU	595	491	2.97	0.258	0.183	0.441	24.26	9.08	0.88	100
3.84wt%SDHU	621	501	2.87	0.264	0.181	0.445	24.35	9.47	3.46	85
5wt%SDHU	561	457	2.94	0.240	0.172	0.412	24.37	9.49	4.26	83
7wt%SDHU	614	470	2.90	0.248	0.196	0.444	24.25	9.64	6.57	73
10wt%SDHU	588	436	2.80	0.231	0.182	0.412	24.27	9.68	10.44	55
Regen. catalyst ^k	-	-	-	-	-	-	-	9.56	5.95	68

^a BET surface area

^b micropore area

^c average pore diameter

^d micropore volume

^e mesopore volume ($V_{\text{pore}} - V_{\text{micro}}$)

^f total pore volume

^g obtained from XRD at lattice plane 533

^{h-i} obtained by XRF

^j relative peak intensities obtained from 2θ angle (6.33° , 10.30° , 12.08° , 15.87° , 18.95° , 20.65° , 23.96° and 27.41°)

^k 7wt%Sn-0.1DeAl.H-USY catalyst after 2nd run of reusability test

DHU means dealuminated H-USY; SDHU means Sn-0.1DeAl.H-USY

The result obtained from nitrogen physisorption analysis is summarized in **Table 6.3**. The commercial H-USY exhibited a BET surface area of 514 m²/g, a micropore volume of 0.220 cm³/g, and a total pore volume of 0.367 cm³/g. After acid treatment, the textural property of the commercial zeolite significantly increased. This could be attributed to the agglomeration of primary particles during acid treatment with 0.1 M HNO₃ solution. Meanwhile, its pore diameter was not significantly affected. The textural property of the dealuminated H-USY decreased respectively following metal insertion at different weights. This result indicates that the accumulation of the tin atoms occurred on the surface of the zeolite. As shown in **Figure 6.2**, the nitrogen adsorption isotherms of the commercial and modified H-USY samples exhibit a type IV isotherm with a hysteresis loop at $P/P_0 > 0.4$, which confirms the existence of mesopores. This result showed that the commercial H-USY zeolite itself possesses both micro and meso pores which is possibly due to interparticle void or agglomerate in the zeolite particles.

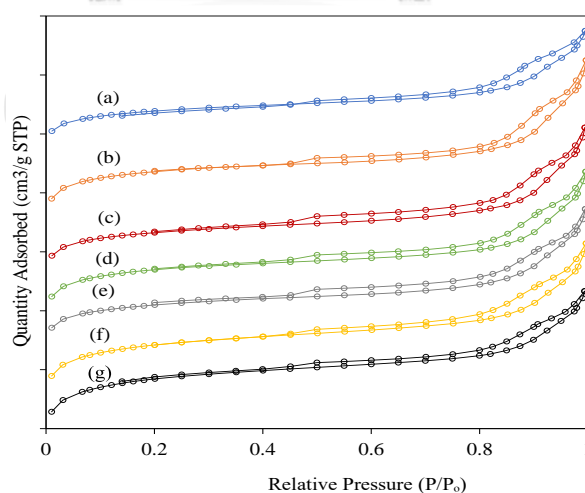


Figure 6.2. N₂ adsorption isotherms of (a) commercial H-USY (b) dealuminated H-USY (c) 1wt% Sn-0.1DeAl.H-USY (d) 3.84wt% Sn-0.1DeAl.H-USY (e) 5wt% Sn-0.1DeAl.H-USY (f) 7wt% Sn-0.1DeAl.H-USY (g) 10wt% Sn-0.1DeAl.H-USY

The FE-SEM image of the commercial and modified H-USY zeolite is presented in **Figure 6.3**. The morphology of the commercial H-USY did not change following acid treatment and metal incorporation. However, the surface of the commercial zeolite became rougher, and the agglomeration of primary particles changed after the acid treatment. Small clusters were seen to be deposited on the surface of the zeolite after metal insertion at 7 wt%, confirming that some tin species were deposited as extraframework species [140]. The walls of the commercial and modified H-USY zeolite, coupled with the clusters observed were all crystalline, consistent with XRD results.

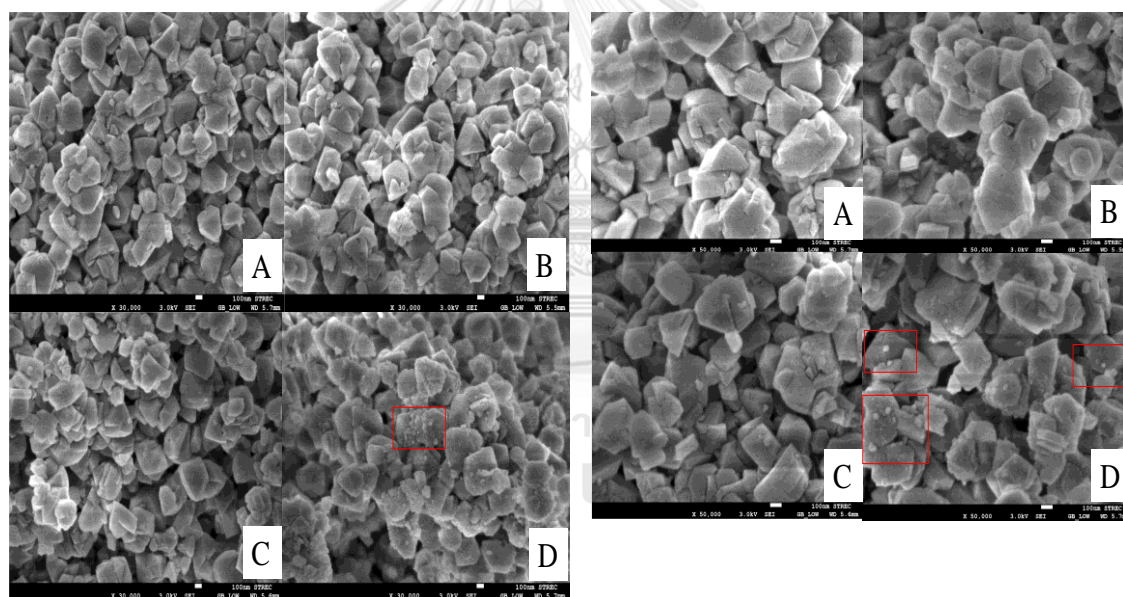


Figure 6.3. FE-SEM images of (A) commercial H-USY (B) dealuminated H-USY (C) 1wt%Sn-0.1DeAl.H-USY (D) 7wt%Sn-0.1DeAl.H-USY at a magnification of 30,000 (Left) and 50,000 (Right)

The result obtained from UV-vis spectroscopy to determine the coordination states of tin in the acid-treated H-USY zeolite is represented in **Figure 6.4**. The absorption band at a wavelength of 205 nm and 231 nm region are typical absorption band for

tetrahedrally-coordinated isolated Sn^{4+} species while the absorption band at 271 nm is typical coordination for higher states of tin species in the zeolite [124,137]. The spectrum of the acid-treated zeolite became broadened for all after the metal insertion. Although, the absorption bands at 205 and 231 nm were slightly broadened whereas the band at 271 nm looks completely broadened, implying that the metal was somewhat incorporated into the framework position and to a large extent as extraframework species, consistent with the SEM result.

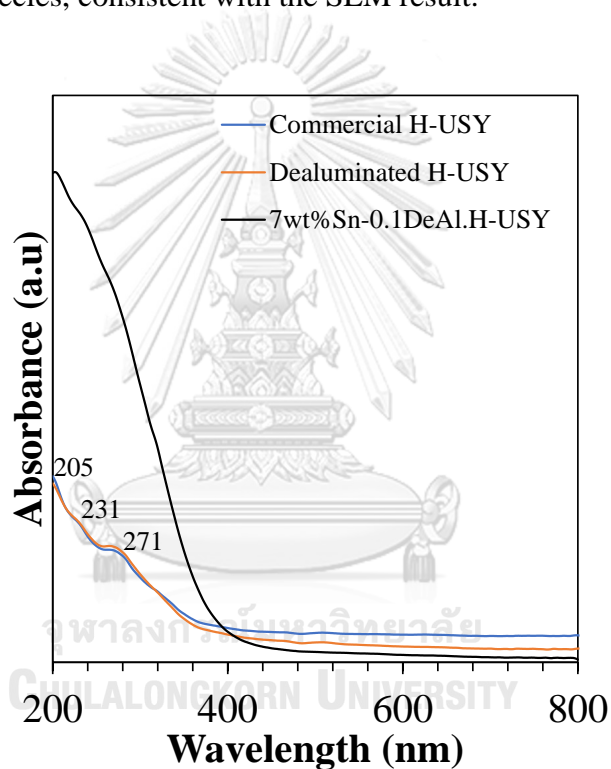


Figure 6.4. UV-vis spectra of commercial and modified H-USY zeolites.

The distribution of acid site and the estimated total acidity for the commercial and modified H-USY zeolites obtained from ammonia-TPD analysis are summarized in **Table 6.4** and their corresponding TPD profiles shown in **Figure 6.5A**. The acid treatment of commercial H-USY zeolite with 0.1 M nitric acid solution increased the area under the TPD spectrum, and thus resulted in increased total acidity. The partial

hydrolysis of the alumina clusters in the parent H-USY framework/extraframework by the acid solution resulted in diverse coordination of aluminum atoms, thus, rendered the acidity increased. The weak and strong acidity were particularly enhanced following acid treatment, but not the moderate acidity. The metal insertion at 1 – 5 wt% decreased the total acidity of the acid-treated zeolite, whereas, at 7 – 10 wt% of the metal loading, the total acidity notably increased. Besides, the weak and strong acidity correspondingly decreased at 1 – 5 wt% of the metal loading. Meanwhile, it correspondingly increased at higher weights. It was evidenced from SEM analysis, that the degree of particle agglomeration increased with the incorporation of the metal precursor at different weights, and tin clusters were seen to be deposited at higher weights as extraframework species. The moderate acidity of the dealuminated zeolite slightly decreased at 1 wt% loading but increased at higher loading. It is expected that the insertion of tin should correspondingly increase zeolite's acidity, however, partial accumulation or agglomeration of the metal on the surface may render the acidity decreased [68].

Table 6.4. Distribution and nature of acid sites for commercial and modified H-USY catalysts.

Catalyst	Acid site distribution (mmol/g) ^a				Nature of acid site (mmol/g) ^b		
	Weak	Moderate	Strong	Total acidity	L	B	B/L ratio
Comm. H-USY	0.715	0.324	0.151	1.191	0.128	0.593	4.63
DHU	0.798	0.313	0.167	1.279	0.133	0.719	5.41
1wt%SDHU	0.768	0.287	0.147	1.202	0.120	0.810	6.73
3.84wt%SDHU	0.614	0.352	0.075	1.041	n.d	n.d	n.d
5wt%SDHU	0.649	0.389	0.048	1.086	n.d	n.d	n.d
7wt%SDHU	0.999	0.356	0.239	1.593	0.129	0.787	6.10
10wt%SDHU	0.924	0.315	0.142	1.382	n.d	n.d	n.d

^a Determined by ammonia-TPD analysis (Weak: 50–200°C, Moderate: 200–350 °C and Strong: 350–500 °C)

^b Determined by Py-FTIR analysis (L – Lewis acidity, B – Brønsted acidity)

n.d – not determined.

DHU means dealuminated H-USY; SDHU means Sn-0.1DeAl.H-USY

The *in-situ* FTIR of pyridine adsorption of the commercial and modified H-USY catalysts is presented in **Table 6.4** and their recorded spectra in **Figure 6.5B**. The quantification of the acid sites provided an estimate of pyridine consumption at the Brønsted acid sites (an absorption band of 1540cm⁻¹) and Lewis acid sites of the catalyst (absorption band of 1450cm⁻¹), while the absorption band at 1490cm⁻¹ was observed for the superimposed vibration of pyridine that interacted with both acid sites. From **Table 6.4**, after acid treatment, the amount of Lewis and Brønsted acidity of the commercial zeolite increased by 0.005 mmol/g and 0.126 mmol/g respectively. As evidenced from the TPD data using ammonia as a probe molecule, this outcome is due to the partial hydrolysis of framework and extraframework aluminum atoms that resulted in various coordination of the aluminum atoms. The ion-exchange process during acid treatment rendered the Brønsted acidity increased by the removal of some extraframework aluminum species [104]. As shown in **Figure 6.6** from the FTIR study of the commercial and dealuminated H-USY obtained thermally at 500 °C before pyridine adsorption, the absorption bands at 3560 cm⁻¹, 3600 cm⁻¹ and 3625 cm⁻¹ are ascribed to the bridging hydroxyl group (Si-OH-Al) in the zeolite's sodalite cage, the bridging hydroxyl group interacting with extraframework species, and the bridging hydroxyl group located in the zeolite's super-cage. Meanwhile, the band at 3670 cm⁻¹ is associated with extraframework hydroxyl groups. The absorption band at

3690 cm^{-1} and 3737 cm^{-1} are typical bands for unperturbed terminal -OH and silanol groups [57,90-91, 104,127,141–142]. After acid treatment, the absorption band at 3670 cm^{-1} associated with the extraframework -OH group increased, indicating that some extraframework aluminum species were hydrolyzed and the content Al-OH_{EF} increased. The band at 3690 cm^{-1} associated with the terminal hydroxyl group was weakened suggesting that some silicon atoms were migrated and condensed with the terminal OH group to form Si-O-Si linkage. The silanol group ($\equiv\text{Si-OH}$), band 3737 cm^{-1} , and the bands associated with the bridging hydroxyl groups, 3560 cm^{-1} , 3600 cm^{-1} , and 3625 cm^{-1} increased after acid treatment, thus, facilitated the increased Brønsted and Lewis acidity.

Upon metal insertion, the content of Lewis acidity decreased whereas the content of Brønsted acidity increased by 0.091 mmol/g and 0.068 mmol/g at 1 wt% and 7 wt% of the metal loading. The decreased Lewis acidity indicates that the metal precursor resulted in further dealumination of the acid-treated H-USY, as evidenced by the XRF data in **Table 6.3**. The interaction of the bridging and extraframework hydroxyl group with Sn atoms occupying the vacant T sites of the acid-treated zeolite enhanced the Brønsted acidity [137]. From the FTIR study in **Figure 6.6**, it was evident that the band at 3737 cm^{-1} assigned to silanol group was slightly weakened at a low weight of the metal incorporation (1 wt%) but was highly weakened at a higher weight (7 wt%), implying that at higher weights tin condensed more with Si-OH nest to form Si-O-Sn linkages, which means that some tin atoms were inserted into framework site [137]. Meanwhile, an intense peak was observed at 3670 cm^{-1} for both weights (1 and 7 wt%) more than the acid-treated zeolite, indicating that the content of the extraframework OH group further increased, due to partial hydrolysis of the

extraframework species by the metal precursor solution. There was no significant change for the terminal hydroxyl groups at band 3690 cm^{-1} , implying that tin atoms were mostly incorporated into the extraframework position, consistent with the result obtained from UV-vis analysis. The interaction of terminal Sn–OH defects in the zeolite framework/extraframework has been demonstrated to contribute to the Brønsted acidity [129,146]. Hence, the increased Brønsted acidity observed with the tin-modified catalysts.

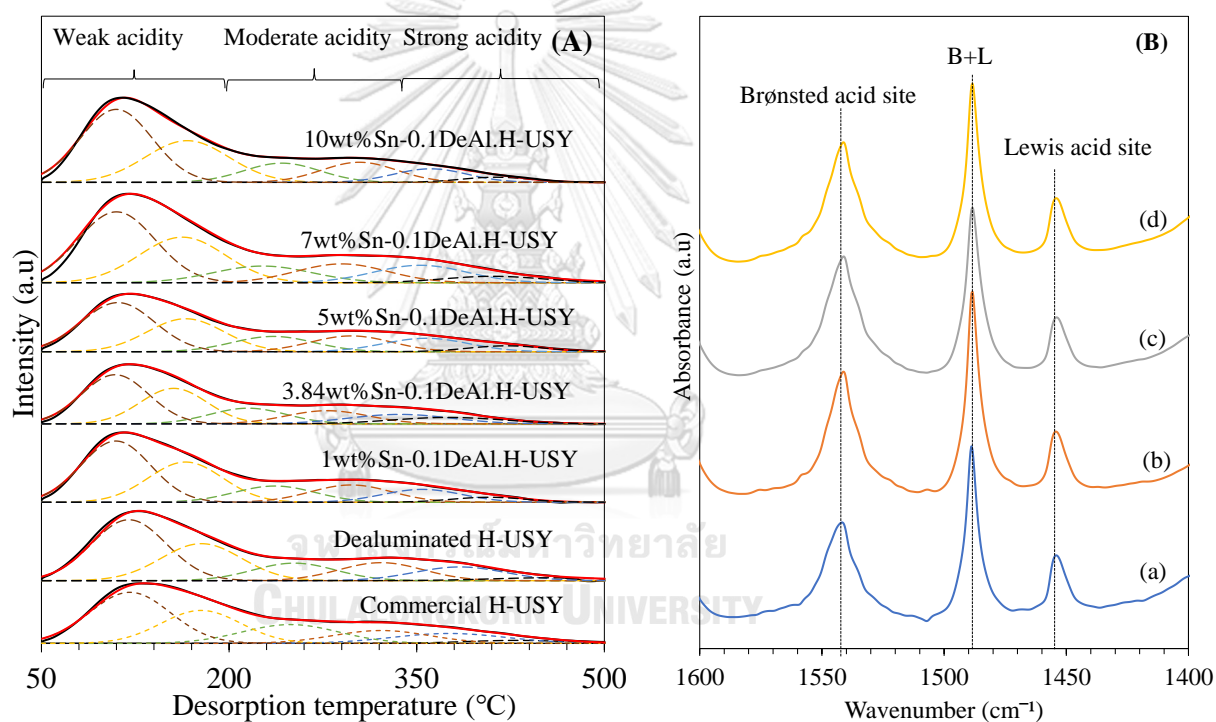


Figure 6.5. (A) NH_3 -TPD deconvoluted profile of all catalysts (B) Py-FTIR spectra of (a) commercial H-USY (b) 0.1DeAl.H-USY (c) 1wt%Sn-0.1DeAl.H-USY and (d) 7wt%Sn-0.1DeAl.H-USY.

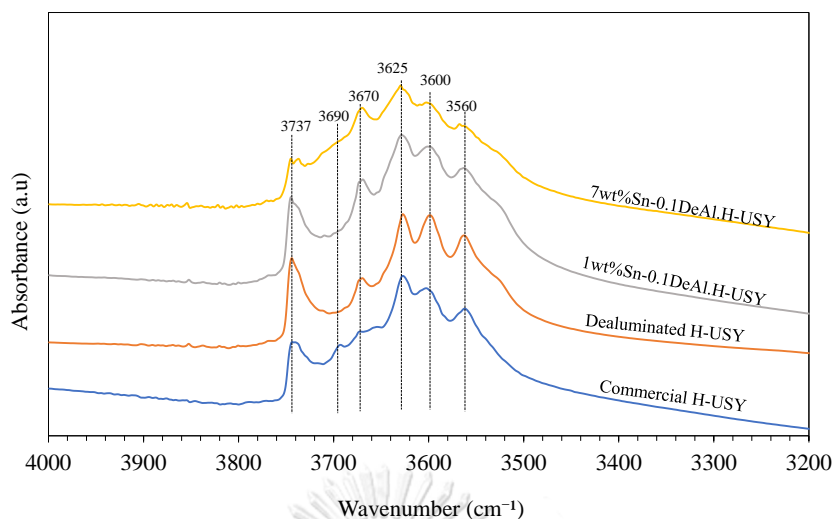


Figure 6.6. FTIR study of commercial and modified H-USY catalysts.

6.2.2. Catalytic study

Figure 6.7 illustrates the pathway to the one-pot acid-catalyzed conversion of cellulose to HMF. Brønsted acid facilitated the hydrolysis or depolymerization of cellulose to glucose. The second step involves the isomerization of glucose formed to fructose through a 1,2-intramolecular hydride shift, facilitated by Lewis acid. The isomerized fructose is then dehydrated at the Brønsted acid centers by removing three molecules of water to form HMF. Formic acid (FA) and levulinic acid (LA) have been widely investigated to be a product of HMF's hydration under a high Brønsted acid content [66]. Furfural was also observed as a by-product in this study, produced from xylose dehydration under the catalysis of Brønsted acid sites [68]. The dehydrated xylose is a product of the retro-aldol condensation of fructose intermediates. Polymeric or soluble humins are unavoidably formed via polycondensation or fragmentation among glucose, fructose, furans, and other reactive intermediates [108]. Studies have shown that by optimizing the total number

of acid sites and the molar ratio of Brønsted/Lewis acidity, the formation of humins can be retarded to enhance the selectivity of HMF [108,109].

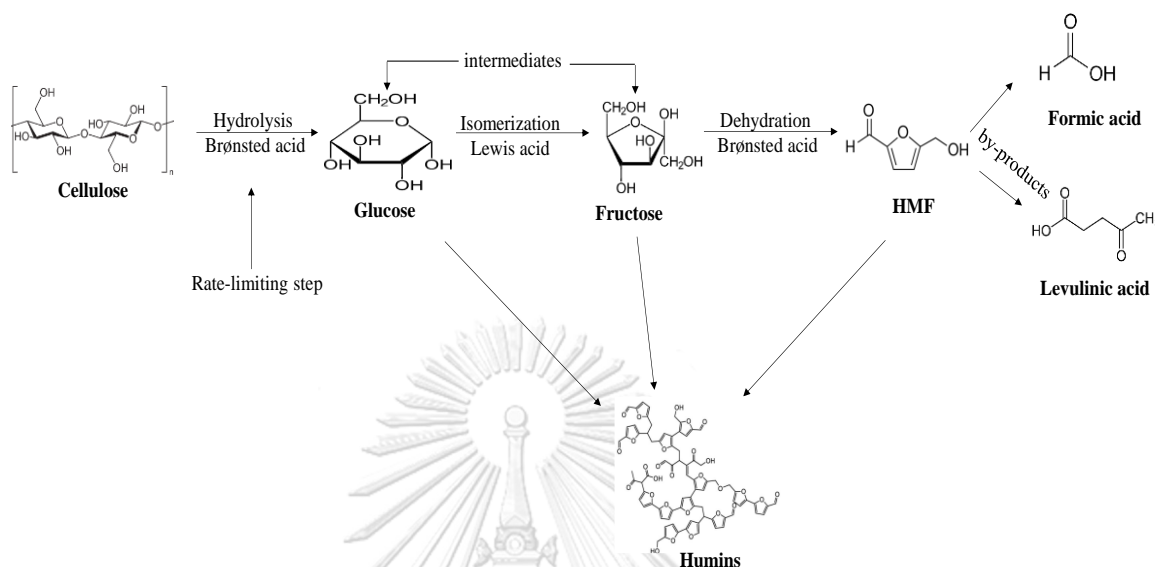


Figure 6.7. Reaction pathway for thermocatalytic conversion of cellulose to HMF and adverse effect of high acidity.

6.2.2.1 Catalytic performance of commercial and acid-treated H-USY catalysts

As earlier discussed, the result obtained from the thermal study of cellulose without a catalyst was significantly low. As shown in **Table 6.5**, cellulose conversion and HMF yield increased by 2.7 and 5.3 folds immediately after commercial H-USY zeolite was introduced into the reaction system, confirming the significant role of solid acid catalysis in lignocellulosic biomass conversion to HMF. The conversion of cellulose and HMF yield increased with increasing temperature with the commercial H-USY. The glucose and fructose content remaining in the solution as the temperature was raised from 170 to 190 °C was found between 10 – 16% and 1 – 4% respectively. Using acid-treated H-USY as catalyst, both conversion and HMF yield were ameliorated. However, the glucose content remaining in the solution was slightly

higher than the commercial one at 190 °C. NH₃-TPD and nitrogen physisorption results revealed that the dealuminated catalyst exhibited a higher acidity (including Brønsted and Lewis acidity) compared to the commercial zeolite. This could have effectively cleaved the β-1,4-glycosidic bond in cellulose units to glucose and to HMF simultaneously. Xing et al. [71] demonstrated that the effective conversion of cellulose to HMF is dependent on the zeolite's acidity. Wu et al. [68] found out that the high acid content of hafnium-containing H-ZSM-5 zeolite promoted the degradation of cellulose to HMF. Levulinic acid and furfural yields increased at elevated temperatures. Based on this outcome, acid-treated H-USY was selected and further modified by metal insertion at different weights for cellulose conversion to a higher HMF yield.

Table 6.5. Catalytic performance of commercial and dealuminated H-USY catalysts on cellulose conversion^a to HMF.

Catalyst	Temp. (°C)	Cellulose conversion (%)	Products Yield [%]					HMF Selectivity (%)
			Glucose	Fructose	LA ^b	HMF	Furfural	
Thermal	170	24.2±2%	12.0	0.0	0.0	8.7	3.5	36.1
Comm. H-USY	170	28.7±2%	12.1	4.4	0.6	8.6	3.1	30.0
Comm. H-USY	180	57.5±2%	15.7	2.2	1.8	33.6	4.4	58.4
Comm. H-USY	190	64.1±2%	9.8	1.2	6.8	46.3	0.0	72.5
0.1DeAl.H-USY	190	88.7±2%	11.4	0	7.38	64.6	5.26	72.9

^a Reaction conditions: catalyst loading, 250 mg; microcrystalline cellulose weight, 3.6 wt%; H₂O-saturated with NaCl, 5 ml; THF, 10 ml; reaction time, 60 min.

^b Levulinic acid

6.2.2.2 Effect of tin incorporation on dealuminated H-USY for cellulose conversion to HMF

Acid amount is largely related to the degree of tin loading in the acid-catalyzed conversion of cellulose to HMF and the catalytic performance was mostly influenced by the acidity. As a result, the synthesized x Sn-dealuminated H-USY catalysts were investigated. As shown in **Table 6.6**, a total conversion of cellulose was obtained with all modified catalysts (1 – 10 wt%). The result obtained from Py-FTIR analysis by using 1 wt% and 7 wt% metal loading revealed that the Brønsted acidity ultimately increased. The mass transfer of cellulose molecules was significantly influenced by the high content of the Brønsted acid sites, thus, induced complete hydrolysis.

HMF yield obtained with various tin loading on acid-treated H-USY is presented in **Table 6.6**. At 1 wt%, the yield of HMF increased from 64.6% (with the dealuminated catalyst) to 72.9%. At 3.84 – 5 wt% loading, a similar HMF yield was obtained as the acid-treated catalyst, however, lower than the one obtained with 1 wt% due to lower total acid content. HMF yield and selectivity reached a plateau of 76.1% when the metal was loaded at 7 wt%. The increased yield is attributed to the highest acidity, high Brønsted acid content, and suitable B/L acid ratio exhibited by this catalyst (**Table 6.4**). Further loading of the metal at a higher weight on the acid-treated zeolite caused HMF yield to decline. The decreased HMF yield may be related to the decreased textural properties such as pore diameter, micropore surface and volume observed with this catalyst.

The yield of glucose left in the reaction mixture increased as the total acidity was decreased at 3.84 wt% and 5 wt% of tin loading. The improved total acidity and Lewis acid content observed at 7 wt% loading accelerated the isomerization step, thus, glucose yield was decreased. Although the total acidity slightly dropped at 10

wt% of the metal loading, probably due to blockage of some acid sites by tin agglomeration, Py-FTIR analysis revealed that the content of Brønsted acidity increased after metal insertion. A high B/L acid ratio played a significant role in this acid-catalyzed conversion of cellulose to HMF. However, it in turn implies a low Lewis acid content. This could have simultaneously affected glucose isomerization to fructose, leaving a high content of glucose in the solution. Fructose, an isomerized product was found in a limited amount in the reaction mixture from 0 – 2%, implying that the Brønsted acidic sites facilitated almost complete dehydration of the formed fructose to HMF. **From Table 6.6**, furfural yields were found in the solution between 6 – 7% as the metal was loaded from 1–10wt%. Meanwhile, due to the nature of the high Brønsted acid content of the x Sn-dealuminated catalysts, the levulinic acid yields observed were obviously high and were found in the reaction mixture between 12 – 20%. Humins deposition on the catalyst's surface increased as the tin content was increased from 1–10 wt%..

Compared to other weights, 7wt%Sn-0.1DeAl.H-USY possessed the highest total acidity and weak-strong acid sites and produced the best catalytic performance. Therefore, it was utilized for reaction condition optimizations to achieve a higher HMF yield from cellulose.

Table 6.6. Effect of tin incorporation on cellulose conversion^a and HMF Yield.

Catalyst	Conversion (%)	Products Yield (%)					HMF Selectivity (%)
		Glucose	Fructose	LA	HMF	Furfural	
1wt%SDHU	>99%	3.3±4.7	0.00	15.8±2.2	72.9±0.8	7.4±2.5	73.3±0.3
3.84wt%SDHU	>99%	7.2±0.1	0.9±1.2	19.6±3.5	66.2±2.7	6.2±0.3	66.2±2.7
5wt%SDHU	>99%	9.5±4.4	1.3±1.8	18.5±2.1	64.5±3.4	6.2±0.7	73.8±3.4
7wt%SDHU	>99%	6.0±4.6	0.00	11.5±2.9	76.1±6.6	6.4±0.9	76.1±6.6
10wt%SDHU	>99%	13.9±1.7	2.3±0.1	13.8±4.3	63.1±6.6	7.0±0.6	63.1±6.6

^a Reaction conditions: catalyst loading, 250 mg; microcrystalline cellulose weight, 3.6 wt%; H₂O-saturated with NaCl, 5 ml; THF, 10 ml; reaction temperature, 190 °C, reaction time, 60 min.

DHU means dealuminated H-USY; SDHU means Sn-0.1DeAl.H-USY

6.2.2.3 Effect of reaction conditions on HMF synthesis over 7wt%Sn-0.1DeAl.H-USY catalyst

Effect of reaction temperature: Cellulose degradation to HMF over 7wt%Sn-0.1DeAl.H-USY catalyst was conducted under three different temperatures from 170 – 190 °C. As depicted in **Figure 6.8A**, reaction temperature has a significant influence on cellulose depolymerization and HMF yield. Cellulose conversion increased from 57% to >99% as the temperature was increased from 170 to 190 °C. Meanwhile, glucose dehydration correspondingly accelerated as the temperature was raised. The responsive dehydration initiated by the increased temperature simultaneously facilitated an increased yield of HMF from 28% to 76.1%. Atanda and co-workers [117], from their work on the kinetic study of cellulose hydrolysis, pointed out that the degradation of cellulose to HMF is temperature dependent. Besides, the elevated temperature completely drove the yield of fructose. Other products such as levulinic

acid and furfural yields showed an increased trend from 3% to 11% and 5% to 6% as the temperature increased. Humins depositions on the catalyst surface increased at elevated temperatures. Based on this result, the reaction temperature at 190 °C was found to be a suitable temperature for cellulose degradation to HMF and was used for other studies.

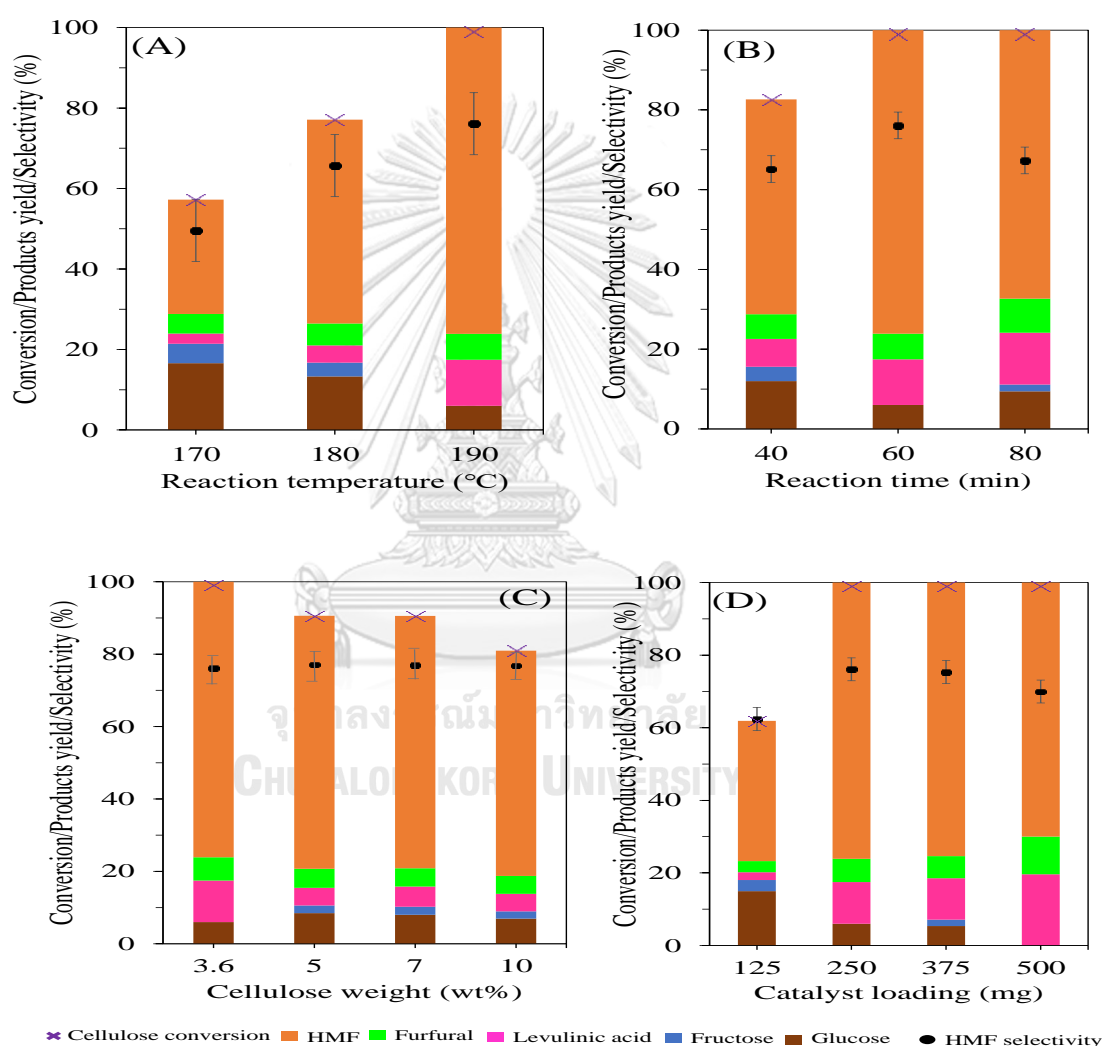


Figure 6.8. Effect of (a) reaction temperature (b) reaction time (c) cellulose weight and (d) catalyst loading in the thermocatalytic conversion of cellulose to HMF with 7wt%Sn-0.1DeAl.H-USY. Central reaction conditions: catalyst loading, 250 mg; microcrystalline cellulose weight, 3.6 wt%; 5 mL H₂O-saturated with NaCl, 10 mL THF, reaction temperature, 190 °C; reaction time, 60 min).

Effect of reaction time: The effect of reaction time was investigated for cellulose conversion to HMF from 40 – 80 min. As shown in **Figure 6.8B**, cellulose conversion increased from 83% to >99% as the reaction time was increased from 40 to 80 min. HMF yield notably increased from 65% to 76.1% for the first 60 min. However, HMF yield and selectivity dropped at a higher reaction time. The prolonged time promoted HMF deterioration and increased levulinic acid yield from 7 to 13%. Besides, the color of the catalyst became darker as the reaction time was increased. Glucose dehydration was accelerated as the reaction time was increased from 40 to 80 min. Furfural as a byproduct was found in the solution between 6% to 9% as the time increased. This implies that at higher reaction time, the dehydration rate of xylose formation was correspondingly promoted. Reaction time of 60 min was found to be suitable for HMF synthesis from cellulose and was used for other reaction studies.

Effect of cellulose weight: The effect of substrate consumption was also examined by using 3.6 – 10 wt% microcrystalline cellulose. As shown in **Figure 6.8C**, cellulose conversion and HMF yield decreased from >99% to 81% and 76.1% to 62% as the substrate weight was increased from 3.6 to 10 wt%. The amount of substrate in the system was more than what the catalyst required at higher weights which concomitantly retarded complete hydrolysis of cellulose and promoted polycondensation routes to unwanted oligomers. Humins deposited on the catalyst surface and soluble oligomers significantly increased as the substrate weight was increased. Glucose dehydration decelerated as the weight of substrate increased and the yield of fructose found in the solution was around 2% at higher weights (5 – 10 wt%). Meanwhile, levulinic acid and furfural yields correspondingly decreased as the

substrate weight increased. Based on this result, 3.6 wt% cellulose was the most suitable weight and was selected for further study.

Effect of catalyst loading: The effect of catalyst dosage was studied for high-yield synthesis of HMF from cellulose by using a dosage range from 125 to 500 mg, as shown in **Figure 6.8D**. The conversion of cellulose increased from 62% to >99% as the catalyst loading was increased from 125 – 500 mg while HMF yield increased from 39 to 76% just at the first increase of the catalyst dosage (250 mg). Increasing catalyst dosage implies increasing the content of acid sites which could promote the hydrolysis, isomerization and dehydration steps respectively. However, higher dosage of the catalyst caused HMF yield and its selectivity to drop, implying that much acid sites were more than required by the reactant in the system and excess acid sites promoted side reactions such as rehydration, furfural formation, and polycondensation routes. Interestingly, levulinic acid and furfural yields notably increased from 2% to 20% and 3% to 10.4% as the dosage increased from 125 to 500 mg. Glucose dehydration was accelerated as the dosage increased and was completely consumed at the highest dosage of the catalyst. Based on this outcome, 250 mg was selected as a suitable dosage for HMF synthesis from cellulose in this work

6.2.3. Reusability study of 7wt%Sn-0.1DeAl.H-USY catalyst

The study was conducted at optimum reaction conditions of 3.6 wt% of microcrystalline cellulose, 250 mg of catalyst, 5 mL water-saturated with NaCl, 10 mL THF, 190 °C, and 1 h reaction time. After the reaction with the fresh catalyst, the catalyst was regenerated by washing with hot water and toluene (twice each) and then dried at 80 °C overnight. The regenerated catalyst was then calcined at 500 °C for 4 h

to remove organic deposits and reused. The cellulose left after the 1st run with the regenerated catalyst decomposed upon calcination. As shown in **Figure 6.9**, the regenerated catalyst was only able to achieve a conversion of 46% and an HMF yield of 16% after the second run.

The result from XRF and XRD analysis shown in **Figure 6.10** of the regenerated catalyst after 2nd run revealed that the degree of leaching only occurred by 9.5% and the crystallinity of the catalyst was maintained, **Table 6.3**. The reduced catalytic activity may be attributed to humins species that were adsorbed on the strong acid sites of the catalyst.

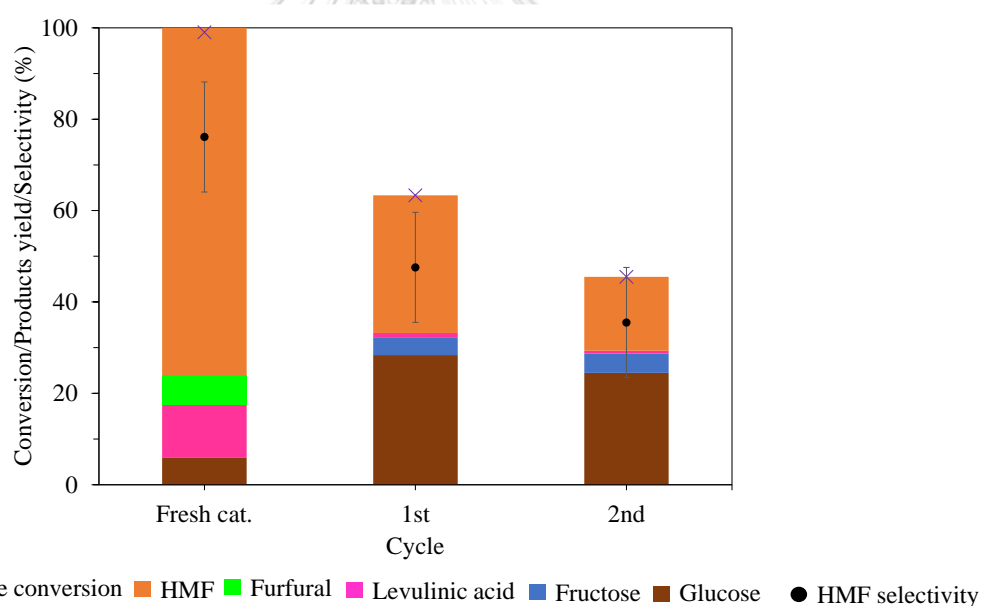


Figure 6.9. Reusability study of 7wt%Sn-0.1DeAl.H-USY catalyst for cellulose conversion to HMF. Reaction conditions: catalyst loading, 5 wt%; microcrystalline cellulose weight, 3.6 wt%; H₂O-saturated with NaCl: THF, 1:2; reaction temperature, 190 °C; reaction time, 60 min.

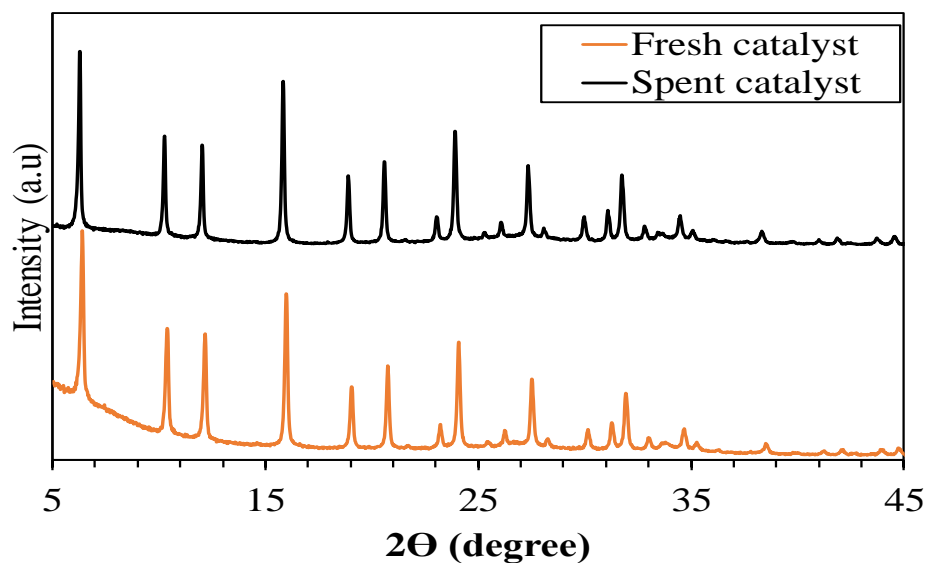


Figure 6.10. Diffraction patterns of fresh and regenerated (spent) 7wt%Sn-0.1DeAl.H-USY catalyst.

6.2.4. Comparison of 7wt%Sn-0.1DeAl.H-USY performance to other zeolite-based acid catalysts

The catalytic performance of 7wt%Sn-0.1DeAl.H-USY was compared to other zeolite-based acid catalysts for the conversion of cellulose to HMF. As shown in **Table 6.7**, based on the result obtained with 7wt%Sn-0.1DeAl.H-USY and the literature reported so far on cellulose conversion to HMF, 7wt%Sn-0.1DeAl.H-USY catalyst exhibited superior catalytic performance. This was majorly ascribed to its high but moderate acidity, enhanced textural properties, and suitable Brønsted & Lewis acid ratio with favorable reaction conditions.

Table 6.7. Comparison of 7wt%Sn-0.1DeAl.H-USY performance to other zeolite-based acid catalysts.

Entry	Catalyst	Solvent	Temp. (°C)	Time (h)	Cellulose conversion (%)	HMF Yield (%)	Ref.
1	5%Hf-HZSM-5	H ₂ O _(NaCl) /THF	190	2	n.d ^a	67.5	[68]
2	Bimodal-HZ-5	H ₂ O	190	4	67	46	[70]
3	Cr-USY	DMSO	160	1.3	n.d	35	[62]
4	Hf-β	H ₂ O _(NaCl) -THF	200	4	86.3	53.4	[71]
5	Cr/β	H ₂ O/THF	150	1.3	n.d	16	[144]
6	Sn-Mon	THF/DMSO	160	3	n.d	39.1	7
7	3.84wt%SDHZ	H ₂ O-NaCl/THF	190	1	83.1	60.2	This work
8	7wt%SDHU	H ₂ O-NaCl/THF	190	1	>99	76.1	This work

n.d means no data.

SDHZ means Sn-0.1DeAl.H-ZSM-5; SDHU means Sn-0.1DeAl.H-USY

CHAPTER 7

CONCLUSION AND FUTURE RECOMMENDATION

The goal of this thesis was to expand the existing knowledge about the possibilities of using modified protonic zeolites for two unique acid-catalyzed reactions, namely, the dehydration reaction of glucose to HMF and the direct conversion of cellulose to HMF.

7.1 Glucose dehydration to HMF – Acid dealumination of commercial H-ZSM-5 zeolite

In summary, a series of acid-treated zeolites were successfully prepared from the commercial H-ZSM-5 through mild dealumination using dilute nitric acid solution. The resulting dealuminated H-ZSM-5 catalysts exhibited preserved crystallinity and morphology. Although the acid treatment slightly affected the aluminum content of the zeolite, the ^{27}Al and ^{29}Si NMR analysis revealed that the chemical environment of aluminum and silicon atoms was locally altered. The mild dealumination removed some extraframework oxide species from the parent H-ZSM-5, and partially hydrolyzed the zeolitic framework, resulting in an increased fraction of coordinatively unsaturated framework aluminum species. Consequently, the total acidity was enhanced after the dealumination process, especially the number of Lewis acid sites in 0.1DeAl.H-ZSM-5 was 5-fold higher than that of the parent H-ZSM-5. 0.1DeAl.H-ZSM-5 was the suitable catalyst, giving the HMF yield of 64.7% at near-complete conversion of glucose. A relatively high content of strong acid sites and a decreased B/L ratio of 0.1DeAl.H-ZSM-5 were crucial for reducing the formation of by-products, and thus increasing the selectivity to HMF. Due to a good reusability and

simple preparation procedure, the mildly dealuminated H-ZSM-5 catalysts found potential for industrial production of HMF from glucose.

7.2 Glucose dehydration to HMF – Acid dealumination of commercial H-ZSM-5 zeolite and tin incorporation

A series of x Sn-dealuminated H-ZSM-5 catalysts were successfully synthesized by acid dealumination of commercial H-ZSM-5 with 0.1 M HNO₃ solution, followed by metal incorporation via excess water impregnation technique. UV-vis spectroscopy revealed that the tin atoms were incorporated into the zeolitic framework and extraframework, and consequently enhanced the zeolite's acidity. Nitrogen physisorption and SEM analysis revealed that agglomeration occurred on the surface of the dealuminated zeolite after impregnation. The result from the pyridine-FTIR analysis confirmed that both Brønsted and Lewis acid centers decreased by 2.5-fold, following impregnation with the metal precursor. Glucose conversion of ~84% was obtained together with 62.3% HMF yield, at an HMF selectivity of 74.3%, under a reaction temperature of 170 °C for 60 min with 3.84wt%Sn-0.1DeAl.H-ZSM-5 catalyst. The reusability study showed that the catalyst can be reused after four runs and still maintain its catalytic activity and stability. This study gives an overview of the effectiveness of tin incorporation in dealuminated H-ZSM- zeolite for efficient transformation of glucose to HMF.

7.3 Cellulose degradation to HMF – Acid dealumination of commercial H-USY zeolite and tin incorporation

Series of x Sn-0.1DeAl.H-USY catalysts were synthesized via acid treatment (using 0.1 M HNO₃ solution) with commercial H-USY zeolite, followed by metal

incorporation using excess water impregnation technique. Mild dealumination with 0.1 M nitric acid solution was very effective in removing some aluminum atoms from the parent's zeolitic framework and extraframework. The hydrolysis/ion-exchange process in the pristine zeolite rendered the Brønsted and Lewis acidity increased and enhanced the textural properties of the commercial catalyst. UV-vis analysis revealed that tin was incorporated into the zeolitic framework and to a large extent as an extraframework species. The result obtained from the FTIR studies confirmed that the Brønsted acidic sites were enhanced following tin incorporation, which in turn aided cellulose hydrolysis and glucose dehydration to HMF and improved the overall performance of the catalyst. The catalyst exhibited excellent catalytic activity in a biphasic system involving a water-NaCl/THF system, achieving a total cellulose conversion and HMF yield of 76.1%. The reusability study for 7wt%Sn-0.1DeAl.H-USY showed that the catalytic active sites were mostly deactivated by strong humins adsorption.

7.4 Future recommendation

From these studies, it can be concluded that mild acid dealumination and metal incorporation greatly enhanced the hydrolysis of cellulose and glucose dehydration to HMF. The utilization of acidic zeolite catalysts greatly promoted the formation of additional products such as levulinic acid, which could be of special interest. Since this work was particularly focused on cellulose conversion to HMF, no special attention was focused on the conversion of cellulose to levulinic acid. This could however be of special interest for future research as the modified H-USY promoted the reaction to some extent.

REFERENCES

- [1] Ambrose, J. (2020). Carbon emissions from fossil fuels could fall by 2.5 bn tonnes in 2020. *The Guardian*, 12.
- [2] Bozell, J. J. and G. R. Petersen (2010). "Technology development for the production of biobased products from biorefinery carbohydrates—the US Department of Energy's "Top 10" revisited." *Green Chemistry* 12(4): 539-554.
- [3] Tong, X., et al. (2010). "Biomass into chemicals: Conversion of sugars to furan derivatives by catalytic processes." *Applied Catalysis A: General* 385(1-2): 1-13.
- [4] Deng, Q., et al. (2016). "Efficient synthesis of high-density aviation biofuel via solvent-free aldol condensation of cyclic ketones and furanic aldehydes." *Fuel Processing Technology* 148: 361-366.
- [5] Hronec, M., et al. (2015). "Bio-derived fuel additives from furfural and cyclopentanone." *Fuel Processing Technology* 138: 564-569.
- [6] Zhao, S., et al. (2011). "One pot production of 5-hydroxymethylfurfural with high yield from cellulose by a Brønsted–Lewis–surfactant-combined heteropolyacid catalyst." *Chemical Communications* 47(7): 2176-2178.
- [7] Wang, J., et al. (2012). "Direct conversion of carbohydrates to 5-hydroxymethylfurfural using Sn-Mont catalyst." *Green Chemistry* 14(9): 2506-2512.
- [8] Georgiev, D., et al. "SYNTHETIC ZEOLITES-STRUCTURE, CLASIFICATION, CURRENT TRENDS IN ZEOLITE SYNTHESIS."
- [9] Walker Costa, T. (2013). *Zeolite Beta-The Conversion of cellulose to HMF*, Faculty of Science and Engineering.
- [10] Baerlocher, C., et al. (2007). *Atlas of zeolite framework types*, Elsevier.
- [11] Loewenstein, W. (1954). "The distribution of aluminum in the tetrahedra of silicates and aluminates." *American Mineralogist: Journal of Earth and Planetary Materials* 39(1-2): 92-96.
- [12] Sanz, J., et al. (1988). "Extraframework aluminium in steam-and SiCl₄-dealuminated Y zeolite. A ²⁷Al and ²⁹Si nuclear magnetic resonance study." *Journal of the Chemical Society, Faraday Transactions 1: Physical Chemistry in Condensed Phases* 84(9): 3113-3119.
- [13] Beers, A. E., et al. (2003). "Optimization of zeolite Beta by steaming and acid leaching for the acylation of anisole with octanoic acid: a structure–activity relation." *Journal of Catalysis* 218(2): 239-248.
- [14] Sand, L. B. and F. A. Mumpton (1978). *Natural zeolites: occurrence, properties, and use*, Pergamon Press, Inc., Elmsford, NY.
- [15] Kianfar, E. and A. Mahler (2020). *Zeolites: properties, applications, modification and selectivity*, Chapter. 1.
- [16] Barrer, R. M. (1982). *Hydrothermal chemistry of zeolites*, Academic press.
- [17] Sankaran, R., et al. (2021). "The expansion of lignocellulose biomass conversion into bioenergy via nanobiotechnology." *Frontiers in Nanotechnology* 3: 96.
- [18] Steinbach, D., et al. (2017). "Pretreatment technologies of lignocellulosic biomass in water in view of furfural and 5-hydroxymethylfurfural production-a review." *Biomass Conversion and Biorefinery* 7: 247-274.
- [19] Sang, S., et al. (2004). "Difference of ZSM-5 zeolites synthesized with various templates." *Catalysis Today* 93: 729-734.
- [20] Kim, S. D., et al. (2004). "Compositional and kinetic study on the rapid crystallization of ZSM-5 in the absence of organic template under stirring." *Microporous and Mesoporous Materials* 72(1-3): 185-192.

- [21] Ghiaci, M., et al. (2004). "Fast and efficient synthesis of ZSM-5 in a broad range of SiO₂/Al₂O₃ without using seeding gel." *Materials research bulletin* 39(9): 1257-1264.
- [22] Bibby, D., et al. (1986). "Coke formation in zeolite ZSM-5." *Journal of Catalysis* 97(2): 493-502.
- [23] Xu, W., et al. (1990). "A novel method for the preparation of zeolite ZSM-5." *Journal of the Chemical Society, Chemical Communications*(10): 755-756.
- [24] Al-Zaidi, B. Y. S. (2011). The effect of modification techniques on the performance of zeolite-Y catalysts in hydrocarbon cracking reactions, The University of Manchester (United Kingdom).
- [25] Jacobs, P., et al. (2001). *Introduction to zeolite science and practice*, Elsevier.
- [26] Powder X-ray Diffraction Patterns. [Website]. Available from: https://asia.iza-structure.org/IZA-SC/ftc_table.php
- [27] Beers, A. E., et al. (2003). "Optimization of zeolite Beta by steaming and acid leaching for the acylation of anisole with octanoic acid: a structure–activity relation." *Journal of Catalysis* 218(2): 239-248.
- [28] Kuehl, G. H. and H. K. C. Timken (2000). "Acid sites in zeolite Beta: effects of ammonium exchange and steaming." *Microporous and Mesoporous Materials* 35: 521-532.
- [29] J. Scherzer. *Advances in Chemistry Series, Symposium Series, Vol. 248*, pages 157{200, 1984.
- [30] Casci, J. and C. Cundy (1983). "RM Barrer Hydrothermal Chemistry of Zeolites. Academic Press, London and New York, 1982. 360 pp. Price£ 31.00 (\$57.50)." *Clay Minerals* 18(2): 223-223.
- [31] P. K. Meher, F. D. Hunter, and J. Scherzer. *Advances in Chemistry Series, Symposium Series, Vol. 101*, page 266, 1971.
- [32] R. von Ballmoos. *Berichte der Bunsengesellschaft fr physikalische Chemie, Vol 86*, page 264265, 1982.
- [33] Ruren Xu, Wenqin Pang, Jihong Yu, Qisheng Huo, and Jiesheng Chen. John Wiley & Sons, 2009. ISBN 9780470822364.
- [34] Lohse, U., et al. (1984). "Adsorption of n-hexane on H—Y and on deep bed treated dealuminated Y zeolites." *Zeolites* 4(2): 163-167.
- [35] Wang, Q., et al. (1991). "Dealumination of zeolites II. Kinetic study of the dealumination by hydrothermal treatment of a NH₄NaY zeolite." *Journal of Catalysis* 130(2): 459-470.
- [36] Müller, M., et al. (2000). "Comparison of the dealumination of zeolites beta, mordenite, ZSM-5 and ferrierite by thermal treatment, leaching with oxalic acid and treatment with SiCl₄ by ¹H, ²⁹Si and ²⁷Al MAS NMR." *Microporous and Mesoporous Materials* 34(2): 135-147.
- [37] Beyerlein, R., et al. (1997). "Effect of steaming on the defect structure and acid catalysis of protonated zeolites." *Topics in Catalysis* 4(1-2): 27-42.
- [38] J. J. Lazaro Munoz, A. Corma Canos, and J. M. Frontela Delgado. US Patent - US5057471, 1991.
- [39] Sherry, H. S. (1968). "Ion-exchange properties of zeolites. IV. Alkaline earth ion exchange in the synthetic zeolites Linde X and Y." *The Journal of Physical Chemistry* 72(12): 4086-4094.
- [40] Kunkeler, P., et al. (1998). "Zeolite beta: the relationship between calcination procedure, aluminum configuration, and Lewis acidity." *Journal of Catalysis* 180(2): 234-244.
- [41] He, J., et al. (2003). "New methods to remove organic templates from porous materials." *Materials chemistry and physics* 77(1): 270-275.
- [42] Corma, A., et al. (1994). "Acidity and stability of MCM-41 crystalline aluminosilicates." *Journal of Catalysis* 148(2): 569-574.

- [43] Melián-Cabrera, I., et al. (2005). "One-pot catalyst preparation: combined detemplating and Fe ion-exchange of BEA through Fenton's chemistry." *Chemical Communications*(16): 2178-2180.
- [44] Ramsaran, A. (1996). Desilicated ZSM-5 zeolite as catalyst for the dehydration of ethanol, Concordia University.
- [45] Halasz, I., et al. (2005). "Molecular spectra and polarity sieving of aluminum deficient hydrophobic HY zeolites." *Microporous and Mesoporous Materials* 84(1-3): 318-331.
- [46] Groen, J. C., et al. (2006). "Desilication: on the controlled generation of mesoporosity in MFI zeolites." *Journal of Materials Chemistry* 16(22): 2121-2131.
- [47] Groen, J. C., et al. (2005). "Mechanism of hierarchical porosity development in MFI zeolites by desilication: The role of aluminium as a pore-directing agent." *Chemistry—A European Journal* 11(17): 4983-4994.
- [48] Gandini, A. and M. N. Belgacem (1997). "Furans in polymer chemistry." *Progress in Polymer Science* 22(6): 1203-1379.
- [49] W. J. Pentz. Quaker Oats - US Patent - US4426460, 1984.
- [50] Román-Leshkov, Y., et al. (2007). "Production of dimethylfuran for liquid fuels from biomass-derived carbohydrates." *Nature* 447(7147): 982-985.
- [51] Van Nguyen, C., et al. (2022). "Highly efficient one-pot conversion of saccharides to 2, 5-dimethylfuran using P-UiO-66 and Ni-Co@ NC noble metal-free catalysts." *Green Chemistry* 24(13): 5070-5076.
- [52] J. J. Bozell, L. Moens, D. C. Elliott, Y. Wang, G. G. Neuenschwander, S. W. Fitzpatrick, R. J. Bilski, and J. L. Jarnefeld. *Resources, Conservation and Recycling*, Vol 28, pages 227-238, 2000.
- [53] M. J. Antal Jr and W. S. L. Mok. *Carbohydrate Research*, Vol 199, pages 91-109, 1990.
- [54] Zhao, H., et al. (2007). "Metal chlorides in ionic liquid solvents convert sugars to 5-hydroxymethylfurfural." *Science* 316(5831): 1597-1600.
- [55] Bicker, M., et al. (2005). "Dehydration of D-fructose to hydroxymethylfurfural in sub- and supercritical fluids." *The journal of supercritical fluids* 36(2): 118-126.
- [56] Asghari, F. S. and H. Yoshida (2006). "Dehydration of fructose to 5-hydroxymethylfurfural in sub-critical water over heterogeneous zirconium phosphate catalysts." *Carbohydrate research* 341(14): 2379-2387.
- [57] Chheda, J. N., et al. (2007). "Production of 5-hydroxymethylfurfural and furfural by dehydration of biomass-derived mono- and poly-saccharides." *Green Chemistry* 9(4): 342-350.
- [58] Seri, K.-i., et al. (2001). "Catalytic activity of lanthanide (III) ions for the dehydration of hexose to 5-hydroxymethyl-2-furaldehyde in water." *Bulletin of the Chemical Society of Japan* 74(6): 1145-1150.
- [59] Mo, H.-b., et al. (2017). "Sustainable synthesis of 5-hydroxymethylfurfural from waste cotton stalk catalyzed by solid superacid-SO₄²⁻/ZrO₂." *Journal of Central South University* 24: 1745-1753.
- [60] Qi, X., et al. (2009). "Sulfated zirconia as a solid acid catalyst for the dehydration of fructose to 5-hydroxymethylfurfural." *Catalysis Communications* 10(13): 1771-1775.
- [61] Armaroli, T., et al. (2000). "Acid sites characterization of niobium phosphate catalysts and their activity in fructose dehydration to 5-hydroxymethyl-2-furaldehyde." *Journal of Molecular Catalysis A: Chemical* 151(1-2): 233-243.
- [62] Sezgin, E., et al. (2019). "Heterogeneous Cr-zeolites (USY and Beta) for the conversion of glucose and cellulose to 5-hydroxymethylfurfural (HMF)." *Cellulose* 26: 9035-9043.

- [63] Atanda, L., et al. (2015). "Catalytic conversion of glucose to 5-Hydroxymethyl-furfural with a phosphated TiO₂ catalyst." *ChemCatChem* 7(5): 781-790.
- [64] Xu, S., et al. (2019). "Direct conversion of wheat straw components into furan compounds using a highly efficient and reusable SnCl₂-PTA/ β zeolite catalyst." *Industrial & engineering chemistry research* 58(22): 9276-9285.
- [65] Moreau, C., et al. (1996). "Dehydration of fructose to 5-hydroxymethylfurfural over H-mordenites." *Applied Catalysis A: General* 145(1-2): 211-224.
- [66] Moreno-Recio, M., et al. (2016). "Brønsted and Lewis acid ZSM-5 zeolites for the catalytic dehydration of glucose into 5-hydroxymethylfurfural." *Chemical Engineering Journal* 303: 22-30.
- [67] Xu, S.-q., et al. (2019). "Enhanced HMF yield from glucose with H-ZSM-5 catalyst in water-tetrahydrofuran/2-butanol/2-methyltetrahydrofuran biphasic systems." *Journal of Central South University* 26(11): 2974-2986.
- [68] Wu, N., et al. (2021). "An effective and inexpensive Hf/ZSM-5 catalyst for efficient HMF formation from cellulose." *Catalysis Letters* 151: 1984-1992.
- [69] Fan, C., et al. (2011). "Conversion of fructose and glucose into 5-hydroxymethylfurfural catalyzed by a solid heteropolyacid salt." *Biomass and bioenergy* 35(7): 2659-2665.
- [70] Nandiwale, K. Y., et al. (2014). "One-pot synthesis of 5-hydroxymethylfurfural by cellulose hydrolysis over highly active bimodal micro/mesoporous H-ZSM-5 catalyst." *ACS Sustainable Chemistry & Engineering* 2(7): 1928-1932.
- [71] Xing, X., et al. (2022). "Hf- β zeolites as highly efficient catalysts for the production of 5-hydroxymethylfurfural from cellulose in biphasic system." *International Journal of Biological Macromolecules* 222: 3014-3023.
- [72] Saenluang, K., et al. (2020). "In situ synthesis of Sn-beta zeolite nanocrystals for glucose to hydroxymethylfurfural (HMF)." *Catalysts* 10(11): 1249.
- [73] Yang, G., et al. (2015). "Catalysis of glucose to 5-hydroxymethylfurfural using Sn-beta zeolites and a Brønsted acid in biphasic systems." *BioResources* 10(3): 5863-5875.
- [74] Chung, N. H., et al. (2020). "Catalytic conversion of glucose into 5-hydroxymethylfurfural over Cu-Cr/ZSM-5 zeolite." *Catalysis Letters* 150: 170-177.
- [75] W. Sanderman. *Holz Roh Werks.* Vol. 31, page 11, 1973.
- [76] Mosier, N., et al. (2005). "Features of promising technologies for pretreatment of lignocellulosic biomass." *Bioresource technology* 96(6): 673-686.
- [77] Edgar, K. J., et al. (2001). "Advances in cellulose ester performance and application." *Progress in Polymer Science* 26(9): 1605-1688.
- [78] Zhang, Y. H. P. and L. R. Lynd (2004). "Toward an aggregated understanding of enzymatic hydrolysis of cellulose: noncomplexed cellulase systems." *Biotechnology and bioengineering* 88(7): 797-824.
- [79] Structure of cellulose. [Website]. Available from: <https://en.wikipedia.org/wiki/Cellulose>.
- [80] M. R. Landisch. *Proc. Biochem. Soc.*, pages 21-25, 1979.
- [81] Faith, W. (1945). "Development of the Scholler process in the United States." *Industrial & Engineering Chemistry* 37(1): 9-11.
- [82] Wooley, R., et al. (1999). Lignocellulosic biomass to ethanol process design and economics utilizing co-current dilute acid prehydrolysis and enzymatic hydrolysis current and futuristic scenarios, National Renewable Energy Lab.(NREL), Golden, CO (United States).
- [83] Bergius, F. (1937). "Conversion of wood to carbohydrates." *Industrial & Engineering Chemistry* 29(3): 247-253.

- [84] Antonoplis, R., et al. (1983). "Production of sugars from wood using high-pressure hydrogen chloride." *Biotechnology and bioengineering* 25(11): 2757-2773.
- [85] Rinaldi, R. and F. Schüth (2009). "Acid hydrolysis of cellulose as the entry point into biorefinery schemes." *ChemSusChem: Chemistry & Sustainability Energy & Materials* 2(12): 1096-1107.
- [86] Harris, J. F. (1985). Two-stage, dilute sulfuric acid hydrolysis of wood: An investigation of fundamentals, US Department of Agriculture, Forest Service, Forest Products Laboratory.
- [87] Zhao, H., et al. (2009). "Regenerating cellulose from ionic liquids for an accelerated enzymatic hydrolysis." *Journal of biotechnology* 139(1): 47-54.
- [88] Heinze, T. and A. Koschella (2005). "Solvents applied in the field of cellulose chemistry: a mini review." *Polímeros* 15: 84-90.
- [89] Onda, A., et al. (2008). "Selective hydrolysis of cellulose into glucose over solid acid catalysts." *Green Chemistry* 10(10): 1033-1037.
- [90] Cairon, O., et al. (2001). "FTIR studies of unusual OH groups in steamed HNaY zeolites: preparation and acid properties." *Microporous and Mesoporous Materials* 46(2-3): 327-340.
- [91] Lohse, U., et al. (1987). "Hydroxyl groups of the non-framework aluminium species in dealuminated Y zeolites." *Zeolites* 7(1): 11-13.
- [92] Van de Vyver, S., et al. (2010). "Sulfonated silica/carbon nanocomposites as novel catalysts for hydrolysis of cellulose to glucose." *Green Chemistry* 12(9): 1560-1563.
- [93] Mohammad, S., et al. (2016). "Influence of Salts on the Partitioning of 5-Hydroxymethylfurfural in Water/MIBK." *The Journal of Physical Chemistry B* 120(16): 3797-3808.
- [94] Nikolla, E., et al. (2011). "One-pot synthesis of 5-(hydroxymethyl) furfural from carbohydrates using tin-beta zeolite." *Acs Catalysis* 1(4): 408-410.
- [95] Kooyman, P., et al. (1997). "Acid dealumination of ZSM-5." *Zeolites* 18(1): 50-53.
- [96] Triantafillidis, C. S., Vlessidis, A. G., Nalbandian, L., & Evmiridis, N. P. (2001). Effect of the degree and type of the dealumination method on the structural, compositional and acidic characteristics of H-ZSM-5 zeolites. *Microporous and Mesoporous Materials*, 47(2-3), 369-388.
- [97] Hoff, T. C., et al. (2017). "Elucidating the effect of desilication on aluminum-rich ZSM-5 zeolite and its consequences on biomass catalytic fast pyrolysis." *Applied Catalysis A: General* 529: 68-78.
- [98] You, S. J. and E. D. Park (2014). "Effects of dealumination and desilication of H-ZSM-5 on xylose dehydration." *Microporous and Mesoporous Materials* 186: 121-129.
- [99] Zhao, S., et al. (2021). "Synergy of Extraframework Al³⁺ Cations and Brønsted Acid Sites on Hierarchical ZSM-5 Zeolites for Butanol-to-Olefin Conversion." *The Journal of Physical Chemistry C* 125(21): 11665-11676.
- [100] Yan, Z., et al. (2003). "On the acid-dealumination of USY zeolite: a solid state NMR investigation." *Journal of Molecular Catalysis A: Chemical* 194(1-2): 153-167.
- [101] Zhang, W., et al. (1999). "A high-resolution solid-state NMR study on nano-structured HZSM-5 zeolite." *Catalysis Letters* 60: 89-94.
- [102] Zhang, W., et al. (2023). "Sn doping on partially dealuminated Beta zeolite by solid state ion exchange for 5-hydroxymethylfurfural (5-HMF) production from glucose." *Journal of Chemical Technology & Biotechnology* 98(3): 773-781.
- [103] Rakiewicz, E., et al. (1996). "Solid-state NMR studies of silanol groups in mildly and highly dealuminated faujasites." *Microporous materials* 7(2-3): 81-88.
- [104] Wu, W. and E. Weitz (2014). "Modification of acid sites in ZSM-5 by ion-exchange: An in-situ FTIR study." *Applied surface science* 316: 405-415.
- [105] Treps, L., et al. (2021). "Spectroscopic expression of the external surface sites of H-ZSM-5." *The Journal of Physical Chemistry C* 125(3): 2163-2181.

- [106] Losch, P., et al. (2017). "Mesoporous ZSM-5 zeolites in acid catalysis: Top-down vs. Bottom-up approach." *Catalysts* 7(8): 225.
- [107] Ju, Z., et al. (2019). "Mechanism of glucose–fructose isomerization over aluminum-based catalysts in methanol media." *ACS Sustainable Chemistry & Engineering* 7(17): 14962-14972.
- [108] Liu, S., et al. (2022). "Advances in understanding the humins: Formation, prevention and application." *Applications in Energy and Combustion Science* 10: 100062.
- [109] Jung, D., et al. (2021). "Kinetic study on the impact of acidity and acid concentration on the formation of 5-hydroxymethylfurfural (HMF), humins, and levulinic acid in the hydrothermal conversion of fructose." *Biomass Conversion and Biorefinery* 11: 1155-1170.
- [110] Khumho, R., et al. (2021). "Glucose conversion into 5-hydroxymethylfurfural over Niobium oxides supported on natural Rubber-derived carbon/silica nanocomposite." *Catalysts* 11(8): 887.
- [111] Yousatit, S., et al. (2022). "Selective synthesis of 5-hydroxymethylfurfural over natural rubber–derived carbon/silica nanocomposites with acid–base bifunctionality." *Fuel* 311: 122577.
- [112] Zhou, C., et al. (2017). "Conversion of glucose into 5-hydroxymethylfurfural in different solvents and catalysts: Reaction kinetics and mechanism." *Egyptian journal of petroleum* 26(2): 477-487.
- [113] Li, X., et al. (2017). "Comprehensive Understanding of the Role of Brønsted and Lewis Acid Sites in Glucose Conversion into 5-Hydroxymethylfurfural." *ChemCatChem* 9(14): 2739-2746.
- [114] Otomo, R., et al. (2014). "Dealuminated Beta zeolite as effective bifunctional catalyst for direct transformation of glucose to 5-hydroxymethylfurfural." *Applied Catalysis A: General* 470: 318-326.
- [115] Li, X., et al. (2018). "Acid-free conversion of cellulose to 5-(hydroxymethyl) furfural catalyzed by hot seawater." *Industrial & engineering chemistry research* 57(10): 3545-3553.
- [116] Zhou, C., et al. (2017). "Conversion of glucose into 5-hydroxymethylfurfural in different solvents and catalysts: Reaction kinetics and mechanism." *Egyptian journal of petroleum* 26(2): 477-487.
- [117] Atanda, L., et al. (2016). "High yield conversion of cellulosic biomass into 5-hydroxymethylfurfural and a study of the reaction kinetics of cellulose to HMF conversion in a biphasic system." *Catalysis Science & Technology* 6(16): 6257-6266.
- [118] Swift, T. D., et al. (2015). "Tandem Lewis/Brønsted homogeneous acid catalysis: conversion of glucose to 5-hydroxymethylfurfural in an aqueous chromium (III) chloride and hydrochloric acid solution." *Green Chemistry* 17(10): 4725-4735.
- [119] Ramesh, A., et al. (2021). "Catalytic conversion of glucose to 5-hydroxymethylfurfural productions over sulphated Ti-Al₂O₃ catalysts." *Biomass and bioenergy* 154: 106261.
- [120] Zhang, Y., et al. (2017). "Synthesis and evaluation of acid-base bi-functionalized SBA-15 catalyst for biomass energy conversation." *Chemical Engineering Journal* 313: 1593-1606.
- [121] Luo, C.-W., et al. (2016). "Influence of reaction parameters on the catalytic performance of alkaline-treated zeolites in the novel synthesis of pyridine bases from glycerol and ammonia." *Industrial & engineering chemistry research* 55(4): 893-911.
- [122] Wei, B., et al. (2020). "Effect of different acid-leached USY zeolites on in-situ catalytic upgrading of lignite tar." *Fuel* 266: 117089.
- [123] Huang, C., et al. (2017). "Heterogeneous catalytic synthesis of quinoline compounds from aniline and C 1–C 4 alcohols over zeolite-based catalysts." *RSC advances* 7(76): 48275-48285.
- [124] Oozeerally, R., et al. (2020). "Gallium and tin exchanged Y zeolites for glucose isomerisation and 5-hydroxymethyl furfural production." *Applied Catalysis A: General* 605: 117798.

- [125] Gautam, R., et al. (2023). "Enhanced Catalytic Activity of Modified ZSM-5 Towards Glucose Isomerization to Fructose." *ChemPlusChem*.
- [126] Song, X., et al. (2021). "Efficient Conversion of Glucose to 5-Hydroxymethylfurfural over a Sn-Modified SAPO-34 Zeolite Catalyst." *Industrial & engineering chemistry research* 60(16): 5838-5851.
- [127] Jin, F. and Y. Li (2009). "A FTIR and TPD examination of the distributive properties of acid sites on ZSM-5 zeolite with pyridine as a probe molecule." *Catalysis Today* 145(1-2): 101-107.
- [128] Moliner, M., et al. (2010). "Tin-containing zeolites are highly active catalysts for the isomerization of glucose in water." *Proceedings of the National Academy of Sciences* 107(14): 6164-6168.
- [129] Kurmach, M., et al. (2016). "Effect of Introduction of B³⁺ OR Al³⁺ Ions in the Structure of Ti-, Sn-, AND Zr-Containing Hierarchical Zeolites on the Concentration of Lewis and Brønsted Acid Centers." *Theoretical and Experimental Chemistry* 52: 190-196.
- [130] Yu, Y., et al. (2000). "Characterization of iron atoms in the framework of MFI-type zeolites by UV resonance Raman spectroscopy." *Journal of Catalysis* 194(2): 487-490.
- [131] Xin, Y., et al. (2013). "Enhanced performance of Zn-Sn/HZSM-5 catalyst for the conversion of methanol to aromatics." *Catalysis Letters* 143: 798-806.
- [132] Dijkmans, J., et al. (2013). "Productive sugar isomerization with highly active Sn in dealuminated β zeolites." *Green Chemistry* 15(10): 2777-2785.
- [133] Samanta, S., et al. (2004). "Mesoporous tin silicate: an efficient liquid phase oxidative dehydrogenation catalyst." *Applied Catalysis A: General* 273(1-2): 157-161.
- [134] Ordonsky, V., et al. (2012). "The effect of solvent addition on fructose dehydration to 5-hydroxymethylfurfural in biphasic system over zeolites." *Journal of Catalysis* 287: 68-75.
- [135] Garcés, D., et al. (2017). "Aqueous phase conversion of hexoses into 5-hydroxymethylfurfural and levulinic acid in the presence of hydrochloric acid: mechanism and kinetics." *Industrial & engineering chemistry research* 56(18): 5221-5230.
- [136] Heda, J., et al. (2023). "Effect of acidity and mesoporosity in H-USY on conversion of wheat straw to ethyl levulinate (Biofuel additive)." *Journal of the Indian Chemical Society*: 100883.
- [137] Yang, X., et al. (2016). "Conversion of dihydroxyacetone to methyl lactate catalyzed by highly active hierarchical Sn-USY at room temperature." *Catalysis Science & Technology* 6(6): 1757-1763.
- [138] Wang, Y., et al. (2017). "Influence of Zirconium Modified USY on Coupled Hydrogenation and Ring Opening of Tetralin Over NiW/USY+ Al₂O₃." *Catalysis Letters* 147: 1704-1713.
- [139] Tang, B., et al. (2019). "Hierarchical FAU-type hafnosilicate zeolite as a robust Lewis acid catalyst for catalytic transfer hydrogenation." *ACS Sustainable Chemistry & Engineering* 7(19): 16329-16343.
- [140] Tosi, I., et al. (2019). "Exploring the synthesis of mesoporous stannosilicates as catalysts for the conversion of mono- and oligosaccharides into methyl lactate." *Topics in Catalysis* 62: 628-638.
- [141] Ward, J. W. (1967). "The nature of active sites on zeolites: I. The decationated Y zeolite." *Journal of Catalysis* 9(3): 225-236.
- [142] Jacobs, P. A. and W. J. Mortier (1982). "An attempt to rationalize stretching frequencies of lattice hydroxyl groups in hydrogen-zeolites." *Zeolites* 2(3): 226-230.
- [143] Yang, H., et al. (2021). "Synthesis of hierarchical Sn-Beta zeolite and its catalytic performance in glucose conversion." *Catalysis Today* 367: 117-123.
- [144] Xu, S., et al. (2019). "Highly efficient Cr/ β zeolite catalyst for conversion of carbohydrates into 5-hydroxymethylfurfural: Characterization and performance." *Fuel Processing Technology* 190: 38-46.

- [145] Gabrienko, A. A., et al. (2010). "Strong acidity of silanol groups of zeolite beta: Evidence from the studies by IR spectroscopy of adsorbed CO and ^1H MAS NMR." *Microporous and Mesoporous Materials* 131(1-3): 210-216.
- [146] Qiu, G., et al. (2022). "Hafnium-tin composite oxides as effective synergistic catalysts for the conversion of glucose into 5-hydroxymethylfurfural." *Fuel* 311: 122628.
- [147] Li, G., et al. (2014). "Synergy between Lewis acid sites and hydroxyl groups for the isomerization of glucose to fructose over Sn-containing zeolites: a theoretical perspective." *Catalysis Science & Technology* 4(8): 2241-2250.



APPENDIX

Calculations and Calibrations for HPLC Analysis

1. Concentrations of nitric acid

The concentrations of the nitric acid were calculated by using mass (weight), percentage purity, and volume of water, based on the following equation.

The mass of concentrated nitric acid needed to prepare x M concentration was obtained by using:

$$\frac{\text{mass}}{\text{molar mass}} = \frac{\text{known concentration} \times \text{required amount of water}}{1000 \times \% \text{purity}}$$

Molar mass of $\text{HNO}_3 = 63.01 \text{ g/mol}$

Required (known) concentration = 0.1 – 0.4 M

Amount of water used = 250 ml

%purity of $\text{HNO}_3 = 65\%$

The calculated mass of HNO_3 required to prepare x M nitric acid was then weighed and dissolved in 250 ml water.

2. Percentage weight of metal impregnated on zeolite.

The weight of tin loaded on the dealuminated zeolite was calculated based on the weight of tin in the tin precursor solution relative to 1 g of the dealuminated zeolite solid used.

$$\% \text{weight of Sn in } \text{SnCl}_4 \cdot 5\text{H}_2\text{O} = \frac{\text{Atomic mass of Sn}}{\text{Molar mass of } \text{SnCl}_4 \cdot 5\text{H}_2\text{O}} \times 100\%$$

Weight (mass) of Sn in Y gram of Sn precursor

$$= \%weight\ of\ Sn\ x\ Y\ gram\ of\ Sn\ precursor$$

Weight% of Sn in 1 g of zeolite sample

$$= \frac{\text{Weight of Sn in Y gram of Sn precursor}}{\text{Weight of Sn in Y gram of Sn precursor} + 1} \times 100\%$$

Atomic mass of Sn = 118.71 g/mol

Molar mass of SnCl₄.5H₂O = 350.71 g/mol

Mass of dealuminated zeolite sample = 1 g

3. SiO₂/Al₂O₃ mole ratio

The Si/Al mole ratio was calculated based on the weight (%) of each element obtained from the XRF result relative to 1 g (100%) of the sample used for analysis divided by their molar masses.

$$\text{Mole of Si or Al} = \frac{\text{mass (wgt\%) obtained from XRF}}{\text{atomic mass of Si or Al}}$$

$$\frac{\text{Si}}{\text{Al}} \text{ mole ratio} = \frac{\text{mole of Si}}{\text{mole of Al}}$$

4. Calibration for HPLC analysis

HPLC was calibrated by measuring the respective area of the concentrations prepared for each chemical standard and internal standard using an HPLC machine. The ratios of the areas obtained for each chemical to the internal standard area were then plotted

against the ratio of their respective concentrations and internal standard, and the calibration equation was obtained.

Table A1. Preparation of stock solutions for HPLC calibration.

Stock solution for Aqueous Phase			
Chemical	Mass (g)	Volume	Concentration (M)
Glucose	1.806	50ml DI water	0.2
Fructose	1.806		0.2
HMF	1.261		0.2
Levulinic Acid	1.161		0.2

A single stock solution for aqueous phase products was prepared by weighing the mass of the chemicals in 50 ml DI water. Then, a single standard solution of 0.02 M containing all the chemicals was made by measuring 2 ml volume from the stock solution (Glucose/Fructose/Levulinic acid (LA)/HMF) and mixed with 18 ml of water, and subsequently, used in preparing other concentration.

A similar procedure was followed for organic phase products containing HMF/Furfural, but THF was used as the solvent medium and not water. Water was not used because furfural does not dissolve in water.

Table A2. Data for HPLC calibration curve (Aqueous phase)

Aqueous phase									
Run	Concentration (M) ^a					Volume used for HPLC analysis (μL)			
	Glucose	Fructose	LA	HMF	2-Butanone	From 0.2M solution	From 0.02M solution	DI Water	2-Butanone
R1	0.02	0.02	0.02	0.02	0.1	800	-	0	200
R2	0.016	0.016	0.016	0.016	0.1	-	640	160	200
R3	0.012	0.012	0.012	0.012	0.1	-	480	320	200
R4	0.008	0.008	0.008	0.008	0.1	-	320	480	200
R5	0.004	0.004	0.004	0.004	0.1	-	160	640	200
R6	0.002	0.002	0.002	0.002	0.1	-	80	720	200

^a prepared concentration

Aqueous phase													
Run	Area from RID ^a					Area ratio from RID ^b				Concentration ratio ^c			
	Glucose	Fructose	LA	HMF	2-Butanone	Glu/B	Fr/B	LA/B	HMF/B	Glu/B	Fr/B	LVA/B	HMF/B
R1	456,066	464,753	294,036	379,666	122,368	3.73	3.80	2.40	3.10	0.20	0.20	0.20	0.20
R2	372,243	380,852	237,484	294,371	119,881	3.11	3.18	1.98	2.46	0.16	0.16	0.16	0.16
R3	275,592	281,600	177,080	232,518	124,382	2.22	2.26	1.42	1.87	0.12	0.12	0.12	0.12
R4	187,644	187,773	118,865	147,772	106,786	1.76	1.76	1.11	1.38	0.08	0.08	0.08	0.08
R5	96,022.90	99,391	61,939.20	74,629.20	102,879	0.93	0.97	0.60	0.73	0.04	0.04	0.04	0.04
R6	51,993.70	52,736.10	32,834.10	41,640.80	110,444	0.47	0.48	0.30	0.38	0.02	0.02	0.02	0.02

^a obtained from HPLC; ^{b-c} determined

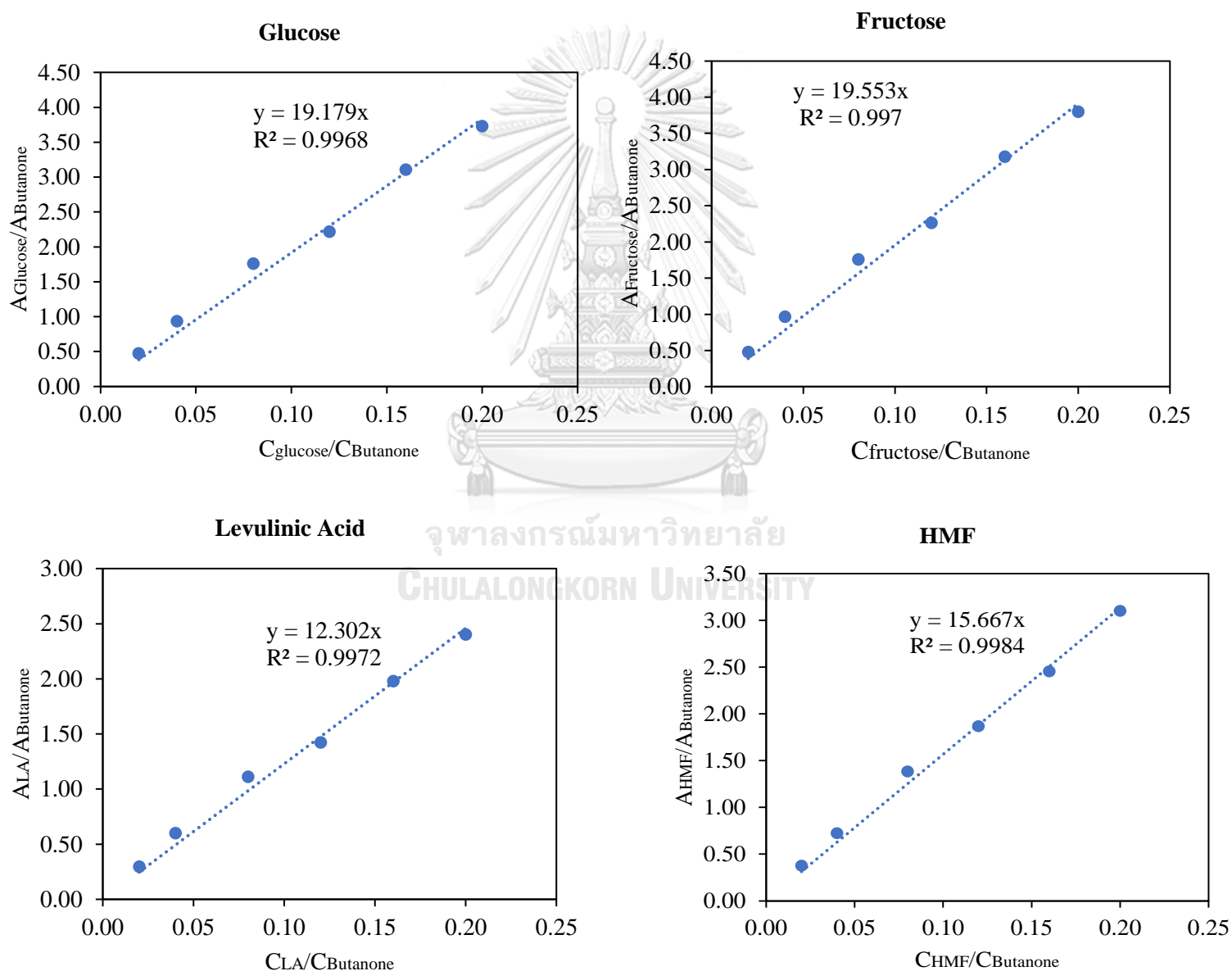


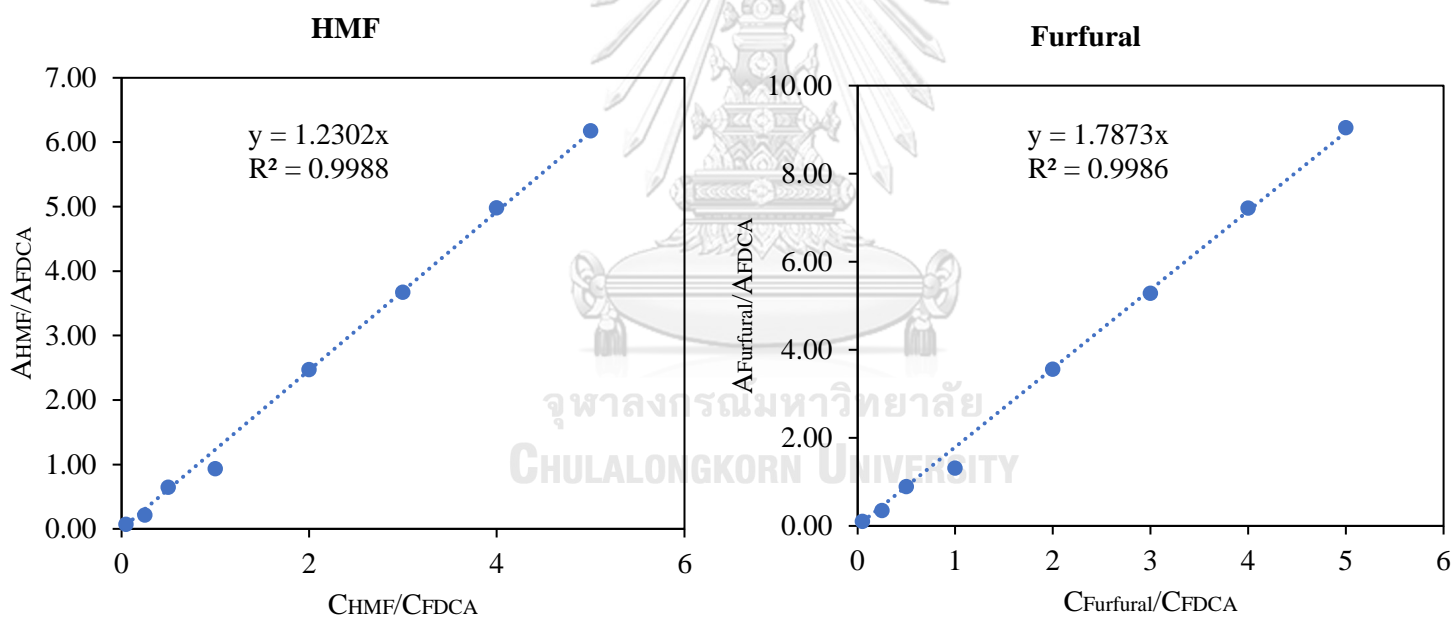
Figure A1. Calibration curve for aqueous phase (chemicals)

Table A3. Data for HPLC calibration curve (Organic phase)

Organic phase														
Run	Concentration (M) ^a			Volume (μ L)				Area from UV detector ^b			Area ratio from UV detector ^c			Concentration ratio ^d
	HMF	FF	FDCA	From 0.1M solution	THF	FDCA	Total (mL)	HMF	FF	FDCA	H/F	FF/F	H/F	FF/F
R1	0.1	0.1	0.02	800	-	200	1	163,064.00	238,772.00	26,410.90	6.17	9.04	5	5
R2	0.08	0.08	0.02	640	160	200	1	137,728.00	199,632.00	27,670.70	4.98	7.21	4	4
R3	0.06	0.06	0.02	480	320	200	1	101,282.00	145,671.00	27,592.90	3.67	5.28	3	3
R4	0.04	0.04	0.02	320	480	200	1	70,785.30	101,865.00	28,637.90	2.47	3.56	2	2
R5	0.02	0.02	0.02	160	640	200	1	26,658.20	37,523.30	28,549.20	0.93	1.31	1	1
R6	0.01	0.01	0.02	80	720	200	1	17,990.20	24,912.10	27,959.50	0.64	0.89	0.5	0.5
R7	0.005	0.005	0.02	40	760	200	1	5,918.38	9,621.02	27,685.80	0.21	0.35	0.25	0.25
R8	0.001	0.001	0.02	8	792	200	1	2,082.46	2,802.35	28,475.70	0.07	0.10	0.05	0.05

^a prepared concentration; ^{b-d} determined

FF or F means furfural; FDCA means 2,5-furan dicarboxylic acid; HMF or H means 5-hydroxymethylfurfural

**Figure A2.** Calibration curve for organic phase (chemicals)

5. Retention Time of Chemicals

Table A4. Retention time of chemicals obtained from HPLC calibration.

Aqueous phase	Retention Time (min)
Glucose	11.839
Fructose	12.819
Levulinic Acid	20.315
HMF	38.511

2-Butanone	34.096
Organic Phase	Retention Time (min)
HMF	37.245
FF	57.083
FDCA	19.23

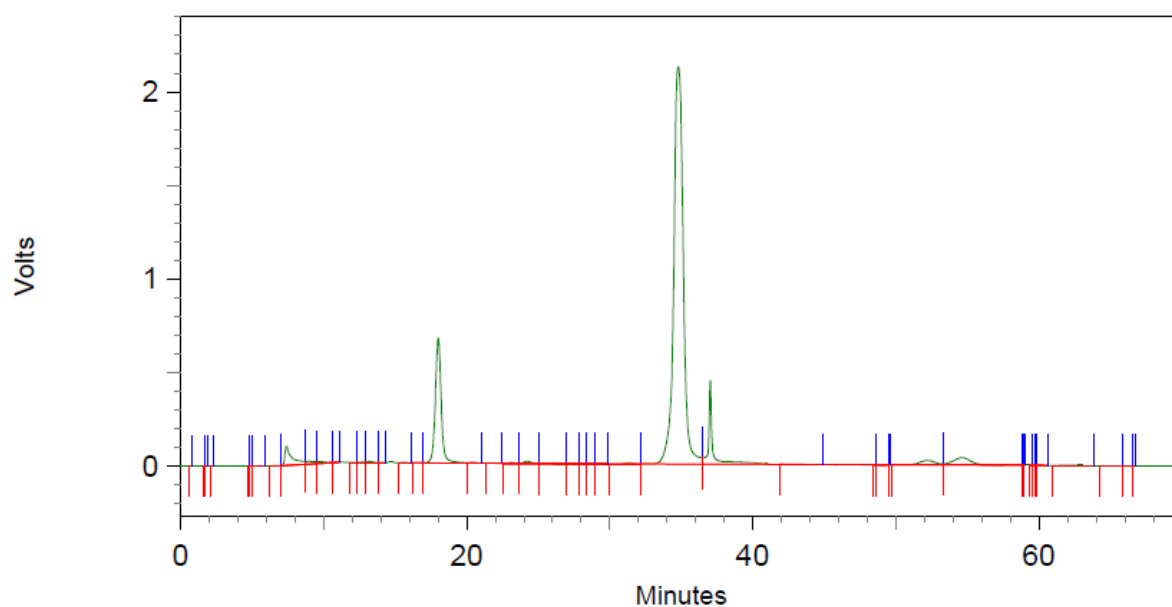


Figure A3. Example of analysis result obtained from HPLC.

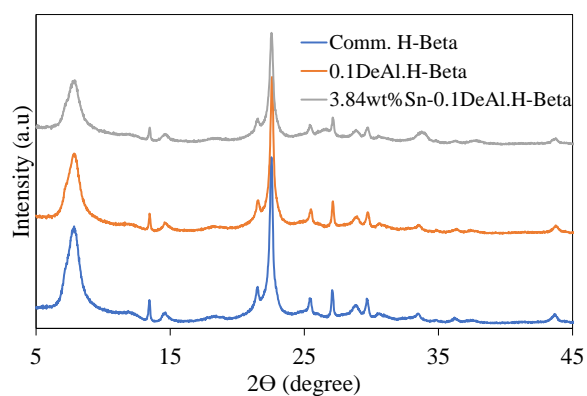


Figure A4. XRD patterns of commercial and modified H-Beta Zeolite

REFERENCES



จุฬาลงกรณ์มหาวิทยาลัย
CHULALONGKORN UNIVERSITY



จุฬาลงกรณ์มหาวิทยาลัย
CHULALONGKORN UNIVERSITY

VITA

NAME Oluwaseyi Ojelabi

DATE OF BIRTH 5 June 1992

PLACE OF BIRTH Nigeria

INSTITUTIONS ATTENDED University of Ilorin, Nigeria

HOME ADDRESS 386, Chang Muaeng 2 Alley, Pracha Songkro Road, Din Daeng, Bangkok

PUBLICATION Ojelabi, O.; Yousatit, S.; Rashid, U.; Ngamcharussrivichai, C. Mild Dealumination of H-ZSM-5 Zeolite for Enhanced Conversion of Glucose into 5-Hydroxymethylfurfural in a Biphasic Solvent System. *Catalysts* 2023, 13, 982. <https://doi.org/10.3390/catal13060982>